AN ABSTRACT OF THE DISSERTATION OF

Iria Gimenez Calvo for the degree of Doctor of Philosophy in Ocean, Earth, and Atmospheric Sciences presented on December 7, 2018.

Title: Ocean Acidification Impacts on Bivalves at Multiple Organizational Levels: From Individual Larvae to Bivalve Aggregations Habitats

Abstract approved: _____

George G. Waldbusser

Many marine bivalves are sensitive to ocean acidification (OA) stress and often show heightened sensitivity during brief early larval and post-larval life stages, potentially leading to population bottlenecks. Most of the evidence to date has been collected in laboratory experiments that focused on physiological responses at the organismal level under stable carbonate chemistry. Bivalves, however, inhabit coastal and estuarine environments where multiple physical and biological processes affect carbonate chemistry and often result in significant temporal and spatial variability and decoupling of carbonate chemistry variables. Furthermore, bivalves often form large shell aggregations where biogeochemical feedbacks relating to inorganic C cycling and alkalinity have not been well constrained and, thus, aggregation-level responses to OA are largely unknown. This dissertation focuses on bivalve responses to OA on two biological organizational levels -organism and habitat- by 1) providing

new frameworks to evaluate environmental variability and 2) measuring the potential of local OA buffering within shell aggregations. These two overarching goals should provide more realistic forecasts of the fate of bivalves under future climate scenarios. Chapter 2 describes a new metric to predict survival of Pacific oyster larvae by integrating their exposure history to variable acidification conditions. Chapter 3 presents a new experimental system capable of decoupling carbonate chemistry parameters and recreate variable exposures under a controlled laboratory environment. Chapter 4 provides the first measurements of alkalinity fluxes in oyster reefs, a type of bivalve aggregation, and evaluates the response of the system to moderate acidification conditions to evaluate the potential of shell aggregations to modify local carbonate chemistry conditions and provide buffering to OA for juveniles. Chapter 5 offers a detailed characterization of the biogeochemistry of a restored oyster reef and the identification of key biogeochemical processes responsible for alkalinity production or regeneration within porewaters. This dissertation suggests that relatively simple modeling and laboratory tools can successfully incorporate temporal variability naturally experienced by bivalves and provide adequate predictions of survival. It further provides first evidence that reef-level biogeochemical feedbacks derived from the collocation of calcium carbonate shell and labile organic matter result in the production of large alkalinity fluxes that, while not very sensitive to increased moderate PCO_2, could indeed buffer corrosive conditions at local spatial scales, providing micro-refugia to sensitive larval and juveniles. Collectively, this body of work is proof of the need to shift from an OA open-ocean paradigm based on stable carbonate chemistry conditions to

improve our understanding regarding OA impacts on sensitive coastal organisms exposed to dynamic carbonate chemistry conditions.

Ocean Acidification Impacts on Bivalves at Multiple Organizational Levels: From Individual Larvae to Bivalve Aggregations Habitats

by
Iria Gimenez Calvo

A DISSERTATION

submitted to

Oregon State University

in partial fulfillment of
the requirements for the
degree of

Doctor of Philosophy

Presented December 7, 2018
Commencement June 2019

Doctor of Philosophy dissertation of Iria Gimenez Calvo presented on December 7, 2018

APPROVED:

Major Professor, representing Ocean, Earth, and Atmospheric Sciences

Dean of the College of Earth, Ocean, and Atmospheric Sciences

Dean of the Graduate School

I understand that my dissertation will become part of the permanent collection of Oregon State University libraries. My signature below authorizes release of my dissertation to any reader upon request.

Iria Gimenez Calvo, Author

ACKNOWLEDGEMENTS

A Ph.D. is no small task. Everybody that has earned a doctorate will, I think, agree. My case is no exception- I have had a ton of support, encouragement, patient guidance, and love. Here goes my attempt to thank everyone that has been instrumental in helping me to accomplish this feat.

First and foremost, I need to thank my Ph.D. advisor, Dr. George Waldbusser, for everything. George, thank you for taking a chance on me, for pushing me to become the best scientist I can be, a good colleague, and a better person. Thank you for being a demanding advisor but always an endless source of support, for patiently guiding me in my professional pursuits, for forcing my brain into thinking in new, creative ways, and for nurturing my self-confidence in times of failure and stress. I have learned so much and so many valuable lessons from you. I could not have asked for a better mentor.

I need to thank the Spanish Fulbright Commission, the National Science Foundation, Oregon Sea Grant and NOAA for providing financial support to my endeavor. I am honored to have had the support of so many institutions, which, in many cases, have afforded me much more than just financial backing. Thank you. I do not take the privilege of conducting research for granted, and I am forever indebted to the program managers that believed in me, in my supervisor's ideas, and in my ability to conduct the work.

I would also like to thanks Dr. Burke Hales for encouraging me to be a rigorous, quantitative scientist, and for, without doubt, making me believe that I can become an engineer

when it is required. I am grateful for all the guidance and mentoring that I have received from you over the years.

Thank you also to the members of my Ph.D. committee: Miguel Goñi, Roberta Marinelli and Inara Scott. Thank you for agreeing to be part of this adventure, for supporting me and encouraging me, and for your helpful contributions along the way.

I am also grateful to Chris Langdon, Matt Gray, Evan Durland, and the entire group at Hatfield Marine Science Center. All I know about bivalve physiology and larval rearing is thanks to you. Thank you for your help, and for always being a supportive crew, even when things never went as planned.

I owe a tremendous thank you to the Whiskey Creek Hatchery for their continuous support of my work. Sue Cudd, Mark Wiegardt, and Alan Barton, your support, help, and guidance carried me over many frustrations. Many times after my work with you had ended, I found myself reminiscing all the lessons I learned from you. Your strength, experience, knowledge, and humility are an example that I hope I can emulate in my future endeavors.

I would also like to thank many people that have contributed to my professional growth during my stay at OSU and Horn Point Laboratory, and whose help and guidance has been invaluable to get to the finish line. In no particular order, Brian Haley, Jennifer McKay, Angelicque White, Rick Colwell, Andrew Thurber, Robert Wheatcroft, Shireen Hyrapiet, Tuba Ozkan-Haller, Ricardo Letelier, Clare Reimers, Joe Jennings, Dale Hubbard, Marnie Jo Zirbel, Jesse Muratli, Andy Ross, Andy Ungerer, Ben Russell, Heather Bergschneider, Lori Hartline,

Robert Allan, Jim Dickson, Mary Hitch, Jason Balderston, Jeffrey Cornwell, Mike Owens, Melanie Jackson. To all of you, thank you.

I cannot thank the Waldbusser lab, including past and present members, enough. Elizabeth Brunner, Rebecca Mabardy, Stephanie Smith, Stephen Pacella, Cameron Allen, Jessamyn Johnson, Cale Miller, and all the fantastic undergraduates that I have interacted with over these years… besides being a group of incredibly smart and driven people, you guys have been my lifeline and an incredible support system, both professionally and personally. You have been there, with beers and hugs, when things were not going well and again, with beers and hugs, when something fantastic needed to be celebrated. You have been a sounding board of frustrations and achievements, a never-ending source of inspiration, and a humble reminder of how incredibly lucky I have been to share part of my life with all of you. Thank you for everything. You are all much more than labmates, and I must thank George again for finding the best students so I could have the best friends. If I ever mentor a group of students, I strive to be select them as well as George has, so the bonds that they will form will be as durable as the ones I have formed with all of you.

Thank you to Emilia, Cristina and Mino, for supporting and rooting me from afar, for conquering your fears to come and visit us, and for never ever complaining about me uprooting your son and brother. I know I have asked a lot from your family and, in turn, I have always received unwavering encouragement. Gracias. I am so lucky to have you in my life.

Thank you also to my Corvallis friends and family. I could not have done any of this without you. Among them, I am particularly grateful to Eduardo Guerrero, Amoreena Guerrero,

Josh Cuzzone and Alejandra Sánchez-Ríos. You have been my rock and my champions during these years, bearing witness to every little step forward and the many steps backwards. This accomplishment is a bit yours too. I have grown personally and professionally by your side, and I am forever grateful to be your friend and count with your unwavering support no matter how hard the situation gets.

Talking about unwavering support, my family deserves almost the biggest thank you of them all. Mamá, Papá, Meritxell, gracias. Truly, for everything. Thank you for making me the person I am today, and for showing me a path for kindness and healthy ambition and for allowing to dream bigger than I thought was possible. None of this would have ever happened without you loving me unconditionally, believing in me and rooting for me since I was born. Thank you for continuing to support me and doing so from all corners of the world. I know I am extremely lucky that all my crazy dreams of becoming a scientist were always supported and encouraged by you three, never once doubting my capability of success even when I did. This is for you.

And, finally, the person that deserves the biggest thank you of all - my loving partner, Alberto. Thank you. No acknowledgment is enough even to begin to describe how grateful I am to have you by my side, supporting me every step of the way, celebrating my every achievement, no matter how small. You nurtured me, championed me, and patiently listened to me when I needed to vent frustrations… to then remind me that life is so much more. You endured 2.5 years of thousands of miles separating us, moved across oceans, and changed career paths just to help me conquer this. You even helped me with experiments and patiently cleaned buckets and

buckets and buckets of seawater! After everything, you continue to be proud of me and are ready to do it all again so I can continue to pursue this dream. Nobody can ask for a better partner. I could not have done this without you and, truly, this is as yours as it is mine.

CONTRIBUTION OF AUTHORS

Dr. Burke Hales contributed to the idea conceptualization for chapter 2, prototype design and development for chapter 3, and data acquisition and interpretation, and writing and reviewing of manuscripts for both chapters 2 and 3.

Dr. Chris Langdon assisted with study design, data acquisition, and manuscript edition for chapter 3.

Dr. Jeffrey Cornwell and Michael Owens assisted with data collection and experimental design for chapters 4 and 5.

Dr. Jeremy Testa, Dr. Wei-Jun Cai, Dr. Jeffrey Cornwell, Dr. Ming Li, and Dr. W. Michael Kemp contributed to study design, and writing and reviewing of manuscripts for both chapter 4 and 5.

TABLE OF CONTENTS

TABLE OF CONTENTS (Continued)

TABLE OF CONTENTS (Continued)

TABLE OF CONTENTS (Continued)

TABLE OF CONTENTS (Continued)

LIST OF FIGURES

LIST OF FIGURES (Continued)

Figure Page

LIST OF FIGURES (Continued)

Figure Page

LIST OF FIGURES (Continued)

Figure Page

LIST OF TABLES

LIST OF TABLES (Continued)

1. CHAPTER I.- Introduction

Combustion of fossil fuels, cement production and land-use changes in the last ~250 years have resulted in unabated releases of anthropogenic carbon dioxide (CO_2) into the atmosphere at rates unprecedented in the last 66 million years (Zeebe et al., 2016). As atmospheric CO_2 increases, approximately a third of the emissions are absorbed by the global oceans (Sabine et al., 2002), increasing partial pressure of CO_2 (PCO_2), and reducing seawater pH and saturation state with respect to calcium carbonate (Ω) (Caldeira and Wickett, 2003; Doney et al., 2009). These shifts in the ocean carbonate chemistry system have been collectively termed ocean acidification (OA) (Caldeira and Wickett, 2003; Orr et al., 2005; Doney et al., 2009).

Open-ocean carbonate chemistry time-series (e.g. Dore et al., 2009; Bates et al., 2014) have demonstrated relative carbonate chemistry stability at hourly and weekly timescales (e g. Hofmann et al. 2010), as well as a tight correlation among carbonate chemistry parameters in these systems. The moderately simple carbonate chemistry dynamics resulting in the observed changes have led to accurate forecasts of future open-ocean mean PCO_2 and pH conditions (e.g. Orr et al., 2005) based on climate projections. The projected open-ocean conditions have been widely accepted by the global research community as standard guidelines to evaluate OA organismal effects (Gattuso et al. 2010).

In recent decades, many taxa and life-stages have been identified as sensitive to OA (Kroeker et al. 2010, 2013; Wittmann and Pörtner 2013). Multiple shell-aggregating bivalve

species have also been shown to respond to acidification stress, displaying mostly adverse biological effects spanning larval to adult life stages (see reviews in Kroeker et al., 2010; Gazeau et al., 2013). Most of the empirical evidence, however, has been collected in isolated, controlled laboratory experiments under constant carbonate chemistry experimental treatments that mimic future average open ocean conditions (as discussed in McElhany and Shallin Busch, 2013; Waldbusser and Salisbury, 2014; Reum et al., 2016) and focused on examining physiological responses at the organismal level. However, as pointed out by Waldbusser and Salisbury, 2014 and Helmuth et al. 2014, open-ocean long-term averages are presumably not physiologically relevant for coastal organisms that experience naturally dynamic and highly variable carbonate chemistry conditions.

Indeed, organisms inhabiting dynamic coastal and estuarine environments and estuaries such as marine bivalves are not subject to the gradual change on tightly correlated carbonate chemistry parameters predicted and observed in open ocean environments (e.g. Waldbusser and Salisbury, 2014; Fassbender et al. 2016; Pacella et al. 2018). Instead, nearshore marine organisms are naturally subject to myriad physical and biological processes that affect the chemistry of their surroundings, thus resulting in a complex mosaic of temporal (Harris et al., 2013; Waldbusser and Salisbury, 2014; Kapsenberg et al., 2015; Hales et al., 2017) and spatial (Hauri et al., 2013a; Chan et al., 2017) variability of the carbonate system (Waldbusser and Salisbury, 2014). Among the drivers of temporal and spatial variability in coastal systems, the most important physical and biogeochemical processes include varying freshwater inputs, tidal and regional circulation, seasonal upwelling, and diel cycles of photosynthesis and respiration,

and calcification and dissolution (Waldbusser et al. 2011; Fassbender et al. 2016; Hales et al. 2017; Pacella et al. 2018), all of which alter the master variables of the carbonate system (dissolved inorganic carbon (DIC) and alkalinity (TAlk)) to various degrees and with different magnitudes. As a result, instances of decoupling of PCO_2, pH and Ω occur in multiple timescales (Cai et al. 2011; Waldbusser and Salisbury 2014; Evans et al. 2015; Hales et al. 2017).

Some authors have argued that the magnitude of projected changes in carbonate chemistry parameters associated with OA lies within the range of the observed natural variability (Duarte et al., 2013). Recent modeling work, however, has demonstrated that the rising baseline of PCO_2 associated with anthropogenic activities will result in increases in the magnitude, duration and frequency of acidified conditions in coastal zones (Harris et al., 2013; Hauri, Gruber, McDonnell, et al., 2013 b).

The need to incorporate habitat-specific future projections of OA conditions and environmental variability in experiments designed to evaluate physiological effects of acidification have been recognized with the research community as key to better predict organismal future outcomes (Takeshita et al., 2015; Wahl et al., 2016; Boyd et al., 2016). The physiological effects of carbonate chemistry temporal and spatial variability, however, are difficult to study and currently poorly constrained, and determining which scales are most relevant for organisms is an active research area.

In a seminal paper, Helmuth et al. (2010) addressed the need to focus on "organismal climatology", or the translation of environmental conditions into realistic and relevant metrics for organisms that then can be applied to improve current fitness forecasts. Building upon

decades of work studying physiological responses to variable temperature, salinity and oxygen conditions, a vast body of research has been accumulated regarding the importance of high frequency variability (e.g. Dillon et al., 2016), the frequency and magnitude of extreme events (e.g. Helmuth et al., 2010), and the need to incorporate small spatial scale variability (e.g. Helmuth and Hofmann, 2001) to better reflect organismal real exposures to current and future environmental conditions.

Relevant temporal and spatial scales, however, can vary among life-stages and are associated with organismal traits that translate into sensitivity or resiliency to environmental conditions. For instance, early larval stages of some marine bivalves display a heightened sensitivity to low Ω during early larval shell formation (e.g. Waldbusser et al. 2015a,b; Waldbusser et al. 2016a). In this case, the relevant temporal scale to accurately describe the exposure history as it relates to acidification stress comprises minutes and hours, as the fast shell building period lasts less than 24 hours (Waldbusser et al. 2016a). As another example, multiple bivalve species respond to varied chemical cues for settlement (Pawlik, 1992; Hadfield and Paul, 2001a; Tamburri et al., 2007), including the corrosivity of sediment (as in clams, see Green et al., 2013; Clements and Hunt, 2014) or specific mineral surfaces in bivalve shells (see Pawlik, 1992). The physiologically relevant spatial scale for bivalves undergoing metamorphosis, therefore, are likely very small, spanning mm to cm. Thus, incorporating environmental variability at the adequate relevant scales is crucial to refine sensitivity thresholds and provide tools to forecast the fate of organisms, particularly at sensitive life-stages that can act as population bottlenecks.

Bivalves, however, often form dense aggregations such as clam beds or oyster reefs (Dame, 2012), thereby forming habitats that can significantly alter biogeochemical dynamics when compared to their surroundings. Thus, organismal exposure within these systems can often be highly variable on small spatial scales and dependent upon habitat-level biogeochemical properties and feedbacks, thereby complicating the prediction of organismal responses based on organismal responses measured on isolated laboratory experiments. Appropriate temporal and spatial scaling is also required in order to assess habitat-level responses to OA and, ultimately, to evaluate the feasibility of OA mitigation strategies targeted to provide local buffering against corrosivity.

The overarching goal of this dissertation was to explore the effects of complex exposures to carbonate chemistry on bivalves by focusing my attention on two biological organizational levels- organismal and habitat. At the organismal level, I centered this research on the larval period, a life-stage with well-demonstrated exacerbated sensitivity to OA and potential to originate population bottlenecks. At the habitat level, I explored the poorly constrained biogeochemical dynamics occurring within a shellfish aggregation, the response of this habitat to moderate OA and, ultimately, the potential for local buffering of detrimental carbonate chemistry conditions for sensitive larvae and juveniles. There is, however, a common thread throughout this work, and while this does not represent the final and definitive assessment of environmental variability and its effects on bivalves' response to OA, I present various tools and frameworks to incorporate this complexity.

Chapter 2 explores the effects of variable carbonate chemistry regimes on Pacific oyster (*Crassostrea gigas*) larvae reared at a commercial hatchery located in Netarts Bay, OR, US and presents an integrated metric that captures accumulated acidification stress over the entire larval period- OASIS, the Ocean Acidification Stress Index for Shellfish. We assessed the effects of environmental variability by comparing survival to pre-settlement on four cohorts of larvae subdivided and raised in naturally variable carbonate chemistry versus stable, buffered, optimal conditions. Results confirmed heightened sensitivity of the early larval stages, as buffering during this early larval stage resulted in significant improvement in overall survival. OASIS predicted survival to pre-settlement in two out of three cohorts with different carbonate chemistry exposures and based on high-frequency aragonite saturation state exposure, therefore providing a promising tool to more realistically predict larval survival that incorporates natural variability.

Related to work from the previous chapter, Chapter 3 proposed a new and automated experimental system to recreate dynamic carbonate chemistry conditions and decoupling of PCO_2, pH, and Ω, instances commonly found in coastal environments, on controlled laboratory experiments. The Dynamic Ocean Acidification Manipulation Experimental System (DOAMES) manipulated DIC and TAlk to successfully decouple pH and Ω, necessary to elucidate mechanisms of sensitivity, while also providing the capability of simulating idealized or natural environmental conditions. DOAMES provides another promising tool to isolate the effects of complex carbonate chemistry exposures to evaluate organismal responses to OA.

Chapter 4 and 5 assessed the biogeochemical processes driving alkalinity production and habitat-level responses to OA on a shellfish aggregation - a restored Eastern oyster (*Crassostrea virginica*) located in Harris Creek, MD, US. Chapter 4 provides, to my knowledge, the first measurements of alkalinity fluxes on oyster reefs, evaluated their response to moderate increases in PCO_2, likely already within the natural range of carbonate chemistry conditions at this habitat. We measured large alkalinity fluxes from the oyster reef to the overlying water, significantly larger than estimates published for many coastal environments and matching reported values for coral reefs. We found no effects of moderate acidification on alkalinity fluxes, although there was substantial variability among samples, likely the result of the intrinsic heterogeneity of the system. We found a key role of shell dissolution in the measured fluxes, likely enhanced by the production of metabolic acids as a result of aerobic respiration of organic rich biodeposits. Inorganic non-carbonate alkalinity contributions to the global alkalinity flux were variable, from zero up to 70%, indicating the potentially important role of anaerobic pathways of organic matter remineralization such as denitrification and sulfate reduction. The results of this chapter suggest that shellfish aggregations can buffer transient local corrosive conditions, likely resulting in microhabitats within the reef of improved carbonate chemistry. The effectiveness of this mitigation strategy, however, requires the collocation of shell and organic biodeposits to favor shell metabolic dissolution and anaerobic remineralization of organic matter and maximize alkalinity generation. Effectively, this means that OA chemical refugia would be associated with living oyster reefs, as opposed to dead shell accumulations.

Building on work from the previous chapter, chapter 5 explores the biogeochemical processes driving the observed porewater distributions of oyster reef cores collected in Harris Creek, MD. Porewater distributions indicate significant production of alkalinity within the framework of the oyster reef. The distributions of alkalinity and DIC support both metabolically-enhanced shell dissolution and net sulfate reduction as main drivers of the alkalinity production. Assessment of calcium, sulfate, hydrogen sulfide and sulfide mineral measurements suggest, however, that net sulfate reduction might be the main porewater alkalinity-generating biogeochemical process. Solid-phase analyses reveal sedimentary organic C contents within the lower end of bivalve aggregation published results, but higher than coastal environments with comparable permeabilities. It is hypothesized that very labile organic C associated with biodeposits might results in high rates of organic carbon remineralization, as observed in other permeable sediments. The results of this work provide the first detailed biogeochemical description of an oyster reef, a necessary framework to better evaluate habitat-level responses to OA in complex and heterogeneous systems like shellfish aggregations and, ultimately, predict potential feedbacks between organisms and their habitat.

Ocean acidification stress index for shellfish (OASIS): Linking Pacific oyster larval survival and exposure to variable carbonate chemistry regimes

Iria Gimenez, George G. Waldbusser, and Burke Hales

Elementa: Science of the Anthropocene
University of California Press
155 Grand Avenue, Suite 400, Oakland, CA 94612-3758
Volume 6, Article 51

2. CHAPTER II.- Ocean acidification stress index for shellfish (OASIS): Linking Pacific oyster larval survival and exposure to variable carbonate chemistry regimes

2.1 Abstract

Understanding larval bivalve responses to variable regimes of seawater carbonate chemistry requires realistic quantification of physiological stress. Based on a degree-day modeling approach, we developed a new metric, the ocean acidification stress index for shellfish (OASIS), for this purpose. OASIS integrates over the entire larval period the instantaneous stress associated with deviations from published sensitivity thresholds to the aragonite saturation state (Ω_{Ar}) over the entire larval period while experiencing variable carbonate chemistry. We measured survival to D-hinge and pre-settlement stage of four Pacific oyster (*Crassostrea gigas*) cohorts with different histories of carbonate chemistry exposure at the Whiskey Creek Hatchery, Netarts Bay, OR, to test the utility of OASIS as a stress metric and document the effects of buffering seawater in mitigating acute and chronic exposure to ocean acidification. Each cohort was divided into four groups and reared under the following conditions: 1) stable, buffered seawater for the entire larval period; 2) stable, buffered seawater for the first 48 hours, then naturally variable, unbuffered seawater; 3) stable, unbuffered seawater for the first 48 hours, then buffered seawater; and 4) stable, unbuffered seawater for the first 48 hours, then naturally variable, unbuffered seawater. Patterns in Netarts Bay carbonate chemistry were dominated by seasonal upwelling at the time of the experimental work, resulting in naturally highly variable Ω_{Ar} for the larvae raised in the unbuffered treatments. Two of the four cohorts showed strongly

positive responses to buffering in survival to 48 hours; three of the four, in survival to pre-settlement. OASIS accurately predicted survival for two of the three cohorts tested (the fourth excluded due to other environmental factors), suggesting that this new metric could be used to better understand larval bivalve survival in naturally variable environments. OASIS may also be useful to an array of diverse stakeholders with increasing access to highly resolved temporal measurements of carbonate chemistry.

2.2 Introduction

Ocean acidification (OA) results from the relatively rapid increase of partial pressure of dissolved CO_2 (PCO_2) through anthropogenic activities (Caldeira and Wickett, 2003; Orr et al., 2005; Doney et al., 2009) decoupled from concurrent changes in total alkalinity or buffering capacity that tend to happen on longer geologic time scales (Honisch et al., 2012; Zeebe, 2012). The current rate of release of anthropogenic CO_2 into the atmosphere is unparalleled in the last 66 million years (Zeebe et al., 2016), while the weathering of carbonate and silicate rocks to buffer the increased PCO_2 operates over time scales of 10,000–100,000 years (Zeebe, 2012). This temporal lag between the main global scale drivers of ocean carbonate chemistry leads to reduced pH and seawater saturation state with respect to calcium carbonate (Ω), shifting the oceans towards more corrosive conditions (Feely, 2004; Honisch et al., 2012).

Adverse biological effects associated with OA have been described across multiple stages of complex bivalve life cycles. These stages include gametogenesis (Parker et al., 2009; Barros et al., 2013), larvae (Kurihara et al., 2007; Talmage and Gobler, 2010; Barton et al., 2012;

Waldbusser et al., 2015a; 2015b), juveniles (Waldbusser et al., 2011; Hettinger et al., 2012; Miller and Waldbusser, 2016) and adult calcification (Gazeau et al., 2007; Amaral et al., 2012). Emerging evidence, however, suggests an exacerbated sensitivity to OA stress during larval stages and, in particular, during the first 48 hours of bivalve larval development (Barton et al., 2012; Waldbusser et al., 2013; 2015a; 2015b; White et al., 2013; 2014). This heightened sensitivity to environmental stress during embryogenesis and early larval shell development is not restricted to acidification, but also to pollution exposure and physiological stress due to sub-optimal temperature and salinity conditions (His et al., 1999).

Bivalves are found in coastal environments and estuaries where myriad physical and biological processes result in high temporal variability in carbonate chemistry at local spatial domains (Hales et al., 2005; Feely et al., 2010; Waldbusser and Salisbury, 2014). The co-occurring modes of temporal variability in these systems include hourly, daily, weekly and seasonal time scales, resulting in complex patterns of carbonate chemistry (Harris et al., 2013; Waldbusser and Salisbury, 2014; Kapsenberg et al., 2015; Hales et al., 2017). Furthermore, the shifting baseline of atmospheric carbon dioxide concentrations (i.e., OA) will result in periods of less favorable chemistry conditions becoming more frequent and of greater magnitude (Harris et al., 2013; Hauri et al., 2013; Evans et al., 2015; Hales et al., 2017).

The physiological effects of high-frequency variability in carbonate chemistry are difficult to study and currently poorly constrained. Consequently, the incorporation of environmental fluctuations into experimental design and model predictions has been identified as a research priority within the OA research community (Takeshita et al., 2015; Wahl et al., 2016;

Boyd et al., 2016). The majority of published work on bivalve larvae involves experimental designs that utilize conditions of fixed levels of high PCO_2, low pH and/or low saturation states that are maintained throughout the exposure period (Kurihara et al., 2007; Gazeau et al., 2011; Timmins-Schiffman et al., 2013; Waldbusser et al., 2015a; 2015b; 2016). In addition, the values chosen for experimental treatments are frequently based on global averages instead of local exposure regimes (McElhany and Busch, 2013), thus often not representative of the range of conditions experienced by organisms in their microhabitats (Helmuth et al., 2010; Helmuth et al., 2014).

Several recent studies have utilized different approaches to integrating the environmental variability of carbonate chemistry into manipulation experiments, aptly summarized by Boyd et al. (2016). Only a very small subset of the reviewed literature, however, concern experimental work performed on the larval stages of marine invertebrates, and currently results have been mixed in terms of whether variable or constant conditions are more favorable to organisms. In a study of two species of mussel larvae, Frieder et al. (2014) found mitigating effects of variable conditions on early development, but mixed effects on growth after eight days. Clark and Gobler (2016) also found both positive and negative effects on three different species of bivalve larvae across different physiological measures. Eriander et al. (2016), however, did not find that variable carbonate chemistry, relative to fixed, affected mean growth of barnacle larvae, although it did elicit a 20-fold increase in variance across the individuals. Overall, interpreting such complex and divergent responses could benefit from the development of conceptual and quantitative frameworks to better assess and predict the effects of dynamic acidification

conditions on organisms. Understanding larval bivalve responses to exposure to variable carbonate chemistry regimes (in situ conditions) is critically dependent on realistic quantification of physiological stress on high frequency time scales and the potential for recovery after transient exposure to harmful conditions.

The effects of environmental variability on physiological stress have been noted previously (Helmuth and Hofmann, 2001), but only recently have been highlighted in OA research frameworks (Waldbusser and Salisbury, 2014) and in the limited experimental work noted above. In a seminal paper, Helmuth et al. (2010) addressed the need to focus on "organismal climatology", or the translation of environmental conditions into realistic and relevant metrics for organisms. The exposure history of organisms that inhabit dynamic environments is driven by the "filtering" of the environmental signal or its translation into what an organism eventually experiences (Helmuth, 2009; Helmuth et al., 2010; Waldbusser and Salisbury, 2014) based on its morphological and behavioral characteristics, thus creating each organism's fundamental physiological niche (Kearney and Porter, 2004; 2009). Organismal climatology is therefore fundamental to the development of realistic predictive models of population dynamics and species distributions (Seabra et al., 2015; Montalto et al., 2016). A wide variety of methods have been proposed, from correlative, descriptive climate-envelope models (Hijmans and Graham, 2006) to highly sophisticated multi-variable mechanistic models (Buckley et al., 2011; Montalto et al., 2016). Nevertheless, translating laboratory experimental results into mechanistic physiological models requires an abundance of physiological and environmental data, and the results are often restrictive in their application (Buckley et al., 2011).

One mechanistic framework widely used across applications and relatively simple to implement is the degree-day (DD) model.

A DD model is widely used to translate the variable thermal exposure of an organism to a metric of biological performance (Bonhomme, 2000). DD models are considered parsimonious, here defined as simple parameterizations with good explanatory power, and have been used to predict crop yield as growing degree-days (GDD), to model plant development and phenology (Moore and Remais, 2014), to estimate fish growth (Neuheimer and Taggart, 2007; Chezik et al., 2014), and to forecast patterns of coral bleaching (Liu et al., 2003; Eakin et al., 2010; Kayanne, 2017). Although there are varying levels of complexity within DD models, all consider the organismal response as the result of the composite of temperature relative to a defined physiological threshold and time. For example, in DD models that predict growth, thermal exposure accumulates when temperature exceeds the minimum threshold for growth but does not surpass a second threshold for impaired physiological activity (Moore and Remais, 2014). Therefore, degree-days are referred to as “thermal time” or “thermal organismal history”.

We propose a reinterpretation of the DD framework to account for accumulated acidification stress on larval bivalves, defining a new metric: ocean acidification stress index for shellfish (OASIS). Akin to a DD model, OASIS integrates an instantaneous acidification stress effect over the larval period, is based on OA stress thresholds identified in laboratory experiments, and includes an additional parameterization that accounts for heightened sensitivity observed in early larval stages. In analogy to DD, OASIS can be described as “acidification time” or “acidification organismal history”.

We assessed the performance of OASIS by following four cohorts of Pacific oyster (*Crassostrea gigas*) larvae subject to a range of carbonate chemistry conditions at a commercial hatchery, Whiskey Creek Hatchery (WCH), Netarts Bay, OR, where ocean acidification has had major impacts on hatchery production of oyster seed (Barton et al., 2012; 2015). The objectives of our study were to: 1) determine differences in acute vs. chronic exposure to acidification stress; 2) document the integrated effects of exposure to buffered larval culture water vs. naturally variable carbonate chemistry on survival in four Pacific oyster larval cohorts; and 3) develop and validate the OASIS index for survival of Pacific oyster larvae to pre-settlement stage.

2.3 Methods

We measured survival to pre-settlement (i.e., pediveliger stage) of four cohorts of Pacific oyster larvae (*C. gigas*) exposed to different carbonate chemistry regimes at WCH: two cohorts in August 2014, one in May 2015, and one in June 2015. The experimental design was an incomplete cross-over in which *C. gigas* larvae were divided into two groups and reared for the first 48 hours post-fertilization, then split again into two more groups for a total of four treatments. Our designation of these treatments include capital "B" or "U", correspoding to buffered (described below) or unbuffered during the first 48 hours, then lowercase "b" or "u" for the same treatment applied during the remaining larval period (see Table 2.1).

2.3.1 Study location

The Whiskey Creek Shellfish Hatchery (WCH) is located in Netarts Bay, OR (45.403°N, 123.944°W), a small tidally dominated estuary located on the north Oregon coast with generally near-ocean salinity in the spring and summer months (Engle et al., 2007). Although almost the entire bay is flushed with every tidal cycle (Whiting and McIntire, 1985), extensive seagrass beds (*Zostera spp.*) covering approximately two-thirds of the total area of the estuary (Whiting and McIntire, 1985) and microphytobenthos on tidal flats appear to significantly modify the Bay's carbonate chemistry (Barton et al., 2012).

WCH installed carbonate chemistry monitoring equipment in 2011, revealing environmental variability on hourly, weekly and fortnightly scales (Vance, 2012; Barton et al., 2012). In 2013, the equipment was upgraded to provide real-time, high frequency measurements of PCO_2 and total dissolved inorganic Carbon (TCO_2) that allow complete parameterization of the carbonate system (Barton et al., 2015). Previously, in 2011, WCH installed an automated system based on pH to buffer seawater, therefore enhancing its favorability for larval shell growth. WCH "buffered" water refers to incoming seawater treated with agricultural grade soda ash (unpurified sodium carbonate, Na_2CO_3) to achieve an aragonite saturation state (Ω_{Ar}) between 4 and 5. WCH "unbuffered" water is untreated and reflects the natural carbonate chemistry variability of Netarts Bay which modifies Pacific Ocean waters.

2.3.2 Experimental system

We constructed a flow-through experimental system consisting of sixteen 23.5-L plastic culture chambers with individual inlets reaching the near-bottom of each chamber and an outlet

at the top of the culture chamber fitted with a “banjo” type filter. The banjo filter consisted of a circular section of 25-cm diameter equipped with nylon mesh screen (Nitex) to allow the flow of seawater and algae but to retain the embryos and larvae. Banjos with larger Nitex were exchanged during the experiment as larvae grew to allow better flushing and minimize clogging. The mesh size was 20 µm the first week and 60 µm from day 7 post-fertilization until the end of the experiment. The locations of the inlet and outlet were designed to maximize mixing and reduce the potential for stratification.

Experimental chambers were maintained at 25°C with four water baths (four chambers per water bath) and individual in-line heaters. The temperature of culture chambers was monitored at least twice a day. Chambers were cleaned every two or three days, coinciding with larval sampling.

The flow of seawater was individually regulated for each culture chamber with rotameter type flow meters and valves maintaining flow between 20 and 23 L hr^{-1} per chamber. We estimated that the residence time of each culture chamber was less than 1.5 hours, except for a few transient occurrences of reduced or stopped flow due to routine hatchery maintenance operations (interruptions less than 2 hours long) and one instance of local disruption in electrical service (less than 8 hours).

All culture chambers were fed continuously to maintain a total approximate concentration of 25,000–30,000 cells mL^{-1} of a mixture of different algal species following the practices of the hatchery (*Isochrysis sp*., both Caribbean and Tahitian strains, *Nannochloropsis sp*., *Chaetoceros gracilis*, and *C. calcitrans*).

2.3.3 Spawn and larval culture

We carried out four independent experiments on 5 August 2014, 12 August 2014, 28 May 2015 and 5 June 2015, providing four independent cohorts. For each experiment, we partnered with the hatchery managers to collect a portion of fertilized eggs from larger, commercial spawns. For each spawn, between 2 and 10 Molluscan Broodstock Program (MBP; Langdon et al., 2003) females and 1–3 MBP males were stripped of their gametes, which were then pooled and fertilized to produce one cohort.

After ~ 1.5 hours post-fertilization, we checked the fertilized eggs for cell division and presence of polar bodies to ensure successful fertilization. Subsequently, we divided the embryos into two groups: "buffered" (B) and "unbuffered" (U) and transferred them into eight culture chambers, four replicates per treatment, at a stocking density of 7 or14 embryos mL^{-1} (Cohorts 1–3: 7 embryos mL^{-1} or 165,000 embryos $chamber^{-1}$; Cohort 4: 14 embryos $mL^{\neg 1}$ or 335,000 embryos $chamber^{-1}$). Cohort 4 was stocked at a higher density to ensure sufficient survival, as this cohort coincided with background high early larval mortality experienced at the hatchery. We allowed the embryos to develop in static conditions (zero flow) for 40 to 45 hours until the Prodissoconch I shell had been fully formed and larvae had reached the D-stage. We then further sub-divided the B and U treatments into the four treatment groups (Bb, Bu, Ub, Uu) resulting in two replicate chambers per treatment. Organismal density was not adjusted for Cohorts 1–3 during the length of the test, but larval density was adjusted for Cohort 4 from 14 embryos mL^{-1} to 7 larvae mL^{-1} after 48 hours post-fertilization when transferred to one of their four respective treatments to match the organismal density of the other cohorts during the remaining larval

period. We terminated the experiments when approximately 50% of the larvae in the Bb treatment appeared to have reached the pediveliger stage and showed signs of competency to settle (i.e., presence of “eye spots” or protrusion of larval “foot”).

2.3.4 Larval survival

Larval abundance was measured at the end of the static culture period and at every chamber cleaning to measure survival. Larvae were collected on a 37-µm screen and concentrated in a known volume of seawater. At least three aliquots of equal volume were then collected and counted at 20x magnification under light microscopy. Sample volumes were adjusted to target 20–100 larvae. Counts were repeated if replicate counts differed by more than 20% among aliquots. The arithmetic mean of the counts was computed and larval survival was reported as the percentage of the total number of embryos stocked in each culture chamber. Cohort 4 survival post-48 hours was computed with respect to the corrected density of larvae.

2.3.5 Carbonate chemistry

Untreated seawater pumped straight from Netarts Bay was characterized continuously by a combined PCO_2/TCO_2 dual analyzer based on Bandstra et al. (2006) coupled with simultaneous measurements of temperature and salinity (SBE 45 MicroTSG, Sea-Bird Scientific) as described in Vance (2012). All measurements were collected at high-frequency temporal resolution (1Hz). Independently calibrated internal gas and liquid standards ensured linearity and accuracy for both parameters.

Discrete samples for carbonate chemistry were collected from one randomly selected culture chamber of each of the two seawater sources (buffered and unbuffered) once or twice a day on larval sampling and non-sampling days, respectively. Samples were preserved in 350-mL amber glass bottles with polyurethane-lined crimp-sealed metal caps and preserved with 50 µL of saturated $HgCl_2$ solution. PCO_2 and TCO_2 were measured following procedures by Bandstra et al. (2006) refined for discrete samples as in Hales et al. (2005) and Hales et al. (2017). The remaining carbonate chemistry parameters were computed following water dissociation constants from Millero (1995), acid equilibration constants from Millero (2010), Dickson (1990) constants for boric acid, and calcite and aragonite solubility constants from Mucci (1983).

2.3.6 Ocean acidification stress index for shellfish (OASIS) description

We opted to base OASIS on Ω_{Ar} based on compelling evidence that this parameter determines growth and development sensitivity to ocean acidification in early larval stages of vulnerable bivalves at modern ambient-water values (Gazeau et al., 2011; Thomsen et al., 2015; Waldbusser et al., 2015a; 2015b). Accordingly, sensitivity thresholds based on Ω_{Ar} have been proposed for some organisms and taxa based on fixed exposures (Barton et al., 2012; Waldbusser et al., 2015a) and used in estimations of historical environmental favorability for bivalve populations (Hales et al., 2017), biogeochemical model projections (Gruber et al., 2012), and shellfish risk assessments (Ekstrom et al., 2015).

2.3.6.1 Definition of OASIS and parameterizations: Ω_{Ar} stress threshold and differential sensitivity term

OASIS provides a measure of accumulated stress by integrating only the area of the Ω_{Ar} time series that falls below the designated threshold over the entire larval period, from fertilization to metamorphosis. Mathematically, OASIS can be described as follows:

$$OASIS = \int_{fertilization}^{settlement} \left[(\Omega_{thrsh} - \Omega_t) \frac{1}{1+D_{pft}} \right] dt, if\ (\Omega_{thrshd} - \Omega_t) > 0 \quad (2.1)$$

where Ω_{thrsh} is the selected acidification stress threshold, Ω_t is the instantaneous value, dt is the time differential (minutes), D_{pft} is day(s) post-fertilization (spawning day = 0), and if (Ω_{thrsh} - Ω_t)> 0 is the truncating condition of the integral, allowing the integral to operate only when the conditions are below the set threshold. The units of OASIS are Ω min day^{-1}. It follows, therefore, that OASIS will have different total integration times depending on developmental rates. Longer periods from fertilization to pre-settlement will result in increased integration time, but only in increased OASIS values if $\Omega_{thrsh} > \Omega_t$.

The most important parameterization of our model is the selection of a physiological relevant threshold. We chose a value of $\Omega_{Ar} = 1.5$ as a conservative stress threshold for OASIS based on recently published work (Barton et al., 2012; Gruber et al., 2012; Ekstrom et al., 2015) that identified this value as a minimum threshold for early development and commercial production-to-settlement competency for *C. gigas*. The second parameterization within OASIS incorporates the increased sensitivity observed in the early larval stages of *C. gigas* by introducing a weight function into the metric, as described by the term

$$\frac{1}{1+D_{pft}} \quad (2.2)$$

This term describes an inverse and injective function with maximum of 1 and horizontal asymptote that approaches 0 when $D_{pft} > 0$; therefore, it works as a simple but useful weight function by placing maximum weight on the early larval stages ($D_{pft} = 0$ corresponds to a weight score of 1; $D_{pft} = 2$, weight score of 0.33; $D_{pft} = 7$, weight score of 0.125).

2.3.6.2 Implementation of OASIS

We computed OASIS for the cohorts described above by combining results of discrete carbonate chemistry sampling for the static portion of the experiment (i.e., embryogenesis to Prodissoconch I shell) with continuous, high-frequency high-resolution data collected by the PCO_2/TCO_2 analyzer for the remainder of the experiment. As the embryos were raised in static conditions for the first 48 hours, we computed the OASIS value for the unbuffered treatment by fitting a linear equation between the initial and final Ω_{Ar} calculated from the results of discrete carbonate chemistry sampling of the embryo culture chamber. We acknowledge that Ω_{Ar} likely varied in a non-linear fashion during these time periods due to respiration and calcification, but decided against taking excessive discrete samples to avoid causing stress to the embryos during this critical life stage. If Ω_{Ar} was above the defined threshold of $\Omega_{Ar} = 1.5$ in the discrete culture chamber, then the OASIS value was 0 during this period. After 48 hours, and thus during the period of flow-through culture, the continuous record was used to calculate OASIS in the unbuffered treatments. OASIS was zero in all buffered treatments for all periods because Ω_{Ar} was always greater than 1.5.

2.3.7 Data analysis

Our experimental design was geared towards an analysis of variance (ANOVA) of larval survival as a function of treatment; however, the survival data did not meet ANOVA assumptions of normality and homoscedasticity even after multiple data transformations were tested. We therefore explored the use of generalized linear models.

Fractional linear regression (Papke and Wooldridge, 1996), a type of generalized linear model, is suitable for fractional responses contained between 0 and 1. It approximates the sample distribution as logistic, allows for overdispersion of the data, and uses iterative weighted least squares to fit a linear model. Also, to address the heteroscedasticity of the data, we computed heteroscedasticity-consistent (HC) standard errors, also known as robust or White-Huber standard errors, and compared them to the regular standard error (SE). Specifically, we used HC3, a version particularly well suited for small sample sizes (Long and Ervin, 2000). Differences between regular and robust standard errors were deemed insignificant, as they did not change statistical significance in any of the parameters, so we decided to report regular SE.

We analyzed survival data at 48 hours post-fertilization and pre-settlement independently, given the autocorrelation of observations over time. All cohorts were grouped for each analysis, using cohort as an independent factor. Therefore cohort had four levels and treatment had two levels (buffered, B; unbuffered, U) for the analysis at 48 hours post-fertilization and four levels (buffered-buffered, Bb; buffered-unbuffered, Bu; unbuffered-

buffered, Ub; unbuffered-unbuffered, Uu) for the analysis at pre-settlement. In all cases, we also tested the interaction of cohort and treatment.

We used standard linear regression to fit survival data to OASIS and we evaluated the statistical significance of the correlation with Pearson's coefficient. All statistical analyses were performed in Rstudio (version 1.0.136).

2.4 Results

2.4.1 Carbonate chemistry

The buffered seawater treatment consistently had greater Ω_{Ar} values than the unbuffered one for all cohorts (Tables 2.2 and 2.3, Figures 2.1 and 2.2). Mean conditions for unbuffered seawater carbonate chemistry during the static culture period (first 48 hours post-fertilization) were below our stress threshold only for Cohort 2 (Ω_{Ar} = 1.34), close to threshold for both Cohorts 1 and 4 (Ω_{Ar} = 2.25 and Ω_{Ar} = 1.87, respectively), and well above the threshold for Cohort 3 (mean Ω_{Ar} = 3.22) (Table 2.3). For the remainder of the larval period, the unbuffered carbonate chemistry conditions experienced by Cohorts 3 and 4 were less acidified than for Cohorts 1 and 2, as evidenced by the reduced overall mean values of PCO_2 (1288 µatm and 882 µatm for Cohorts 3 and 4, compared to 1445 µatm and 1520 µatm for Cohorts 1 and 2, respectively) and, conversely, overall greater values for pH (7.76 and 7.79 for Cohorts 3 and 4, versus 7.60 for Cohort 1 and 7.54 for Cohort 2) and Ω_{Ar} (2.14 and 2.13 for Cohorts 3 and 4, compared to 1.38 for Cohort 1 and 1.18 for Cohort 2). The mean unbuffered Ω_{Ar} was slightly lower than the defined threshold for physiological stress for Cohorts 1 and 2 (Ω_{Ar}<1.5), but

slightly higher for Cohorts 3 and 4 (Ω_{Ar} > 2.0). Buffered treatments were always above the physiological threshold (Ω_{Ar} > 4.0) (Table 2.3). The temperature remained reasonably stable around 24.3°C (± 0.8°C standard deviation, STD) due to the controlled heating of water in the hatchery, and salinity was generally high (33.0 ± 0.9 STD).

Our culture chambers reflected the dynamics of the source water to the hatchery as evidenced by the general agreement of the discrete chamber samples with the continuous high-resolution carbonate chemistry record (see Figures 2.2 and 2.3). Small discrepancies, more evident in PCO_2 and pH than in Ω_{Ar}, were likely the result of a combination of processes including the heating of the water to 24.4°C, the interplay of larval calcification and net respiration, and the addition of concentrated CO_2-enriched algal cultures.

2.4.2 Larval survival

Larval survival at 48 hours post-fertilization and pre-settlement are shown in Figures 2.3 and 2.4. Analysis of all cohorts together yielded a highly significant effect of treatment on survival to 48 hours post-fertilization ($F_{1,28} = 51.51$, $p = 2.04 \times 10^{-7}$), while cohort ($F_{3,28} = 7.05$, $p = 0.0015$) and the interaction between cohort and treatment ($F_{3,28} = 9.90$, $p = 0.00020$) were also significant, limiting overall inferential power. Survival to 48 hours post-fertilization varied among treatments and across cohorts (Figure 2.3, Table 2.3). Cohort 1 showed a strong survival response to buffering (B = 88.6 ± 7.8% SE versus U = 7.6 ± 8.6% SE), while Cohorts 2 and 4 showed possible trends towards increased survival (B = 53.7 ± 4.4% SE versus U = 38.5 ± 13.5% SE for Cohort 2; B = 96.0% ± 6.9% SE and U = 85.5% ± 15.3% SE for Cohort 4). In

contrast, Cohort 3 displayed a possible reverse trend, though the mean survivals were similar (B = 79.3% ± 6.1% SE versus U = 81.5% ± 7.5% SE; Figure 2.3, Table 2.3).

Three of the four cohorts, however, showed strong buffering effects in pre-settlement survival (Figure 2.4). We decided to exclude Cohort 4 from the analysis, after suspicions that other factors beyond our treatments had affected the survival responses (see Discussion). After excluding Cohort 4, survival was influenced by both treatment ($F_{3,23} = 3.39$, $p = 0.041$) and cohort ($F_{2,23} = 4.91$, $p = 0.020$), but not their interaction. However, none of the post-hoc Tukey pair-wise comparisons were significant, due to the overall high variance; therefore, any observed differences have to be interpreted with caution.

As expected for all cohorts, we found that Cohorts 1 and 2 showed higher survivorship for buffered larvae, compared to those exposed to naturally unbuffered conditions. For Cohort 1 only those larvae buffered during the early larval stage (i.e., first 48 hours post-fertilization) survived to pre-settlement stage (5.4% ± 5.4% SE and 1.6% ± 0.6% SE, for Bb and Bu, respectively, versus 0.0% ± 0.0% SE for all unbuffered). In contrast, Cohort 2 survival was highest for those larvae buffered during the whole experiment (12.9% ± 1.9% SE) and lowest for those unbuffered (5.5% ± 5.5% SE), but was similar for those buffered only for the first 48 hours (8.1% ± 3.1% SE) and those buffered only after this period (8.1% ± 2.2% SE). For Cohort 3, the pattern observed for Cohort 1 was repeated: larvae buffered during early stages outperformed those that were not buffered, although Cohort 3 seemed to benefit from exposure to natural variability after initial buffering (11.1% ± 7.8% SE for Bb; 18.6% ± 2.0% SE for Bu; 1.2% ± 0.9% SE for Ub; and 1.9% ± 1.7% SE for Uu). Finally, Cohort 4 showed an unexpected pattern

of survival, in which buffering the water seemed to have a detrimental effect, and survival was highest in larvae not exposed to buffered water at any point during the experiment (3.4% ± 0.3% SE for Bb; 2.6% ± 2.6% SE for Bu; 1.9% ± 1.4% SE for Ub and 12.0% ± 2.6% SE for Uu).

Competency to settle in the fully buffered (Bb) treatment was reached at different days post-fertilization for each cohort, resulting in varying duration of the experiments. Cohort 1 did not reach pediveliger stage until 22 days post-fertilization, whereas Cohort 2 reached competency to settlement at 16 days, and Cohorts 3 and 4 at 17 days (Table 2.3).

2.4.3 OASIS

The Ω_{Ar} time series for Cohorts 1, 2 and 3 and the associated computed OASIS values are shown in Figure 2.5. We excluded Cohort 4 from OASIS calculations given the odd pattern of survival (see Discussion).

The unbuffered Ω_{Ar} during the first 48 hours was above the stress threshold for Cohorts 1 (mean $\Omega_{Ar} = 2.25$) and 3 (mean $\Omega_{Ar} = 3.22$), so the accumulated OASIS during this stage is 0 for all treatments of these two cohorts (Figure 2.5 A,C). For Cohort 2, we assumed that Ω_{Ar} increased linearly from $\Omega_{Ar} = 1.00$ to $\Omega_{Ar} = 1.67$ during the first 48 hours (Figure 2.5 B). The cumulative OASIS value for Bb for all three of these cohorts was 0, as Ω_{Ar} never reached values below the stress threshold.

Given that OASIS was 0 for the first 48 hours for Cohorts 1 and 3, OASIS values for Bu and Uu were identical: 741 Ω min day^{-1} for both values for Cohort 1 and 253 Ω min day^{-1} for Cohort 3. In the case of Cohort 2, the OASIS values for Bu, Ub, and Uu were 499, 557, and 1056

Ω min day^{-1}, respectively. The integration period was longer for Cohort 1 (22 days) compared to Cohorts 2 and 3 (16–17 days) as a consequence of its slower development.

OASIS predicted survival for 2 of the 3 cohorts tested. The regression fit between survival and OASIS for Cohorts 1, 2, and 3 is shown in Figure 2.6. We excluded from the computation two treatments from Cohort 1 (Ub and Uu) due to concern about the validity of a cumulative stress index to assess pre-settlement survival when no survival to the end of the larval stage was achieved. Survival reached 0% at 2 and 5 days post-fertilization for Cohort 1 Uu and Bu, respectively. As two data points have been excluded in the case of Cohort 1, the relationship is a perfect fit (%Survival = –0.005[OASIS] + 5.352). We recognize that fitting a linear regression to the remaining two points is problematic, and only provide the values to compare the slopes of the two cohorts. We found a significant linear regression for Cohort 2 (%Survival = –0.007[OASIS] + 12.346; $R^2 = 0.957$, $p < 0.05$), but no correlation for Cohort 3 ($R^2 < 0.1$).

2.5 Discussion

This study was designed to address three main objectives related to the effects of variable carbonate chemistry on larval oyster survival. First, we assessed the effect of acute exposure (first 48 hours post-fertilization) to naturally occurring carbonate chemistry on larval survival and compared it to larvae cultured in buffered seawater. Second, we determined chronic effects of buffering as an OA mitigation strategy for the entire larval stage. Third, we tested the performance of OASIS as a predictor of survival to settlement competency on larval stages exposed to different carbonate chemistry regimes.

Inquiry into the effects of buffering as a mitigation strategy for acute exposure to acidification stress (first 48 hours post-fertilization) revealed that high ΩAr during embryogenesis dramatically increased survival to 48 hours post-fertilization in Cohort 1, with either a possible trend towards increased survival or else no effect detected in the other cohorts (Figure 3). These results appear generally consistent with earlier work (Gazeau et al., 2011; Thomsen et al., 2015; Waldbusser et al., 2015a; 2015b), showing reduced acute sensitivity in development and growth to ambient-water ΩAr values exceeding 1.5. However, comparisons with previously published work are difficult, as survival is a different metric than development and growth. Further complicating comparisons, some experimental studies have been conducted at temperatures that span the range of sub-optimal conditions for larval growth and survival (Bochenek et al., 2001).

Cohorts 1 and 4 had very similar chemistry conditions of about ΩAr = 2.0 during the first 48 hours yet showed remarkably dissimilar responses. Secondary effects from other carbonate chemistry parameters are unlikely to have been responsible for these divergent results, given that PCO2 was lower for Cohort 1 than for Cohort 4 (Table 2.3). Although no definitive studies on survival are available, robust experimental data have demonstrated the sensitivity of development and growth to ΩAr, but not to PCO2 and pH at the embryological stage (Waldbusser, 2015a). We propose, therefore, that the strong response of Cohort 1 to buffering might be related to additional environmental stressors or to broodstock quality that resulted in an overall poorer condition. Cohort 1 larvae might have had greater sensitivity to acute exposure at higher Ω_{Ar} if their overall fitness had already been compromised. The overall longer larval

period, suggesting developmental delays (as in Timmins-Schiffman et al., 2013), might also be evidence for reduced fitness.

Buffering seawater during embryogenesis resulted in significantly greater pre-settlement survival in three of the four cohorts (Figure 2.4). Buffering only after this early stage seemed to improve survival to pre-settlement in only one cohort when compared to survival in continuously unbuffered seawater (Figure 2.4 B), highlighting again the heightened sensitivity to early exposure and the importance of delayed effects.

We hypothesize that the unbuffered Ω_{Ar} conditions experienced by Cohort 3 during embryogenesis ($\Omega_{Ar} > 3.0$) were not sufficiently unfavorable to elicit an acute mortality response, but may have resulted in sub-lethal effects. Such delayed effects are evidenced by an order of magnitude greater survival to pre-settlement for larvae that were buffered during this early stage compared to those that experienced unbuffered conditions (Figure 2.4 C). These results also confirm observations made by hatchery managers and in other studies of carryover effects that the impacts of early exposure to acidification stress often manifest themselves later in the larval cycle (Barton et al., 2012; 2015; Hettinger et al., 2012).

The overall beneficial effect of buffering agrees with observations made by multiple hatchery operators on the US West Coast (Barton et al., 2015). Better bivalve larval performance at elevated Ω_{Ar} ($\Omega_{Ar} > 1.5$) during embryological and early larval development has also been shown in multiple laboratory experiments (Gazeau et al., 2011; Timmins-Schiffman et al., 2013; White et al., 2013; 2014; Thomsen et al., 2015; Waldbusser et al., 2015a; 2015b). In this study, we exposed some of the larvae to acute stress followed by chronic stress (Uu). The overall

response of larvae to chronic stress in the Uu treatments may represent a conservative estimate of the effects of chronic exposure, as we were evaluating only the survivors of acute stress that might have been selected for increased tolerance to stress.

The overall survival-to-settlement competency size in this study fell below commercial hatchery targets (30–60%; A Barton, personal communication; Breese and Malouf, 1975) for all cohorts, but was within the range of other published studies for oyster larvae (Talmage and Gobler, 2012; Eierman and Hare, 2013; Ko et al., 2013). To our knowledge, however, laboratory studies that have measured long-term larval survival under acidification have not captured embryological exposure to acidified conditions, only the exposure of larvae at least 24 hours old (Talmage and Gobler, 2010; Ko et al., 2013; 2014), potentially underestimating deleterious effects. While our results generally show better survival for larvae raised in buffered water, differences in survival are complicated to assess statistically given the limited number of replicates due to logistical constraints, including limited laboratory space that prevented the installation of more culture chambers, lack of feasibility of sampling efforts, and the prioritization of repetition of the experiment (i.e., more cohorts) over increased sample replication. Our unbuffered treatment was also a function of natural variability, making the magnitude of the acute stress exposure variable by design.

Cohort 1 performed better under buffered conditions, but showed lower overall survival across treatments, both at 48 hours post-fertilization and pre-settlement, compared to the other three treatments (Figures 2.3 and 2.4). This reduction in overall fitness suggests possible parental effects, including lower maternal lipid contribution to eggs (Gallager and Mann, 1986) or an

unfavorable condition of the broodstock (Utting and Millican, 1997). The overall poorer performance of Cohort 1 compared to the other cohorts is also evident by the notably longer time to reach settlement competency (22 days, compared to 16–17 days for the other cohorts). Although arrested or slow larval development might sometimes be an effective strategy to survive stress (Moran and Manahan, 2004), in general a longer pelagic larval stage increases the probability of loss by predation (Underwood and Fairweather, 1989) or dispersal away from favorable settlement substrates and habitats (Strathmann, 1985). Therefore, developmental larval delays can have significant detrimental effects on survival to post-metamorphosis and juvenile growth (Pechenik, 1990; 2006) and, ultimately, affect population dynamics (Pechenik, 1999).

Cohort 4 responded differently in pre-settlement survival with respect to buffering than the other three cohorts, resulting in highest survival in the continuously unbuffered treatment (Figure 2.4 D). In 2015, an unprecedented harmful algal bloom (HAB) of diatoms, *Pseudo-nitzschia spp*., producers of neurotoxin domoic acid (DA), was detected along the West Coast of the US (Cavole et al., 2016; Du et al., 2016; McCabe et al., 2016; McKibben et al., 2017). One particularly severe peak coincided with the culture of Cohort 4 in early June 2015 (Du et al., 2016; Figure 4 in McCabe et al., 2016), coinciding with low embryo survival and arrested growth of later larval stages at WCH. The concentrations of particulate DA recorded during this HAB (~ 20,000 ng mL^{-1} in California (McCabe et al., 2016)) were 2–3 orders of magnitude higher than levels reported to cause impaired bivalve larval development, growth, survival and immune system functioning (De Rijcke et al., 2015; Liu et al., 2007). Various non-mutually exclusive mechanisms to trigger DA production and toxicity have been proposed (reviewed by

Lelong et al., 2012; Lewitus et al., 2012), including elevated production of DA with increasing pH (pH from 7.9 to 8.9; Lundholm et al., 2004; Trimborn et al., 2008; but see Sun et al. 2011) and greater availability of Fe in Fe-depleted acclimated cells (reviewed by Trainer et al., 2012). We hypothesize that the negative response to buffering observed in Cohort 4 could be associated with an increased production of DA in buffered water due to higher pH (mean $pH_{unbuffered}$ = 7.79 versus mean $pH_{buffered}$ = 8.15; Table 2.2), and with increased levels of Fe associated with the WCH-buffered water (Waldbusser, limited unpublished data), possibly due to impurities in the agricultural grade Na_2CO_3 used as buffering reagent. These observations suggest the need for better evaluation of the efficiency of routine buffering practices at commercial larval hatcheries during HABs. Importantly, if the increased pH due to buffering were to result in greater DA levels during HABS, this outcome would suggest a possible narrowing of effective ocean acidification mitigation strategies during HABs, which are predicted to increase in frequency and duration (McKibben et al., 2017). At least for early larval stages, current studies suggest that the development of buffering strategies that increase Ω_{Ar} while limiting changes in pH (Waldbusser et al., 2015a; 2015b; 2016) would be useful to mitigate OA effects on larval development without stimulating increases in DA production.

The ultimate objective of this study, however, was to present a framework to translate temporal variability of environmental carbonate chemistry into a physiological stress index. OASIS adequately predicted survival due to variable acidification exposure for two cohorts of Pacific oyster larvae in 2014 (Figure 2.6). Given the high Ω_{Ar} corresponding to exposure during embryogenesis for Cohorts 1 and 3, Bu and Uu values were equal. In the case of Cohort 2,

similar values for Bu and Ub are striking and suggest that the accumulated acidification stress only for the first 48 hours was as severe as the cumulative stress from day 2 to pre-settlement stage.

Comparing the correlations between survival and OASIS for both Cohort 1 and 2 reveals that the slopes of the regressions are very similar, but the intercepts are different (Figure 2.6). Although assessing the intercept of Cohort 1 requires caution, given that only two points were included in the regression, we hypothesize that the differences in intercept may be hinting at general fitness of the cohorts. Fundamentally, the intercept models survival in the absence of acidification stress (Bb). The smaller intercept for Cohort 1, which performed worse than the other three cohorts (Figure 2.4 and 2.5), might be another piece of evidence pointing towards overall lower cohort fitness possibly attributable to broodstock quality (Utting and Millican, 1997) or maternal lipid investment (Gallager and Mann, 1986). This observation suggests that besides predicting survival associated with exposure to variable acidified conditions, OASIS might be able to help identify differences in overall performance among cohorts exposed to similar variability in the natural environment, aiding in identifying particular strains and families with better resistance to acidification for genetic selection (de Melo et al., 2016).

An advantage of OASIS is that it offers a flexible parameterization that can easily incorporate multiple thresholds across larval stages, potential harmful effects associated with high rates of change in environmental conditions, and physiological recovery. For this study, we chose a conservative physiological stress threshold ($\Omega_{Ar} = 1.5$) already applied to other studies (Gruber et al., 2012; Ekstrom et al., 2015; Hales et al., 2017) and derived from hatchery

production observations (Barton et al. 2012) and laboratory experiments measuring early development and growth (Waldbusser et al., 2015a; 2015b). Survival, however, may be more sensitive to reduced Ω_{Ar} conditions, particularly in early larval stages, as evidenced by the contrasting responses observed with Ω_{Ar} values around 2.0.

Although we account for changes in sensitivity through a weighting function, OASIS currently assumes a constant stress threshold over the entire larval stage. A secondary threshold that would result in a certain level of cumulative sub-lethal stress when early larval exposure Ω_{Ar} is > 1.5 and < 4.0 might be needed, as evidenced by the reduced pre-settlement survival of Cohort 3 larvae exposed to Ω_{Ar} > 3.0 during the first 48 hours. More work is needed to assess if the results obtained with Cohort 3 are the result of a new secondary threshold for this larval stage. Multiple thresholds, however, could be incorporated to further refine stress exposures over the entire larval cycle, or to include the presence of multiple known or unknown stressors (for example, HABs in this study and Talmage and Gobler, 2012; hypoxia in Keppel et al., 2015, and Clark and Gobler, 2016).

Additional terms can also be added to OASIS to incorporate additional stress due to highly dynamic environmental conditions like those experienced by Cohort 3 at eight days post-fertilization when Ω_{Ar} decreased from 3.39 to 1.18 in less than 2 hours (Figure 2.5 C). Some organisms have already been found to be sensitive to rapidly changing conditions in laboratory experiments. For example, Kamenos et al. (2013) demonstrated that coralline algal structure is more sensitive to a rapid change of PCO_2 conditions than to the magnitude of the perturbation.

Finally, the potential for physiological recovery during times when carbonate chemistry is more favorable has not been adequately explored in the literature yet. Currently, OASIS only integrates stressful conditions; it is, therefore, a truncated integral. Similarly, we lack enough data to parameterize the potentially additive deleterious effect of persistent harmful conditions. As more data regarding physiological effects of variable carbonate exposure are collected, recovery thresholds and parameters to account for continuous unfavorable chemistry can be implemented in OASIS. At this stage in its development, the current parsimonious description of OASIS predicted survival in two of the three cohorts tested without adding more layers of complexity. The effectiveness of OASIS for the other two cohorts appears to be limited not by the approach but by the lack of OA stress in the first 48 hours for Cohort 3 and by an unprecedented HAB that appeared to overcome any OA effects, including the possibility of increased toxicity in the buffered conditions, for Cohort 4. Therefore, OASIS represents an encouraging advance towards the task of translating laboratory results into more meaningful metrics that accurately capture accumulated physiological stress due to organismal exposure to variable acidification conditions, but more work is needed to further validate its performance and better understand the role of multi-stressors.

We believe that OASIS, a re-interpretation of DD models, is a promising step towards understanding the effects of variable carbonate chemistry experienced by bivalve larvae in the field. More data regarding experimental exposure to fluctuating treatments are needed to better understand the underlying physiological mechanisms of sensitivity to variable carbonate chemistry and to reconcile conflicting published results (Frieder et al., 2014; Keppel et al., 2015;

Eriander et al., 2016; Clark and Gobler, 2016), but OASIS is a flexible framework that can continue to be refined to distill the increased complexity in responses and facilitate the prediction of outcomes (Helmuth et al., 2014; Boyd et al., 2016). Multiple strategies should be pursued simultaneously: continued monitoring efforts to characterize and analyze environmental conditions in temporal and spatial scales relevant to organisms (Helmuth et al., 2010; Dillon and Woods, 2016); development and validation of mechanistic models that incorporate physiological sensitivity into biological performance (this study; Kearney and Porter, 2009; Helmuth et al., 2014; Bozinovic and Pörtner, 2015); and integration of these models into local, regional and global climate models to assess the future of populations and their distributions (Buckley et al., 2011).

2.6 Conclusions

Although a growing body of experimental work has advanced our understanding of the effects of ocean acidification on marine bivalves, key vulnerable taxa, important questions remain regarding the effects of highly variable carbonate chemistry commonly found in bivalve habitats on larval stages and the effectiveness of buffering mitigation strategies in current use and the effects on larval stages of highly variable carbonate chemistry commonly found in their habitats within commercial larval hatcheries. Our work supports the benefits of buffering seawater, particularly during embryogenesis and the formation of the prodissoconch I shell, on overall larval survival. Increasing coverage of high frequency monitoring of carbonate chemistry is demonstrating that carbonate chemistry is dynamic in coastal environments. Translating those

variable data into reasonable approximations of success for sensitive species and taxa is important for predicting OA effects on populations and communities. To help translate the effects of dynamic acidification conditions on bivalve larvae survival, we propose a new quantitative framework, the ocean acidification stress index for shellfish (OASIS), based on a conservative threshold derived from past observations that accounted for differential sensitivity across the larval stage. OASIS predicted survival for two of the three larval cohorts exposed to different carbonate chemistry regimes, thus representing an important step towards distilling physiological responses to complex carbonate chemistry conditions into synthetic metrics useful to industry managers and policy-makers as predictive tools.

Acknowledgements

The authors thank the Whiskey Creek Hatchery personnel for providing space, broodstock, and countless support in conducting the work within the hatchery. Particularly, the authors would like to thank Sue Cudd, Mark Wiegardt, and Alan Barton from WCH for their support, encouragement and professional experience. This work was supported by Oregon Sea Grant grant #NA10OAR4170059 awarded to Dr. George G. Waldbusser, Dr. Burke Hales, and Dr. Chris J. Langdon.

Table 2.1. Description of experimental treatments and their nomenclature.

Treatment during first 48 h post-fertilization	Treatment after first 48 h post-fertilization	Nomenclature
Static, buffered (B)	Flow-through, stable buffered (b)	Bb
Static, buffered (B)	Flow-through, naturally variable unbuffered (u)	Bu
Static, unbuffered (U)	Flow-through, stable buffered (b)	Ub
Static, unbuffered (U)	Flow-through, naturally variable unbuffered (u)	Uu

Table 2.2. Mean experimental conditions in the culture chambers assessed from discrete seawater samples. Values are standard deviations and represent environmental variability, not measurement uncertainty.

Cohort	Treatment	N	T (°C)	S	Alkalinity (µeq kg^{-1})	TCO_2 (µmol kg^{-1})	PCO_2 (µatm)	HCO_3^- (µmol kg^{-1})	CO_3^{2-} (µmol kg^{-1})	pH_t	Ω_{Ca}	Ω_{Ar}
1	Buffered	24	24.1 ± 0.6	33.1 ± 0.6	2792 ± 209	2435 ± 121	609 ± 732	2143 ± 113	274 ± 87	8.07 ± 0.27	6.49 ± 2.06	4.32 ± 1.37
	Unbuffered	26	24.2 ± 0.5	33.0 ± 0.6	2228 ± 87	2142 ± 100	1445 ± 849	2011 ± 106	88 ± 43	7.60 ± 0.23	2.08 ± 1.05	1.38 ± 0.68
2	Buffered	16	23.5 ± 0.8	33.0 ± 0.4	2907 ± 94	2492 ± 68	368 ± 111	2167 ± 84	314 ± 51	8.17 ± 0.09	7.44 ± 1.22	4.95 ± 0.81
	Unbuffered	13	24.3 ± 0.5	33.3 ± 0.4	2234 ± 25	2169 ± 50	1520 ± 497	2051 ± 57	74 ± 23	7.54 ± 0.14	1.75 ± 0.54	1.18 ± 0.36
3	Buffered	18	24.4 ± 0.7	32.6 ± 1.0	2782 ± 256	2388 ± 235	527 ± 843	2074 ± 226	298 ± 81	8.14 ± 0.24	7.10 ± 1.91	4.73 ± 1.27
	Unbuffered	18	24.4 ± 0.9	32.5 ± 0.9	2280 ± 136	2131 ± 213	1288 ± 1833	1965 ± 217	128 ± 68	7.76 ± 0.32	3.06 ± 1.62	2.14 ± 1.01
4	Buffered	16	24.3 ± 0.8	33.7 ± 0.7	2909 ± 225	2490 ± 205	396 ± 177	2164 ± 202	315 ± 63	8.15 ± 0.12	7.43 ± 1.52	4.95± 1.01
	Unbuffered	16	24.9 ± 0.9	33.5 ± 0.5	2378 ± 192	2208 ± 191	882 ± 365	2047 ± 191	135 ± 45	7.79 ± 0.16	3.20 ± 1.06	2.13 ± 0.71

Table 2.3. Summary of mean environmental conditions by cohort and treatment in the culture chambers with larval survival responses. Mean values for Ω_{Ar} (with range, to indicate variability); mean values for PCO_2 in µatm (with range, to indicate variability). Mean % survival ± standard error (SE).

Cohort	Mean environmental conditions 0–48 h		Mean environmental conditions 0 h–pre-settlement				Survival 0–48 h (%)		Survival to pre-settlement (%)				Larval period (days)
	B	U	Bb	Bu	Ub	Uu	B	U	Bb	Bu	Ub	Uu	
1	Ω_{Ar} = 4.93 (4.78–5.08) PCO_2 = 325 (309–342)	Ω_{Ar} = 2.25 (2.20–2.31) PCO_2 = 636 (620–651)	Ω_{Ar} = 4.32 (0.65–5.41) PCO_2 = 609 (300–3044)	Ω_{Ar} = 1.55 (0.45–5.08) PCO_2 =1421 (309–4154)	Ω_{Ar} = 4.06 (0.65–5.41) PCO_2 = 649 (300–3044)	Ω_{Ar} = 1.38 (0.45–3.30) PCO_2 = 1444 (458–4154)	88.6 ± 7.8	7.6 ± 8.6	5.4 ± 5.4	1.6 ± 0.6	0.0 ± 0.0	0.0 ± 0.0	22
2	Ω_{Ar} = 5.40 (5.36–5.43) PCO_2 = 343 (330–356)	Ω_{Ar} = 1.34 (1.00–1.67) PCO_2 = 1293 (919–1667)	Ω_{Ar} = 4.95 (2.80–5.69) PCO_2 = 368 (296–671)	Ω_{Ar} = 1.74 (0.75–5.43) PCO_2 =1433 (330–2194)	Ω_{Ar} = 4.50 (1.00–5.69) PCO_2 = 477 (296–1667)	Ω_{Ar} = 1.18 (0.75–1.71) PCO_2 = 1439 (378–2194)	53.7 ± 4.4	38.5 ± 13.5	12.9 ± 1.9	8.1 ± 3.1	8.1 ± 2.2	5.5 ± 5.5	17

Table 2.3. Continued.

Cohort	Mean environmental conditions 0–48 h		Mean environmental conditions 0 h–pre-settlement				Survival 0–48 h (%)		Survival to pre-settlement (%)				Larval period (days)
	B	U	Bb	Bu	Ub	Uu	B	U	Bb	Bu	Ub	Uu	
3	Ω_{Ar} = 4.92 (4.34–5.22) PCO_2 = 285 (239–337)	Ω_{Ar} = 3.22 (3.04–3.41) PCO_2 = 352 (305–400)	Ω_{Ar} = 4.73 (3.70–6.15) PCO_2= 527 (239–490)	Ω_{Ar} = 2.32 (0.99–5.19) PCO_2= 885 (239–1879)	Ω_{Ar} = 4.77 (3.04–6.15) PCO_2 = 342 (271–490)	Ω_{Ar} = 2.14 (0.99–4.29) PCO_2 = 1288 (305–1879)	79.3 ± 6.1	81.5 ± 7.5	11.1 ± 7.8	18.6 ± 2.0	1.2 ± 0.9	1.9 ± 1.7	16
4	Ω_{Ar} = 5.96 (5.84–6.07) PCO_2 = 316 (307–324)	Ω_{Ar} = 1.87 (1.67–2.08) PCO_2 = 837 (728–945)	Ω_{Ar} = 4.95 (2.77–6.26) PCO_2 = 396 (260–858)	Ω_{Ar} = 2.73 (1.27–6.07) PCO_2 = 792 (307–1769)	Ω_{Ar} = 4.43 (1.67–6.26) PCO_2 = 461 (260–945)	Ω_{Ar} = 2.13 (1.27–3.26) PCO_2 = 882 (382–1769)	96.0 ± 6.9	85.5 ± 15.3	3.4 ± 0.3	2.6 ± 2.6	1.9 ± 1.4	12.0 ± 2.6	16

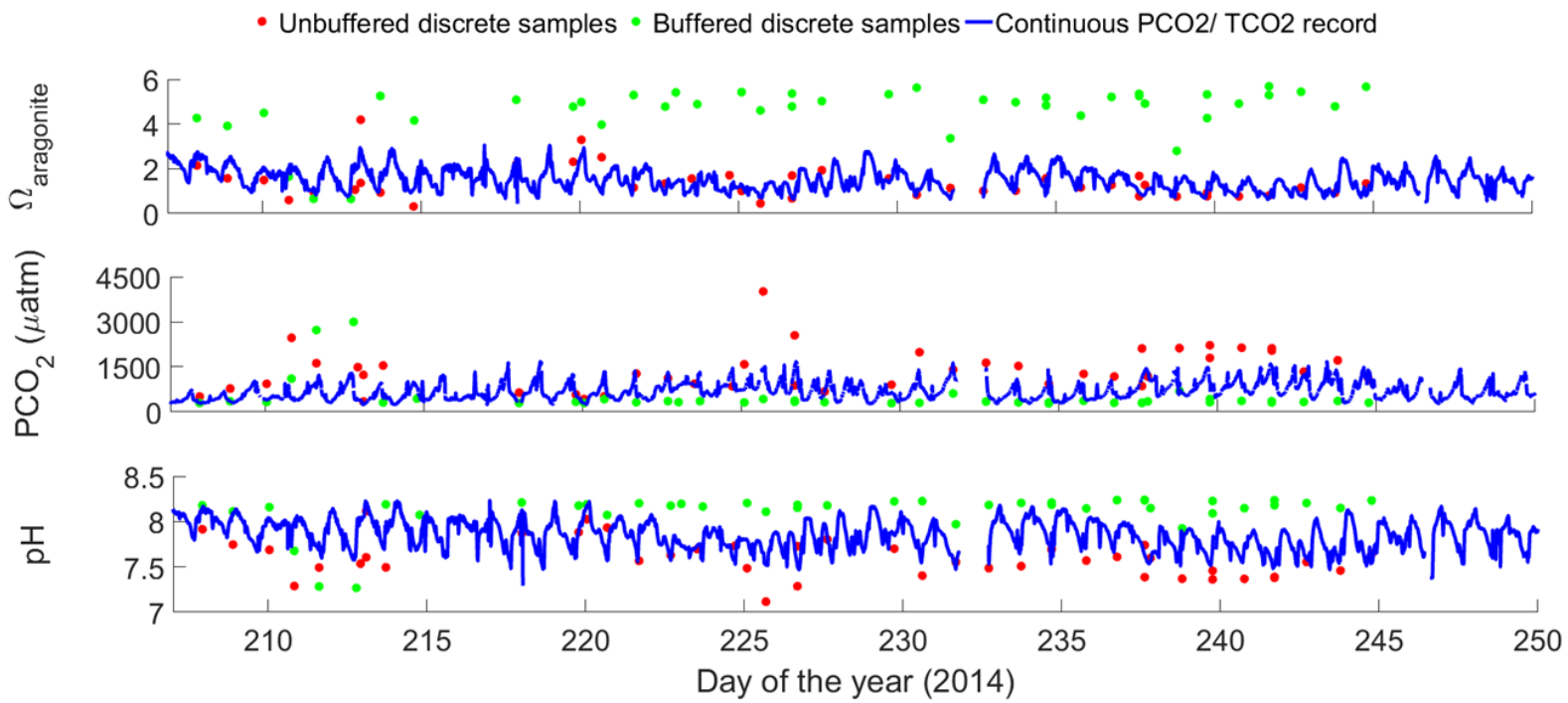

Figure 2.1. Time series of Netarts Bay carbonate chemistry during Cohort 1 and 2 experiments in 2014.
In blue, high-frequency, high-resolution monitoring data collected immediately after Whiskey Creek Hatchery seawater intake. Top panel represents Ω_{Ar}; middle panel, PCO_2; and bottom panel, pH. Red dots are discrete seawater samples from randomly selected unbuffered culture chambers; green dots, discrete seawater samples from randomly selected buffered culture chambers. The few buffered samples that have unusually low Ω_{Ar} and pH and high PCO_2 could be the result of sample mishandling or a transient failure of the buffering system.

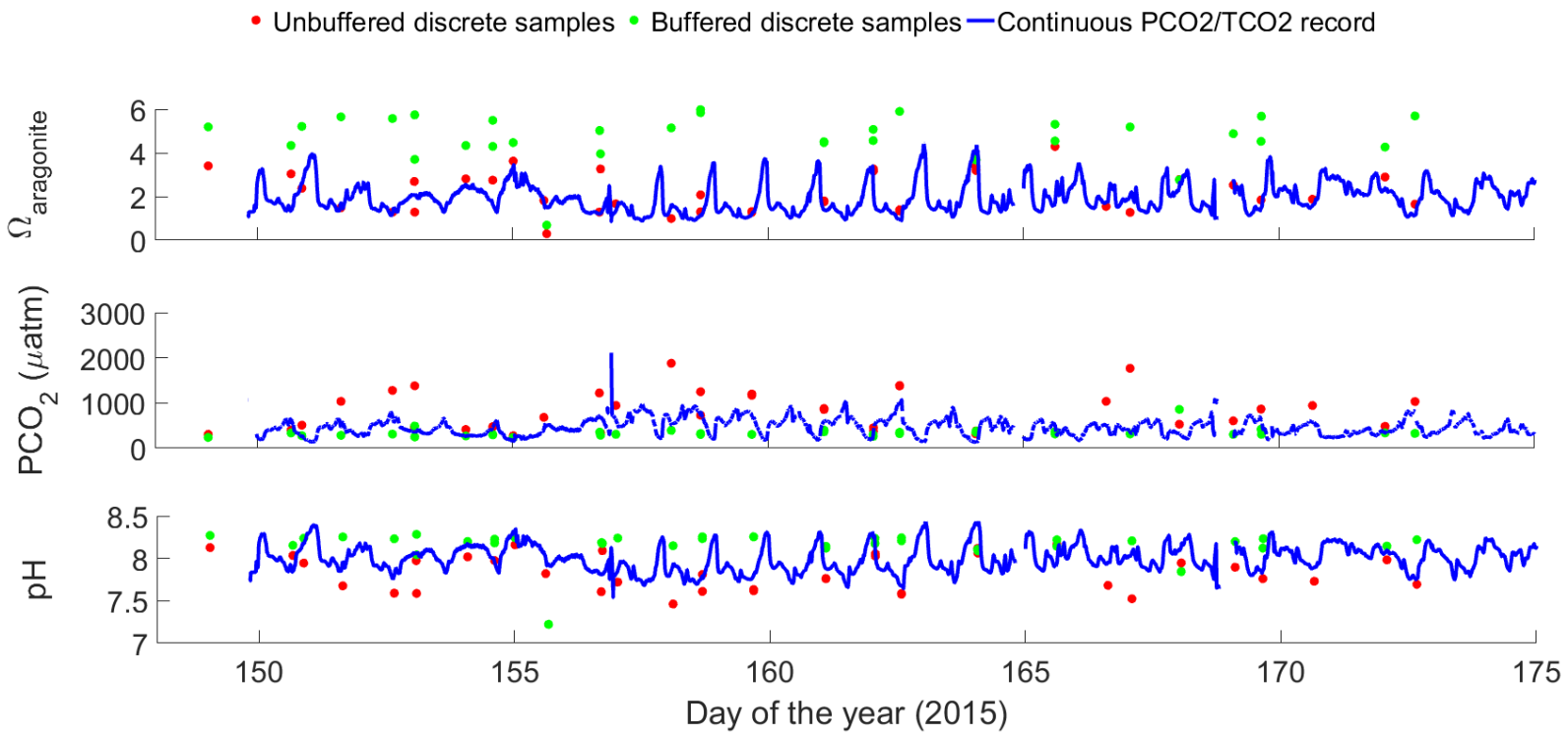

Figure 2.2. Time series of Netarts Bay carbonate chemistry during Cohort 3 and 4 experiments in 2015.
Blue lines indicate high-frequency, high-resolution monitoring data collected immediately after Whiskey Creek Hatchery seawater intake. Top panel represents Ω_{Ar}; middle panel, PCO_2; and bottom panel, pH. Red dots represent discrete seawater samples from unbuffered, randomly selected culture chambers; green dots represent discrete seawater samples from buffered, randomly selected culture chambers. The few buffered samples that have unusually low Ω_{Ar} and pH and high PCO_2 could be the result of sample mishandling or a transient failure of the buffering system.

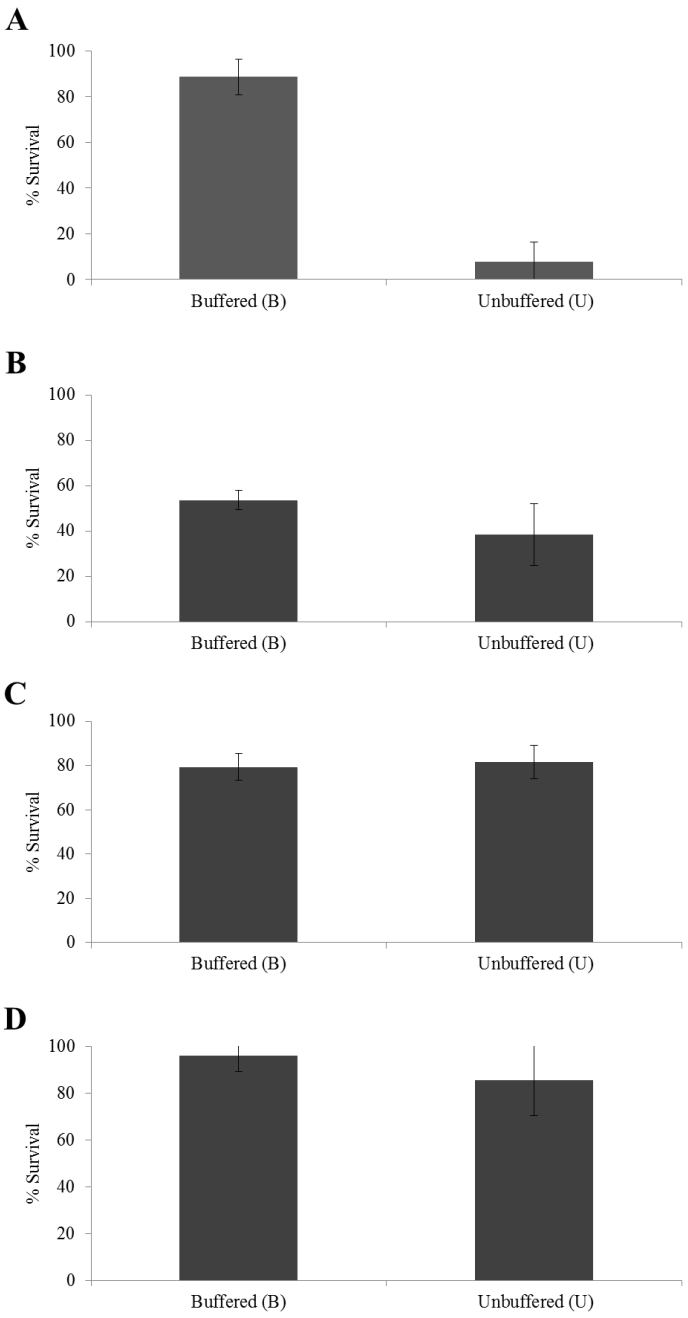

Figure 2.3. Larval survival at 48 hours post-fertilization for all cohorts.
Percent survival 48 hours post-fertilization for buffered (B) and unbuffered (U) culture treatments for A) Cohort 1; B) Cohort 2; C) Cohort 3; and D) Cohort 4. Error bars indicate standard error.

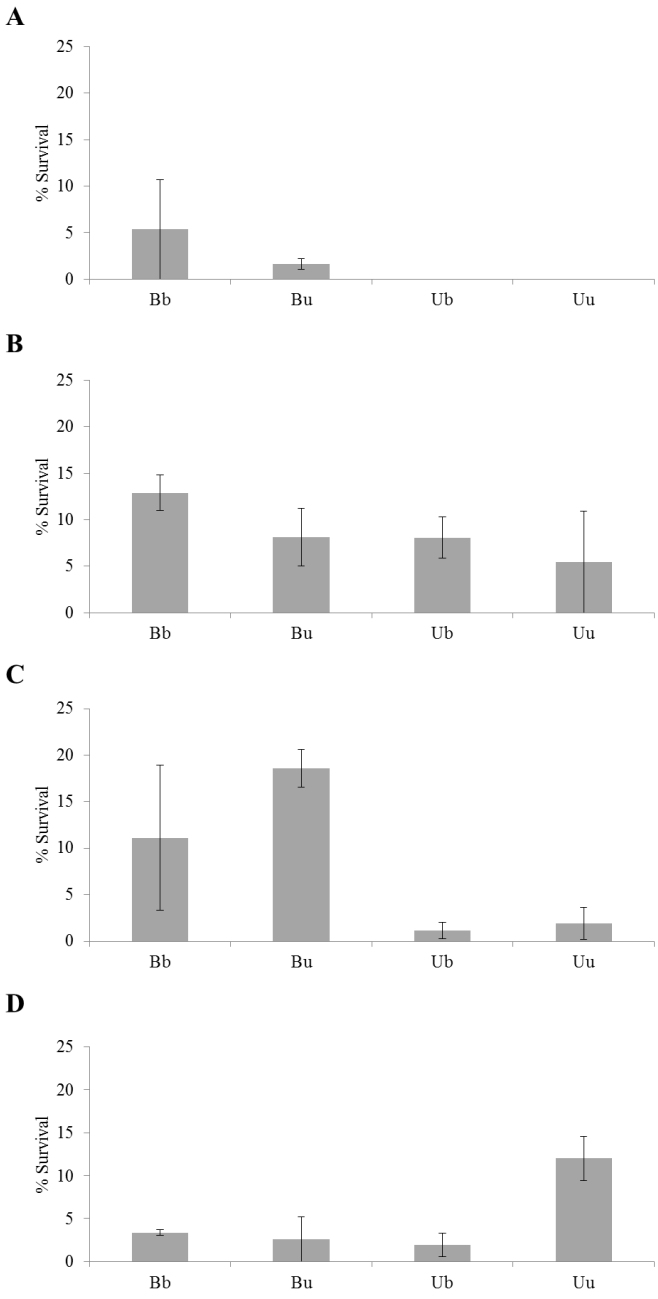

Figure 2.4. Larval survival at pre-settlement for all cohorts.
Percent survival pre-settlement for A) Cohort 1; B) Cohort 2; C) Cohort 3; and D) Cohort 4. Pre-settlement occurred at different days post-fertilization for the different cohorts: day 22 post-fertilization for Cohort 1, Day 17 post-fertilization for Cohort 2, and day 16 post-fertilization for both Cohorts 3 and 4. Error bars indicate standard error.

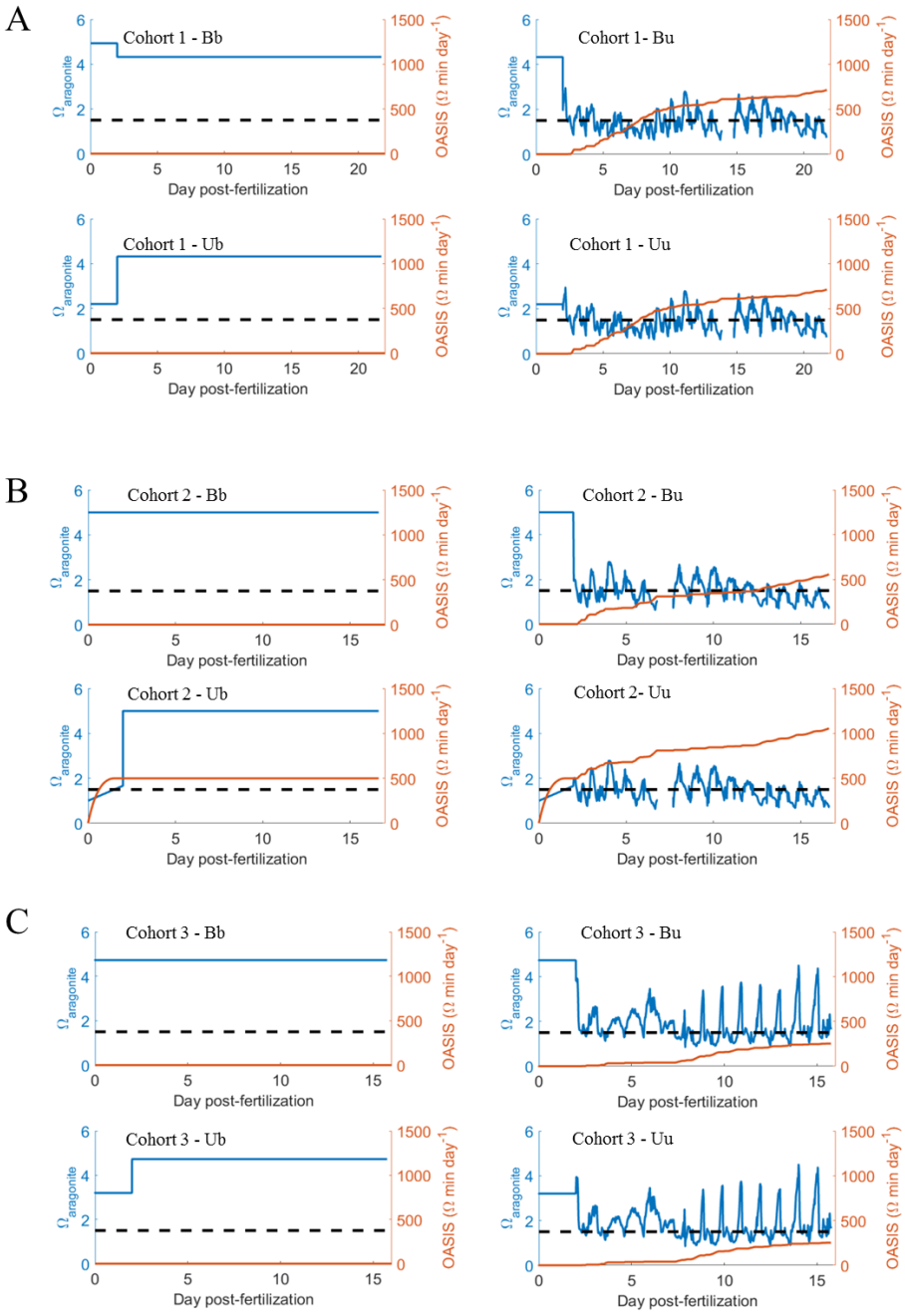

Figure 2.5. Time series of Ω_{Ar} values and OASIS index for Cohorts 1, 2 and 3. Results from all four treatments (Bb, Bu, Ub, Uu) are shown for A) Cohort 1, B) Cohort 2, and C) Cohort 3. Blue lines indicate Ω_{Ar} values; light red lines, cumulative OASIS values; and dashed black lines, the Ω_{Ar} stress threshold chosen for the computation of OASIS.

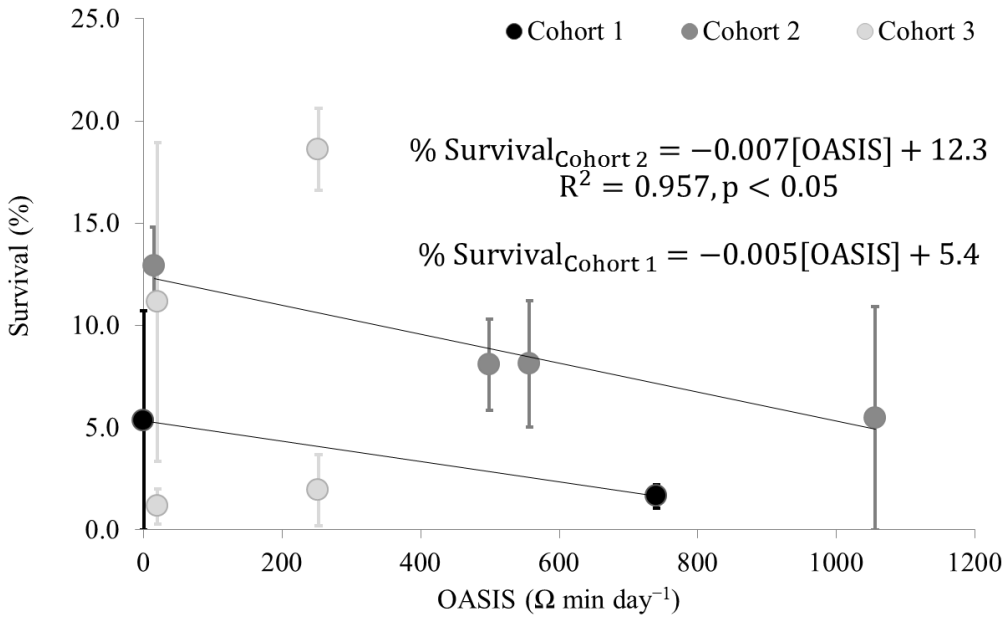

Figure 2.6. Percent survival predicted by OASIS for Cohorts 1, 2 and 3.
Black circles indicate Cohort 1; dark grey, Cohort 2; and light grey, Cohort 3. Cohort 2 and 3 data points associated with OASIS value of zero have been slightly offset to improve visual clarity and avoid data overlap. For Cohort 1, only the results of Bb and Uu treatments are included in the relationship due to concerns about the validity of an integrated stress measure to predict pre-settlement survival when the treatment caused 100% mortality earlier than day 7 post-fertilization. Linear models were fit to the data for Cohorts 1 and 2; in the resulting equation for Cohort 2, R^2 corresponds to the coefficient of determination, and the p-value to Pearson's coefficient of correlation. Error bars indicate standard error.

The Dynamic Ocean Acidification Manipulation Experimental System (DOAMES): Separating carbonate variables and simulating natural variability in laboratory flow-through experiments.

Iria Gimenez, George G. Waldbusser, Chris J. Langdon, Burke R. Hales

Accepted for publication in Limnology and Oceanography: Methods
5400 Bosque Blvd., Suite 680
Waco, TX 76710

3. CHAPTER III.- The Dynamic Ocean Acidification Manipulation Experimental System (DOAMES): Separating carbonate variables and simulating natural variability in laboratory flow-through experiments.

3.1 Abstract

Carbonate chemistry variables such as PCO_2, pH and mineral saturation state (Ω) are commonly thought of as co-varying in open-ocean settings, but have decoupled over geologic time-scales and among modern dynamic coastal margins and estuaries. Predicting responses of vulnerable coastal organisms to past, present and future ocean acidification (OA) scenarios requires the empirical identification of organismal sensitivity thresholds to individual carbonate chemistry parameters. Conversely, most OA experiments involve chemistry manipulations that result in co-variance of carbonate system variables. We developed the Dynamic Ocean Acidification Manipulation Experimental System (DOAMES)- a feed-forward, flow-through carbonate chemistry control system capable of decoupling PCO_2, pH or Ω by independently manipulating total alkalinity (TAlk) and total inorganic carbon (TCO_2). DOAMES proof-of-concept can manipulate source seawater with stable or variable carbonate chemistry, and produce experimental treatments with constant and dynamic carbonate chemistry regimes. The combination of dynamic input and output allows for off-set treatments that impose a ΔPCO_2 on naturally variable conditions. After overcoming several operational challenges, DOAMES is capable of simultaneously generating three different experimental treatments within 1% ± 1% of TCO_2 and TAlk targets. The achieved precision and accuracy resulted in the successful

decoupling of pH and Ω_{Ar} in five trials. We tested the viability of sensitive bivalve embryos raised in DOAMES-manipulated seawater and found no difference in development when compared to the control, demonstrating DOAMES suitability for organismal studies. DOAMES provides a novel tool to evaluate organismal effects of exposure to decoupled carbonate system variables and to past, current and future carbonate chemistry scenarios.

3.2 Introduction

The uptake of atmospheric anthropogenic CO_2 by ocean surface waters has caused ocean acidification (OA) (Caldeira and Wickett 2003; Doney et al. 2009); a collective shift in marine carbonate chemistry that results in increased PCO_2 and reduced pH and calcium carbonate saturation state (Ω) (Feely 2004; Hönisch et al. 2012). OA is the consequence of the rapid increase in PCO_2 that cannot be compensated for by weathering of continental rocks or dissolution of marine carbonates (Zeebe 2012; Hönisch et al. 2012). In contrast, geologic periods when the CO_2 release to the atmosphere was significantly slower than today such as the Miocene, Oligocene, and Cretaceous, were associated with long-term decoupling of PCO_2, pH and Ω due to the ability of Earth's system to partially buffer the rise in CO_2 (Zeebe 2012; Hönisch et al. 2012).

Instances of decoupling do occur in the modern ocean over daily and monthly time-scales and result from the interaction of myriad physical and biological processes that alter carbonate chemistry (Fassbender et al. 2016). Decoupling, however, is more common on dynamic margins and coastal systems. For instance, in open ocean oligotrophic regions, where temperature and

salinity, and thus alkalinity, do not vary significantly, net community production (NCP), air-sea gas exchange, and mixing dominate daily and seasonal changes in PCO_2. Consequently, PCO_2 is generally tightly negatively correlated to pH and Ω, while pH and Ω are generally tightly positively correlated to each other (Dore et al. 2009; Bates et al. 2012, 2014), although moderate seasonal and intra-regional decoupling occurs due to differential thermal and salinity sensitivity (Takahashi et al. 2014). Conversely, in dynamic coastal environments and estuaries, temperature and salinity vary significantly across daily and seasonal timescales, and numerous physical and biological processes affect carbonate chemistry, including freshwater inputs, tides and regional circulation, seasonal upwelling, and diel cycles of photosynthesis and respiration, and calcification and dissolution (Waldbusser et al. 2011; Fassbender et al. 2016; Hales et al. 2017; Pacella et al. 2018), all of which alter TCO2 and TAlk to different extents. As a result, instances of decoupling of PCO_2, pH and Ω occur in daily, fortnightly and seasonal timescales (Cai et al. 2011; Waldbusser and Salisbury 2014; Evans et al. 2015; Hales et al. 2017). The differential decoupling of carbonate system variables today versus in the geologic past and the complex carbonate chemistry dynamics in coastal and estuarine systems have broad implications for understanding species responses to OA in an evolutionary context, as well as how we design experiments to better predict future changes in marine communities.

Most OA experiments to date rely on injection or bubbling of CO_2 gas as the mechanism to generate carbonate chemistry treatments (see reviews by Kroeker et al. 2010; Cornwall and Hurd 2015) . CO_2 bubbling typically generates tightly controlled experimental conditions that closely mimic changes in marine carbonate systems associated with the very rapid anthropogenic

perturbation of atmospheric CO_2. Thus, this approach was codified after the publication of the "Guide to best practices for OA research and data reporting" guidelines (Gattuso et al. 2010). Experiments based on CO_2 bubbling, therefore, have been crucial in documenting the adverse physiological effects associated with OA across multiple taxa and life-stages (reviewed in (Kroeker et al. 2010, 2013; Wittmann and Pörtner 2013). While mimicking the current global changes in marine carbonate chemistry, this manipulation technique, however, results in the co-variance of PCO_2, pH, and Ω, and thus leads to equivocal experimental interpretations as the true driver of response is difficult to empirically isolate. Similarly, field observations across naturally co-varying acidification gradients (e.g., Cigliano et al. 2010; Kroeker et al. 2011) provide valuable insight but often lack the power to discriminate physiological mechanisms underlying responses (i.e., Waldbusser et al. 2015a, b). Thus, the interpretation of physiological responses to OA is confounded, due to the inability to attribute which variable is causing the observed effects, therefore precluding a mechanistic understanding of the drivers of organismal sensitivity. Hence, carbonate chemistry manipulation techniques that empirically de-couple PCO_2, pH and Ω are essential.

Short-term physiological responses to different carbonate system variables have been explored by the development of batch-culture manipulation laboratory techniques specifically designed to decouple carbonate chemistry parameters. For instance, techniques based on altering total inorganic Carbon (TCO_2) and/or Total Alkalinity (TAlk) have been used to study biocalcification in corals, bivalve larvae and coccolithophores (Schneider and Erez 2006; Jury et al. 2010; Gazeau et al. 2011; Bach et al. 2013; Waldbusser et al. 2015a; b; Thomsen et al. 2015a;

Comeau et al. 2017). In these experiments, biocalcification was largely insensitive to pH and PCO_2, but controlled by Ω_{Ar} (Waldbusser et al. 2015a; b), [CO_3^{2-}] (Gazeau et al. 2011), or [HCO_3^-/H^+] (Jokiel 2013; Bach et al. 2013; Thomsen et al. 2015a), although combinations of multiple variables have also been invoked (e.g. Bach et al. 2013; Comeau et al. 2017). Conversely, respiration on early-larval mussels is negatively impacted by low pH (Waldbusser et al. 2015b), while feeding responses in early bivalve larvae appear to be driven by PCO_2 or Ω_{Ar} (Waldbusser et al. 2015b, Gray et al. 2017). The diversity of carbonate chemistry drivers of short-term physiological responses warrants further exploration to elucidate modes of action of long-term exposure to acidified conditions and, ultimately, mechanisms of sensitivity to improve our predictions of OA long-term effects in organisms.

Long-term exposure experiments, crucial to investigate multi-generational and chronic or sub-lethal physiological effects of ocean acidification, require different experimental approaches. While batch-culture experimental techniques have provided very valuable insight, they are less suitable for long-term exposure experiments, can result in “bottle effects” on carbonate chemistry and limit approaches designed to assess organismal responses to dynamic chemistry conditions (e.g., Frieder et al. 2014; Clark and Gobler 2016). Long-term exposure experiments that utilize destructive sampling generally require higher density of organisms and, therefore, benefit from flow-through culture systems that prevent targeted carbonate chemistry conditions from deviations resulting from in situ respiration and photosynthesis (e.g., Rost et al. 2008; Gradoville et al. 2014) and reduce the accumulation of metabolic waste products. Furthermore, flow-through experimental designs allow for the simulation of variable carbonate chemistry

conditions often experienced by organisms in the coastal environment, a research priority identified by the OA community (Takeshita et al. 2015; Wahl et al. 2016; Boyd et al. 2016).

In order to bridge the insight to be gained from experiments that decouple carbonate chemistry variables and the need for flow-through systems allowing for longer-term experiments, we: 1) adapted the short-term, batch-culture techniques developed in Waldbusser et al. 2015a,b and Waldbusser et al. 2016 (see also Schneider and Erez 2006; Jury et al. 2010; Keul et al. 2013), into the Dynamic Ocean Acidification Manipulation Experimental System (DOAMES) - a feed-forward, flow-through carbonate chemistry control system capable of long-term, automatic decoupling of carbonate chemistry parameters (i.e. pH and Ω_{Ar}) by performing precise manipulations of TAlk and TCO_2; 2) evaluated DOAMES performance with variable and stable source seawater inputs and with dynamic and off-set carbonate chemistry targets; and 3) performed a proof-of-concept validation of DOAMES by exposing sensitive early stages of bivalve larvae to highly acidified seawater that DOAMES manipulated back to favorable conditions.

3.3 Materials and procedures

3.3.1 Experimental system overview

DOAMES independently and automatically manipulates TAlk and TCO_2, the master variables of the carbonate system, in two stages: 1) real-time measurement of source seawater PCO_2 and TCO_2 through a continuous Non-Dispersive Infrared (NDIR)-based analyzer and

computation of all carbonate chemistry variables; and 2) a feed-forward control system to achieve user-defined targets of TAlk and TCO_2 via high-precision mineral acid-base additions to the source seawater (Figure 3.1).

3.3.1.1 Description of DOAMES Hardware: NDIR-based continuous PCO_2 and TCO_2 analyzer

The PCO_2 and TCO_2 analyzer measures inlet water chemistry by temporally alternating the analysis of PCO_2 and TCO_2, and is based on published designs of high-frequency, continuous PCO_2 and TCO_2 systems (Hales et al. 2004; Bandstra et al. 2006; Vance 2012). In this application (described further below), it was necessary to recirculate water between the holding tank and the experimental apparatus, and so a microporous hydrophobic membrane contactor (3M™ Liqui-Cel™ EXF-2.5x8 Series Membrane Contactor, Liqui-Cel) was used for PCO_2 equilibration (following Hales et al., 2004; Bandstra et al., 2006) rather than a gravity-draining showerhead-style equilibrator. Briefly, filtered (1-10 µm, nominally) seawater was routed through a thermosalinograph (SBE 45 MicroTSG, Sea-Bird Scientific) to measure salinity and temperature at a flow rate of 2-6 L min^{-1}. Flow subsequently entered the LiquiCel unit, where rapid gas transfer between the recirculated gas analytical stream and the water stream ensured efficient gas-phase equilibration of the gas stream with the water PCO_2. The equilibrated gas-stream is then routed through an NDIR absorbance CO_2 detector (LI-840A, LI-COR) for analysis. In parallel with this flow regime, a split of sample water is drawn from the main sample flow (one to 4 times per hour for three minutes at a time) at a flow rate of 20 mL min^{-1} and acidified with 10% HCl to convert all carbonate and bicarbonate to $CO_{2,aq}$. This aqueous CO_2 is

then stripped from solution using a 900 mL min^{-1} flow of CO_2-free gas in a smaller membrane contactor (3M™ Liqui-Cel™ MM-1.0x5.5 Series Membrane Contactor, Liqui-Cel). The mass-balance-determined CO_2 content of this strip-gas stream is subsequently determined by the NDIR CO_2 detector. Temperature, salinity, and gas stream CO_2 content measurements were made at 1 Hz, and the response times of the PCO_2 and TCO_2 measurements are estimated at 5 and 15 sec, respectively, as shown in Hales et al., 2004, and Bandstra et al., 2006.

Every 6 hours automatically, or at any user-defined interval, the NDIR detector is calibrated using 2 or more certified gas standards (CO_2 in Ultrapure AirTM, Scott-Marrin). Similarly, 3 or more liquid TCO_2 standards are also analyzed to calibrate the TCO_2 measurements across the expected measurement range. Finally, upon user-input, the analyzer can be used to measure PCO_2 and TCO_2 in discrete samples by temporarily pausing continuous measurements and utilizing the sample-equilibrator mode. In discrete mode, we measured PCO_2 by equilibrating the sample headspace gas and bypassing the membrane contactor, and TCO_2 by analyzing the discrete sample instead of the seawater streamflow.

These measurements and calibrations are used to continuously and automatically calculate the remaining parameters of the carbonate system following water dissociation constants from (Millero 1995), carbonic acid equilibration constants from Millero (2010), Dickson (1990) constants for boric acid and calcite and aragonite solubility constants from Mucci (1983). The DOAMES carbonate chemistry manipulation software (detailed below) then incorporates all the calculated data.

The PCO_2/TCO_2 software, based in LabVIEW™ (National Instruments, NI, version 2012), integrates communication and automatic control of all pumps, mass flow controllers, sensors and data acquisition boards through a user-friendly control panel (Figure 3.2). Additionally, we designed the software to automatically log data and metadata, as well as process, compute and visualize preliminary data. A version of this continuous PCO_2/TCO_2 analyzer is commercially available under the brand name Burke-O-Lator (Dakunalytics, LLC).

3.3.1.2 Description of DOAMES Hardware: Feed-forward TCO_2 and TAlk manipulation system

The carbonate chemistry manipulation component of DOAMES coordinates the delivery of seawater and reagents necessary to produce the desired experimental treatments. Following DOAMES experimental system diagram (Figure 3.3, blue box), source seawater is routed from the outlet of the membrane contactor through in-line heaters (Heater for External Canister Filters, Hydor) and heated to the targeted experimental temperature. Subsequently, one metering, positive displacement pump (FMI QV, Fluid Metering Inc.) coupled with a variable flow pump head (RH1, Fluid Metering Inc.) delivers heated seawater for each manipulation channel (i.e., experimental treatment). A variable speed controller (V300, Fluid Metering Inc.), set via an analog voltage signal, drives the pump. We gravimetrically calibrated each combination of controller and pumps to obtain a voltage-flow linear relationship. The minimum and maximum flows tested were 73 mL min^{-1} and 113 mL min^{-1} for each treatment, which corresponded to 50% and 70% of the maximum voltage signal, respectively.

Each manipulation channel consists of two pairs of variable flow, programmable syringe pumps (NE-100, New Era Pump Systems Inc.): 1) one pair delivers the mineral acid reagent: 0.1 N HCl, gravimetrically diluted from certified 1.0N HCl (5620-07, J.T. Baker, or BDH7202-7, BDH VWR Chemicals); and 2) one pair delivers the mineral base reagent: a concentrated solution of reagent-grade Na_2CO_3 (7527-06, Macron Fine Chemicals) and $NaHCO_3$ (7412-06, Macron Fine Chemicals) in deionized water with the Na_2CO_3:$NaHCO_3$ ratio targeted to produce approximately ambient atmospheric pCO_2 values so that the effects of gas-exchange were minimized during preparation and transfer to gas-impermeable bottles. All syringe pumps are fitted with gravimetrically calibrated 60 mL luer-lock polypropylene syringes (309653, BD Medical) to ensure volumetric dispensing accuracy. Each pair of reagent pumps connects to a four-port, two-position switch valve (C22, Valco Instruments Company Inc.). One port is plumbed to the reagent reservoir, two ports are linked to each of the paired syringes, and the fourth port connects to the reagent outflow. The valve's position determines two flow paths: 1) reservoir to the filling syringe, and 2) injecting syringe to outflow (Figure 3.4). An electric actuator controls the switch between flow paths, interfacing with the manipulation software to synchronize refilling-injection routines and ensure constant delivery of reagent.

Both reagent outflows are combined in a mixing coil prior to their injection into each manipulation channel to avoid mineral precipitation observed in earlier versions, a result of the direct addition of a strong base to seawater. The injection point is located immediately downstream from the seawater metering pumps and consists of an in-line T-fitting with an

associated one-way polypropylene or styrene-acrylonitrile check-valve (PP695-2B2BF HAST, Pneuline Supply Inc.; or EW-30505-92, Cole-Parmer) to prevent seawater back-flow.

3.3.1.3 Description of DOAMES: Manipulation Software

DOAMES' controlling software integrates the calculation of target reagent flows based on source seawater carbonate chemistry and the automatic control of DOAMES' hardware components (Figure 3.3, orange box). A stand-alone program developed using LabVIEW™ controls each manipulation channel, thereby providing a level of architectural redundancy that prevents the stop of all manipulation channels in the event of a single pump communication failure. Before initialization of the program, the user manually sets the experimental targets for both TAlk and TCO_2 (based on desired targets of Ω, pH and/or PCO_2), the flow rate of the seawater-delivery pump for each manipulation channel, base reagent (TAlk and TCO_2) and acid reagent concentrations, and the target temperature for the experimental treatments. All of these experimental parameters are entered in the front-screen of the controlling software (Figure 3.5) and can be modified at any time. Although DOAMES does not control any of these experimental parameters, they are incorporated in the calculations to determine reagent flow rates.

Upon initialization, the software reads real-time-processed data from the TCO_2/PCO_2 analyzer at a frequency of 1Hz and updates source-seawater measurements of temperature, salinity, PCO_2, TCO_2 and calculated TAlk values. These data, along with the experimental parameters defined by the user discussed above, are then used to compute reagent flow rates automatically. Flow rates of reagents depend on the desired targets of TAlk and TCO_2 and the

initial carbonate chemistry values of the source seawater but generally range between one and five percent of the total seawater flow rates.

A subroutine then communicates with each pair of syringe pumps, updates the injecting flow rates and the volume dispensed by injecting syringes, determines the refilling flow rate on the refilling syringes, and controls switching of both reagent valves. Additionally, the software automatically performs data logging of all relevant input and calculated data.

3.3.2 Laboratory tests-

We evaluated the performance of DOAMES in eight trials conducted between 2015 and 2017 at the Hatfield Marine Science Center (HMSC), Newport, OR (Table 3.1). In these trials, we assessed DOAMES capability to decouple pH and Ω_{Ar}, as well as to manipulate a dynamic source of seawater and simultaneously produce stable, dynamic and off-set experimental treatments.

3.3.2.1 Modes of carbonate chemistry manipulation experiments-

Decoupling of pH and Ω_{Ar}-

We performed seven trials between 2015 and 2017 to experimentally decouple pH and Ω_{Ar} due to the recent interest in this topic (Cyronak et al. 2016; Waldbusser et al. 2016b; Fassbender et al. 2016). We first developed the manipulation software to accept user inputs of TAlk and TCO_2 targets that remained stable during the test (Figure 3.5, “manual”). We designed DOAMES three simultaneous manipulation treatments to cover a constant Ω_{Ar} across a range of

three pH values (from 7.55 to 7.85), one for each manipulation channel. We conducted these experiments at two different temperatures (18°C and 25°C) and, therefore, target Ω_{Ar} values varied between 2.00 and 3.00 (Table 3.2).

We carried the decoupling experiments with stable source seawater by partially filling 1,500 L reservoir tanks with an approximate volume of 1,250 L of filtered seawater. The seawater at the laboratory tended to have significantly supersaturated PCO_2 and so was vigorously aerated with outdoor ambient air for a minimum of 8 hours to stabilize its PCO_2 value before carbonate chemistry manipulations. There are seawater targets that require removing TCO_2 to reach target values (e.g., low Ω_{Ar}), and for these, seawater may need to be stripped of TCO_2 and TAlk before manipulations. For this reason, in some trials, source seawater's TAlk was partially titrated through the addition of reagent-grade, concentrated HCl, and subsequently TCO_2 was stripped by vigorous aeration. It is important to note that the bubbling is not a critical step in the procedure, since the true TCO_2 and PCO_2 values were measured continuously before the manipulation reagents were added.

The seawater was continuously recirculated from the holding tank to the PCO_2/TCO_2 analyzer, except for the necessary flow of water needed for treatments (a maximum of ~350 mL min^{-1}). In these trials, designed to mimic the optimal conditions to run Pacific oyster larvae experiments (Waldbusser et al. 2015a), the temperature of the recirculating source seawater was kept below 15°C to minimize pathogenic bacterial growth (*Vibrio spp*) by use of a seawater chiller (C-0500, Resun). The manipulated seawater was, therefore, heated inline to match the target temperature before delivery to experimental containers.

Dynamic Source Seawater-

In some instances, performing experimental studies without reservoir tanks and directly from a seawater feed-line might be advantageous. For instance, if there are concerns regarding water quality deterioration over time due to stagnation, if there is interest in replicating natural carbonate chemistry variability, or if the capability to hold salinity or temperature constant is compromised. As a consequence, we tested DOAMES performance in a reservoir-less manipulation trial conducted in June 2016 to assess the capability of the system to reliably produced manipulated treatments with dynamic sources of seawater. To that end, we performed this experiment by directly analyzing and manipulating the laboratory incoming seawater continuous streamflow.

Stable, Dynamic, and offset Targets-

We ran a one-week long trial using the dynamic live seawater system from the HMSC in June 2016 (Table 3.1). In this trial, we produced three simultaneous different carbonate chemistry treatments: a stable set of targets, a combination of idealized dynamic TCO_2 and stable TAlk, and an offset from the naturally variable water coming into the system.

In the stable manipulation channel, the TCO_2 and TAlk targets were manually set (Figure 3.5, "manual") to 2,750 µmol kg^{-1} and 2,980 µmol kg^{-1}, respectively, throughout the entire trial.

In the second manipulation channel, we modified the software to allow for user input of mean, amplitude, and frequency of the sinusoidal signal (Figure 3.5, "sinusoidal"). We then tested this capability by defining an idealized sinusoidal pattern for TCO_2 that mimic a

semidiurnal signal centered around a value of 2,750 µmol kg^{-1} with a mean amplitude of 200 µmol kg^{-1} (2,750± 200 µmol kg^{-1}) and a frequency of 2 cycles day^{-1}. Simultaneously, we kept the TAlk target constant (3,000 µmol kg^{1} for the first six days; 2900-2950 µmol kg^{-1} for the last day of the experiment).

Both first and second manipulation channels TCO_2 and TAlk targets fell outside the usual range found in marine environments. These values, however, were chosen as a rigorous test for DOAMES dynamic capabilities, as they imposed demanding reagent delivery requirements.

In the third manipulation channel, we created a set of constant offset conditions meant to utilize the truly dynamic conditions from a given location and added a constant amount of anthropogenic carbon to those conditions (Figure 3.5, "RCP 6.0"). This type of carbonate chemistry manipulation test calculated the TCO_2 target based on an offset ΔPCO_2 imposed on the continuous source seawater PCO_2 values. We estimated ΔPCO_2 as the difference between current, global atmospheric CO_2 and the 2100 atmospheric CO_2 predicted from future IPCC projections according to different Representative Concentration Pathways (e.g., RCP6.0, Pachauri et al. 2015) (Figure 3.5, "RCP 6.0"). We designed the software logic to continually compute the instantaneous source seawater PCO_2 by adding ΔPCO_2 to the measured PCO_2 value. Subsequently, DOAMES computed the resulting TCO_2 value with the corrected source seawater PCO_2, together with the original TAlk and temperature, salinity values. The software then updated the resulting TCO_2 value as the manipulation target value. We allowed the TAlk target to dynamically vary mimicking the naturally variable alkalinity value of the source seawater.

3.3.3 Organismal exposure to manipulated carbonate chemistry test-

In April 2015, we tested DOAMES applicability to organismal acidification stress experiments by exposing early stages of Pacific Oyster (*Crassostrea gigas*) larvae to manipulated seawater from fertilization to 48 hours post-fertilization. We utilized static culture chambers as controls to help separate any potential effects of flow from the carbonate chemistry manipulations on larval development. In previous work, we have demonstrated the ability to culture oyster larvae with high fidelity, resulting in upwards of 80% embryo development (Waldbusser et al. 2015a; b, 2016a). Therefore, we must ensure DOAMES does not have a significant effect on the development of larvae.

To do this, we acidified and stripped the source seawater to reduce the TCO_2 and TAlk, and manipulated the carbonate chemistry back to the control, unaltered conditions of the source seawater. Initially, both the unaltered and manipulated flow-through reservoir tanks were filled with filtered seawater heavily aerated with outside, ambient air. DOAMES reservoir tank was then acidified and purged with ambient air to reduce the TAlk and TCO_2 by ~80%. In this experiment, we used only one manipulation channel and targets for both TAlk and TCO_2 where set to 2145 µmol kg-1 and 1958 µmol kg-1, respectively, matching the carbonate chemistry values of the control seawater measured at the start of the experiment. Embryos were then raised in both control and manipulated water, in both static and flow-through conditions. As a negative control, embryos were also reared in static, acidified, un-manipulated source seawater from DOAMES reservoir tank.

3.3.3.1 Spawn and larval culture -

Spawning, fertilization, and embryo viability assessments were conducted following previous protocols (Waldbusser et al. 2015a; b). Briefly, we obtained multiple males and females Pacific Oyster broodstock from Whiskey Creek Hatchery (WCH), and manually stripped them of their gametes on April 7th, 2015. The gametes were subsequently pooled and fertilized in filtered seawater. After 2 hours post-fertilization, we checked fertilization success by assessing the appearance of polar bodies. Developing embryos were then transferred to 500 mL biological oxygen demand (BOD) bottles or 1L borosilicate glass culture chambers (1397-1L, Corning®), for static or flow-through culture, respectively. The embryos were cultured in five replicate culture jars per treatment and at stocking densities of 10 embryos mL^{-1} for static and 25 embryos mL^{-1} for flow-through cultures. Each flow-through culture jar inlet was connected to DOAMES manipulation channel outflow, while the outlet was plumbed to a peristaltic pump that regulated an equal inflow of manipulated water at a constant flow-rate of 1 mL min-1 across all treatment replicate culture jars. The outlet was also fitted with a 20 μm "banjo-type" Nitex filter to allow for the flow of seawater but prevent the loss of organisms.

The experiment terminated approximately at 48 hours post-fertilization. Larvae from each BOD bottle and culture chamber were collected and preserved with 10% formalin buffered to a pH of ~8.15. We examined larvae under inverted light microscopy to evaluate the proportion of normally developed larvae with respect to the total number of larvae following established criteria (His et al. 1997(Waldbusser et al. 2015a; b, 2016a).

3.3.4 Discrete carbonate chemistry samples-

Discrete carbonate chemistry samples from experimental treatments were routinely obtained from the outflow of each manipulation channel or from the outflow of culture chambers. Samples were collected in 350 mL amber glass bottles with polyurethane-lined crimp-sealed metal caps and immediately analyzed or preserved with 100 µL of saturated $HgCl_2$ solution for posterior analysis. In situ temperature and salinity values were recorded and TCO_2 and PCO_2 were measured in the above-mentioned PCO_2/TCO_2 analyzer by temporarily switching from continuous mode to discrete sample analysis. Alternatively, we analyzed preserved samples in an analogous PCO_2/TCO_2 system dedicated to discrete sample analysis. The estimated, combined analytical uncertainty is 0.2% for TCO_2 and 2% for PCO_2 (Hales et al. 2017), based on analysis of certified reference materials (CRM) provided from A. Dickson's laboratory at the Scripps Institution of Oceanography.

3.3.5 Data analysis-

3.3.5.1 Carbonate chemistry manipulations-

We assessed the overall performance of DOAMES, in terms of accuracy and precision of the carbonate chemistry manipulations, by evaluating the relative error as the difference between actual conditions and target values, divided by the target values. We report the absolute value of this error, and assessed systematic errors in the sign-retaining error through one-sample Student's t-tests. We further evaluated the successful separation of pH treatments under constant Ω_{Ar} through one-way analysis of variance (ANOVA) with manipulation treatment as a factor.

3.3.5.2 Larval development-

We square-root arcsine-transformed the larval development data and analyzed them through one-way analysis of variance (ANOVA) with treatment as a factor. All statistical analyses were performed in Rstudio (version 1.0.136).

3.4 Assessment

3.4.1 Overall accuracy and precision of carbonate chemistry manipulations-

Although the overall accuracy and precision of the system, excluding 2017 trials, is 2.1% ± 2.4% for TCO_2, and 2.9% ± 3.1% for TAlk (Table 3.1), DOAMES is capable of 1.2% and a precision of ± 0.9% for both TCO_2 and TAlk when mechanical and software operation challenges are minimized, thereby a more representative assessment of DOAMES' capabilities (Table 3.1).

Initial target achievement was 2.3% and 3.8% for TCO_2 and TAlk respectively, with an associated precision of 2.7% for TCO_2 and 5.1% for TAlk. After we identified several operational problems, including mechanical and software inadequacies, we implemented system modifications including enhancements of syringe pumps' mechanical stability, redesign of the reagent injection system, including check-valves and switching valves, and improvements of the communication between syringe pumps and controlling software. As we overcame these challenges, manipulation's accuracy improved by two-fold (TCO_2) to three-fold (TAlk), while

precision improved three- to six-fold for TCO_2 and TAlk, respectively, when comparing stable manipulations between April 2015 and March 2016 (Table 3.1, Figure 3.6).

We chose syringe pumps because the linear-actuation mechanism coupled with a high-resolution stepper-motor controller in theory provides the greatest dynamic range of positive-displacement flow control; however, syringe pumps in general, and NE-100 pumps in particular, provided several operational challenges. First, syringe pumps required a pair of pumps for each reagent and complicated logic to monitor flow volume and control rates through switching procedures. Across all trials, a pattern emerged of periodical outliers of discrete sample values with % relative error greater than 7% for either (or both) manipulated variables, sometimes associated with overlapping switching routines for both reagent pumps, resulting in transient instances (<30 seconds) of completely paused manipulations. The overall effect of these transient reagent delivery failures on experimental treatments depends on the frequency of occurrence, the residence time of the culture chambers, and the difference in carbonate chemistry conditions between the source seawater and the experimental treatment. Second, the NE-100 pumps had a relatively inefficient linear-actuator screw drive, with interference, rather than square or lead-screw threads designed to minimize friction and "thread-jumping" that resulted in failures in reagent delivery. Last, the NE-100 flow-control mechanism included several parts made of materials (Delrin, Silicone) with low resistance to acid solutions that failed after extended use. We heavily modified the pumps to eliminate these components and ultimately achieved acceptable performance, but alternate delivery mechanisms should be considered (see recommendations).

Although we did not detect systematic errors across all trials through visual inspection of sign-retaining percent errors (Figure 3.6), t-test statistical analyses showed a small bias towards under-delivery of both reagents, slightly greater for the acid reagent. The reagent under-delivery resulted in mean negative values of % relative error for both TAlk (-0.58%, $t_{376,375} = -2.29$; $p=0.023$) and TCO_2 (-1.01%, $t_{376,375} = -5.40$; $p<0.001$). The increase of % relative error and standard deviations for both TAlk and TCO_2 for the trials conducted between July 2016 and March 2017 is evidence of progressive mechanical fatigue in the syringe pumps, leading to loss of accuracy and precision (Table 3.1 and Figure 3.6). Accordingly, we have excluded the 2017 data for further analysis, as the mechanical integrity of some of the syringe pumps seemed significantly compromised and, therefore, the results do not provide a reliable evaluation of the manipulation system.

3.4.2 Decoupling of carbonate chemistry parameters: pH and Ω_{Ar}

DOAMES was generally able to deliver statistically significant experimental treatments that successfully decoupled pH and Ω_{Ar} by producing a range of carbonate chemistry conditions with a common, stable Ω_{Ar} within 0.7 units of target and across a range of pH values (Table 3.2 and 3.3, Figure 3.7). DOAMES effectively decoupled these carbonate chemistry variables even in the experiments conducted in July and August 2016 (Figure 3.7 g-j), when syringe pumps' developing mechanical fatigue was already decreasing accuracy and precision of the manipulations (Table 3.1). Despite the overall success in decoupling of carbonate chemistry parameters, there were, however, several instances of high pH experimental treatment

overlapping with the medium pH treatment (Figure 3.7 b, f, j), resulting in treatments not being statistically different from each other. Overlapping in treatments result from the disproportionate effect of small, opposite signs % relative errors of TAlk and TCO_2 on pH in the least manipulated chemistries (i.e., lowest absolute values of TAlk and TCO_2).

Although the observed variability in Ω_{Ar} and pH in our trials is greater than usually found in published laboratory studies conducted through precise CO_2 gas injections (i.e. pH up to 0.03 units in Standard Deviation (SD), and up to 0.4 SD units for Ω_{Ar}; Talmage and Gobler 2010; Hettinger et al. 2012; Barros et al. 2013), our results are still within the variability of published batch-culture studies aimed at decoupling carbonate chemistry parameters (Gazeau et al. 2011; Waldbusser et al. 2015a; Thomsen et al. 2015a; Waldbusser et al. 2015b, 2016a). DOAMES is, therefore, performing within the range of current community standards for the types of manipulations we are conducting.

3.4.3 Dynamic source seawater input and variable targets test-

Under moderately variable source seawater conditions (Figure 3.8), DOAMES simultaneously produced stable, dynamic, and offset experimental treatments by using each of the three controller channels for a given manipulation (Figure 3.9).

Although we did achieved a moderately dynamic source seawater (Figure 3.8), the continuous seawater stream-flow at HMSC laboratories originates from HMSC facility-wide reservoir tanks that do not fill continuously. Rather, seawater is pumped twice a day during high tide from Yaquina Bay, OR and stored in reservoir tanks for further distribution through HMSC

laboratories, effectively dampening the high-frequency natural variability expected from a tidally-influenced estuary (Barton et al. 2012; Hales et al. 2017).

The combined precision and accuracy across the three manipulation channels is better than DOAMES overall values, with overall better performance in obtaining TCO_2 targets relative to TAlk (Table 3.1). We then assessed each manipulation channel potential performance and potential for systematic errors by evaluating their mean signed-retaining error. For the stable treatment, both TCO_2 and TAlk manipulations achieved great accuracy and performed similarly regarding precision (-0.2 ± 2.7 % for TCO_2 compared to -0.1 ± 2.7% for TAlk). The idealized TCO_2 dynamic treatment performed slightly worse in terms of accuracy for both TCO_2 and TAlk, but better for TCO_2 precision (1.1 ± 1.6 % for TCO_2; -0.6 ± 3.8% for TAlk) when compared to the stable target manipulation. Finally, the best performing manipulation channel was the dynamic offset (-0.0 ± 1% for TCO_2 compared to 1.6 ± 1.4% for TAlk), which is to be expected considering that it is the least "manipulated" system and, therefore, requires the lowest reagent additions. These results suggest that DOAMES is indeed capable of responding to dynamic source seawater inputs and to simultaneously produce stable and dynamic treatments with TCO_2 and TAlk targets that range across 2050 to 2950 μmol kg^{-1}.

3.4.4 Larval exposure experiment-

Bivalve embryos developed normally on DOAMES-manipulated water to successfully mimic control seawater after stripping ~80% of the TCO_2 and TAlk (Figure 3.10, Table 3.4). Manipulated conditions were, on average, approximately 0.3% lower for TCO_2, close to

analytical uncertainty, and 1.9% greater for TAlk and with respect to the static control (Table 3.4). These unequal deviations from TAlk and TCO_2 targets resulted in slightly elevated mean Ω_{Ar} and pH values in the flow-through manipulated water with respect to the static control (Table 3.4). These deviations, however, are less than 0.5 units Ω_{Ar} and 0.06 for pH, within the experimental conditions variability reported on other carbonate chemistry parameter decoupling studies (Gazeau et al. 2011; Thomsen et al. 2015; Waldbusser et al. 2015b, 2016a).

Bivalve larval development at 48 hours post-fertilization was not statistically different in control-simulating manipulated water treatment compared to untreated control water (Figure 3.10). The mean percentage of normally developed larvae was 90.9 ± 1.5% for the static control, 88.1 ± 5.6% for the flow-through control, 86.0 ± 3.3% for the manipulated flow-through treatment, 81.6 ± 2.6% for the manipulated static, and 0.2 ± 0.4% for the un-manipulated static. These developmental responses agree with published results on early Pacific oyster larvae development that identified a favorable threshold of Ω_{Ar} >~2.3 that corresponded with more that 80% normally developed larvae and a sensitivity threshold of Ω_{Ar} <1.4 that was associated with significant proportions of abnormal larvae present (Waldbusser et al. 2015a). It is important to note that one of the five replicates of the manipulated, static treatment resulted in near zero normal development. Upon further analysis of the carbonate chemistry, we hypothesize that the BOD bottle was probably filled with a combination of manipulated and transient un-manipulated water, as the TAlk and TCO_2 values were consistent with partially manipulated water. We speculate that this replicate bottle was filled before the manipulation system had stabilized and, as a result, was excluded from further analysis.

We found a highly significant effect of treatment on development to day two post-fertilization (Table 5, $F_{4,19}$=536.7, p<0.0001), mostly driven by the detrimental effects of the un-manipulated treatment. Indeed, upon further exploration of the post-hoc multiple comparisons, we found no significant differences among controls (both static and flow-through) and the flow-through, manipulated water (Figure 3.10).

These results suggest that DOAMES allows for the adequate development of embryos in a flow-through environment and that there are no inherent negative effects of manipulated water to mimic control seawater conditions on larvae development. We, therefore, conclude that this is a successful proof-of-concept of the suitability of our novel manipulation system for experimental work on marine organisms.

3.5 Discussion

DOAMES proof-of-concept results demonstrate its capability to decouple Ω_{Ar} and pH in a flow-through setting, a key tool to determine chronic organismal and population-level sensitivities to past, current and future carbonate chemistry scenarios and, ultimately, provide adequate forecasts of the future fate of taxa vulnerable to OA. Indeed, DOAMES-manipulated water supported normal embryo development during the most vulnerable stage of bivalve larvae. Since the organismal exposure experiment discussed here, we have utilized DOAMES to successfully raise fertilized embryos to 48 hours old larvae at seven times higher organismal densities (200 embryos mL^{-1}) and thirteen times higher flow-rates (~14 mL min^{-1}) (unpublished

data). DOAMES, therefore, can support experimental work that requires elevated densities of organisms due to either expected high initial mortality (White et al. 2013), or the need for abundant biomass for specific analysis (e.g. transcriptomics (De Wit et al. 2018); lipid extraction (Waldbusser et al. 2016a; Brunner et al. 2016). DOAMES flow-through capabilities support experimental designs that need higher flows to optimize organismal development (e.g. Howes et al. 2014), or when deviations from target carbonate chemistry conditions as a result of metabolic processes need to be minimized (e.g. Gradoville et al. 2014). Additionally, DOAMES flow-through configuration allows for long experimental exposures (e.g. Ko et al. 2013) and multi-generational experiments of organisms (e.g. Parker et al. 2015; Griffith and Gobler 2017), providing an empirical framework to explore potential differential carry-over effects (e.g. Hettinger et al. 2012, 2013) of exposure to different carbonate chemistry parameters.

Resolving sensitivity mechanisms to different carbonate variables is more relevant in coastal environments where carbonate chemistry variables naturally decouple (e,g. Fassbender et al. 2016, Hales et al. 2017), habitat for organisms with identified heightened vulnerability to OA such as corals and bivalves (Kroeker et al. 2013). From an evolutionary perspective, many of the extant taxa of bivalves, for instance, evolved during the Triassic and Cretaceous periods, with extensive evolutionary radiation occurring during the latter (Crame 2000). Both of these geological periods coincided with likely episodes of natural decoupling of pH and Ω_{Ar} (Kump et al. 2009; Zeebe 2012; Hönisch et al. 2012), therefore observed bivalve differential sensitivities to carbonate chemistry parameters such as PCO_2, pH and Ω_{Ar} in present conditions (Waldbusser et al. 2015a; b; Thomsen et al. 2015b; Waldbusser et al. 2016a) might stem from evolutionary

adaptations. DOAMES capabilities for long-term empirical decoupling, therefore, are a necessary tool to assess the long-term physiological effects of individual carbonate chemistry variables.

Decoupling in coastal zones will also likely be exacerbated in the future, as modeled projections forecast increased high-frequency carbonate chemistry variability and different rates of change for PCO_2, pH and Ω_{Ar}. For instance, Pacella et al. (2018) found that increased PCO_2 due to anthropogenic activity lowers buffering capacity in a seagrass habitat, therefore amplifying the effect of diel community metabolic cycles. The increased amplitude in TCO_2 changed daily maximum PCO_2 and minimum pH and Ω_{Ar} values more than 1.5x faster than the change in their median values. Changes in the seasonal variability of these carbonate parameters are also predicted and observed in open-ocean environments where decoupling is not prevalent (Kwiatkowski and Orr 2018; Landschützer et al. 2018). It follows, therefore, that to better predict future responses to OA of marine coastal organisms, current and future variability in carbonate chemistry variables need to be incoporated in laboratory experimental design.

DOAMES supports experimental treatments with dynamic TCO_2 (or TAlk) targets, simulating carbonate chemistry variability naturally found in coastal systems to assess its effects on organismal physiology. Though determining organismal responses to naturally variable carbonate chemistry conditions is an identified research priority within the OA community (Wahl et al. 2016; Boyd et al. 2016), variable carbonate chemistry conditions are technically difficult to recreate in laboratory settings (but see Frieder et al. 2014; Burrell et al. 2016; Eriander et al. 2016; Clark and Gobler 2016). DOAMES dynamic target mode allows for the

exploration of the effects of high and low-frequency carbonate chemistry variable conditions and comparison of physiological responses to those of stable treatments, thereby providing empirical evidence to help reconcile observed divergent responses across multiple taxa and life-stages.

Carbonate chemistry variable treatments have been shown to mitigate, exacerbate or elicit the same physiological response when compared to stable OA treatments in species such as micro and macroalgae (Cornwall et al. 2013; Li et al. 2016), bivalve larvae (Frieder et al. 2014; Eriander et al. 2016; Clark and Gobler 2016), adult bivalves (Keppel et al. 2015), recruits and adult corals (Dufault et al. 2012), and fish (Jarrold 2017). DOAMES' flexibility to incorporate complex dynamic TAlk and TCO_2 target regimes also supports the design of experiments that can test the relative impact of transient extremes on organisms, previously identified as important drivers of physiological responses to temperature (Helmuth et al. 2010). Ultimately, DOAMES' ability to create complex but controlled dynamic exposures to OA enables the testing and validation of stress indexes designed to capture physiological stress due to variable natural conditions (e.g. Gimenez et al. 2018).

Finally, DOAMES is capable of mimicking future environmental conditions on variable coastal environments by applying system-specific offsets based on CO_2 emission scenarios to naturally variable carbonate chemistry conditions. In this work, we tested the ΔPCO_2 approach to simulate future OA conditions (Feely et al. 2010; Hales et al. 2017; Pacella et al. 2018), assuming constant disequilibrium between atmospheric CO_2 and seawater PCO_2. We believe, however, that DOAMES is capable of projecting future conditions based on the ΔTCO_2 method (Pacella et al. 2018 and references therein) that assumes constant disequelibrium between the

measured TCO_2 and the computed TCO_2 if the observed system was in equilibrium, likely a more appropriate method for coastal environments in where metabolic processes significantly affect the carbonate chemistry and their buffering capacity. Experimental designs that involve carbonate parameter decoupling or variable environmental conditions are technically complex and require high precision in the chemical manipulations, and therefore are particularly challenging in longer-term experiments.

DOAMES high degree of automation requires minimal user-input to initialize an experiment and its feed-forward control logic reduces hysteresis and provides stability to the manipulated treatments, even in highly complex experimental designs as the dynamic and offset targets discussed above. Some of the published flow-through experimental systems designed for ocean acidification experiments rely on sufficently long gas equilibration times to ensure experimental treatment stability (e.g. Fangue et al. 2010; Eriander et al. 2016). Conversely, the experimental systems that do rely in some control logic almost invariably do so by using feed-back control (McGraw et al. 2010; Wahl et al. 2016; Burrell et al. 2016; Sordo et al. 2016).

For reasonably constrained systems, feed-forward control is a viable option that provides increased stability and, presumably, reduced hysteresis when compared to feedback-controlled systems (Hovd and Bitmead 2009). Constrained systems are those for which the most important controlling variables are known and measurable and their effect on the output can be fully predicted. The carbonate system, governed by well-known thermodynamic relationships, can be therefore considered a constrained system and, therefore, suitable for feed-forward control. We acknowledge that the ideal experimental system would incorporate an adaptive feed-forward or a

combination of feed-forward and feed-back controllers, although this approach is often unfeasible due to logistical and financial constraints. For DOAMES, a dual feed-forward and feed-back approach would require an additional PCO_2/TCO_2 analyzer downstream from the manipulation channels that would continuously monitor both parameters for each channel and, more importantly, a complex logic to adjust future manipulation targets balancing both the input from the source seawater carbonate chemistry signature and the measured experimental conditions.

3.6 Comments and Recommendations

DOAMES modular flexibility allows for multiple manipulation channels and different experimental treatment configurations, including simultaneous coupling or decoupling of carbonate variables, and stable, dynamic and offset carbonate chemistry targets. The current proof-of-concept described in this work includes three simultaneous manipulation channels, but we can foresee the addition of more with minimal software changes. Thus, DOAMES affords experimentalists a high degree of customization to tailor to their specific research needs, and we provide some suggestions to facilitate its adaptation.

First, the constraint of processes inherent to the experimental design that can lead to deviations from targets is key in feed-forward controlled systems like DOAMES. We suggest, therefore, that future DOAMES users should consider exploring alternative reagent delivery systems, as DOAMES current reagent injection design is responsible for most of the deviations

from targeted manipulation values and for the small but significant systematic under-delivery of base and acid reagents. Within the injection system, the weakest component has been identified: the syringe pumps.

Syringe pumps are very affordable, easy to program and interface with the manipulation controller software, and they can provide precise volume delivery across an extended range of flow rates. These attributes originally made syringe pumps an obvious choice for DOAMES; however, alternative reagent delivery systems that minimize the need for switching valves and limit mechanical fatigue that can lead to manipulation errors will reduce the frequency of reagent delivery failures and, thus, increase DOAMES' robustness. We suggest, therefore, alternative options as programmable, high-precision peristaltic or valve-less metering pumps. Although significantly more expensive, these pumps will eliminate the need of having dual syringe pumps per reagent and channel, as they can deliver volume continuously, and, therefore, also mitigate the need for switching valves.

Second, selecting the right combination of reagent pumps depends on the desired carbonate chemistry targets and the required total experimental treatment seawater flow-rate (i.e. flow rate to each replicate culture chambers multiplied by total number of replicates). As a first approximation, however, reagent flow rates are typically less than 10% of the total experimental treatment seawater flow-rate, even if the source seawater has been stripped of TCO_2 and TAlk. We suggest, therefore, that users identify first the total flow required and then select the appropriate combination of reagent pumps to suit their needs.

Finally, we suggest the use of intermediate holding seawater tanks for manipulated water when designing low flow, high residence-time experiments. Although the use of pumps that can continuously deliver reagents will significantly lower the occurrence of manipulation errors associated with reagent delivery failures, transient breaks in carbonate chemistry manipulations can still occur. Instances of delivery of under- or un-manipulated water can have an outsized effect in low flow, high residence time experimental designs; thus, an intermediate holding seawater tank can buffer high-frequency variability resulting from brief manipulation errors and produce experimental treatments with very stable carbonate chemistry. We recommend optimizing the volume of these intermediate holding tanks to ensure adequate flushing rates that limit bacterial growth that could result in decreased overall water quality.

Acknowledgments

This work was supported by National Science Foundation OCE CRI-OA #1041267 to GGW, BH, and CJL. The authors would like to thank Greg Hutchinson for his invaluable help in designing, implementing and supporting the flow-through organismal culture setup, as well as his numerous contributions during biological tests. The authors are also grateful to Matthew Gray for imaging and analysis of bivalve larvae and general support during biological tests; Dylan Howell and David Madison for their support during manipulation tests; Dale Hubbard and Joe Jennings for technical support in the design and troubleshooting of the carbonate chemistry manipulation system; Stephanie Smith, Cameron Allen, Stephen Pacella, and Jessamyn Johnson for their support during biological tests; Blaine Schoolfield, Evan Durland, Kimberley Preston,

and the Molluscan Broodstock Program for general support at HMSC; and Alan Barton, Sue Cudd, and Mark Wiegardt from Whiskey Creek Hatchery for providing *Crassostrea gigas* broodstock.

Table 3.1. DOAMES accuracy and precision across trials. 2017 trials were excluded from the overall accuracy and precision due to mechanical fatigue of reagent pumps (see discussion). Best DOAMES performance was achieved on March 2016.

Date	Type of source seawater	Type of manipulation targets	TCO_2 % Absolute Relative Error ± SD	TAlk % Absolute Relative Error ± SD
April 2015	Stable	Mimic control conditions	2.3 ± 2.7	3.8 ± 5.1
October 2015	Stable	Constant Ω_{Ar} and varying pH	2.0 ± 2.8	3.2 ± 3.8
March 2016	Stable	Constant Ω_{Ar} and varying pH	1.2 ± 0.9	1.2 ± 0.9
April 2016	Stable	Constant Ω_{Ar} and varying pH	4.1 ± 1.3	4.6 ± 1.4
June 2016	Dynamic	Stable, Dynamic and Off-set	1.5 ± 1.5	2.3 ± 1.9
July 2016	Stable	Constant Ω_{Ar} and varying pH	4.9 ± 2.9	4.5 ± 2.5
August 2016	Stable	Constant Ω_{Ar} and varying pH	4.8 ± 2.6	4.9 ± 3.1
February 2017	Stable	Constant Ω_{Ar} and varying pH	5.1 ± 3.0	5.0 ± 4.1
March 2017	Stable	Constant Ω_{Ar} and varying pH	3.6 ± 4.8	5.1 ± 7.0
Overall (excluding 2017)			2.1 ± 2.4	2.9 ± 3.1
Best performance			1.2 ± 0.89	1.2 ± 0.9

Table 3.2. Ω_{Ar} and pH_t decoupling experiments mean experimental results. ± are Standard Deviations.

Date	T (°C)	S	Manipulation Channel 1		Manipulation Channel 2		Manipulation Channel 3	
			Target	Observed	Target	Observed	Target	Observed
October 2015	20.1 ± 0.5	32.7 ± 0.0	Ω_{Ar} = 2.50 pH_t = 7.85	Ω_{Ar} = 2.19 ± 0.57 pH_t = 7.79 ± 0.13	Ω_{Ar} = 2.50 pH_t = 7.70	Ω_{Ar} = 3.03 ± 1.66 pH_t = 7.77 ± 0.18	Ω_{Ar} = 2.50 pH_t = 7.50	Ω_{Ar} = 2.17± 0.66 pH_t = 7.50 ± 0.13
March 2016	20.2 ± 0.2	28.6 ± 0.0	Ω_{Ar} = 2.52 pH_t = 7.89	Ω_{Ar} = 2.50 ± 0.27 pH_t = 7.89 ± 0.05	Ω_{Ar} = 2.50 pH_t = 7.74	Ω_{Ar} = 2.61 ± 0.24 pH_t = 7.75 ± 0.04	Ω_{Ar} = 2.47 pH_t = 7.58	Ω_{Ar} = 2.77± 0.38 pH_t = 7.63 ± 0.06
April 2016	19.4 ± 0.3	31.8 ± 0.0	Ω_{Ar} = 2.52 pH_t = 7.89	Ω_{Ar} = 2.46 ± 0.04 pH_t = 7.85 ± 0.02	Ω_{Ar} = 2.50 pH_t = 7.74	Ω_{Ar} = 2.87 ± 0.60 pH_t = 7.77 ± 0.09	Ω_{Ar} = 2.47 pH_t = 7.58	Ω_{Ar} = 2.85± 0.48 pH_t = 7.62 ± 0.07
July 2016	25.1 ± 0.4	33.2 ± 0.3	Ω_{Ar} = 3.00 pH_t = 7.85	Ω_{Ar} = 2.89 ± 0.20 pH_t = 7.84 ± 0.03	Ω_{Ar} = 3.00 pH_t = 7.70	Ω_{Ar} = 3.18 ± 0.54 pH_t = 7.74 ± 0.07	Ω_{Ar} = 3.00 pH_t = 7.55	Ω_{Ar} = 3.38± 0.80 pH_t = 7.62 ± 0.10
August 2016	25.1 ± 0.2	33.7 ± 0.0	Ω_{Ar} = 3.00 pH_t = 7.85	Ω_{Ar} = 2.59 ± 0.64 pH_t = 7.78 ± 0.13	Ω_{Ar} = 3.00 pH_t = 7.70	Ω_{Ar} = 2.95 ± 0.47 pH_t = 7.70 ± 0.07	Ω_{Ar} = 3.00 pH_t = 7.55	Ω_{Ar} = 3.00 ± 0.39 pH_t = 7.57 ± 0.06

Table 3.3. Analysis of variance (One-way ANOVA) of Ω_{Ar} and pH_t decoupling experiments.

Date	Source of pHt Variance	Degrees of freedom	Sums of Squares	F-value	p-value
October 2015	Treatment	2	1.080	27.54	<0.0001
	Error	61	1.196		
March 2016	Treatment	2	0.606	118.10	<0.0001
	Error	51	0.131		
April 2016	Treatment	2	0.115	11.96	0.0029
	Error	9	0.043		
July 2016	Treatment	2	0.159	12.07	0.0005
	Error	18	0.119		
August 2016	Treatment	2	0.113	6.23	0.0116
	Error	14	0.126		

Table 3.4. Experimental conditions in 2015 Pacific oyster larval experiment.

Treatment	Temperat. (°C)	Salinity	TAlk (µmol kg^{-1})	TCO_2 (µmol kg^{-1})	PCO_2 (µatm)	pHt	Ω_{Ca}	Ω_{Ar}
Static Control	25.0	29.0	2125	1934	515	7.94	3.54	2.36
Flow-through Control	25.0	29.0	2121	1926	502	7.95	3.60	2.40
Flow-through Manipulated	25.0	30.8	2166	1928	485	7.99	4.22	2.81
Manipulated Static	25.0	30.9	2185	1948	436	8.00	4.17	2.78
Unmanipulated Static	25.0	29.9	460	452	562	7.28	0.19	0.13

Table 3.5. Analysis of variance (One-way ANOVA) of Pacific oyster (*Crassostrea gigas*) early larval development in response to carbonate chemistry treatment.

Source of Variance	Degrees of freedom	Sums of Squares	F-value	p-value
Treatment	4	5.625	536.7	<0.0001
Error	19	0.050		

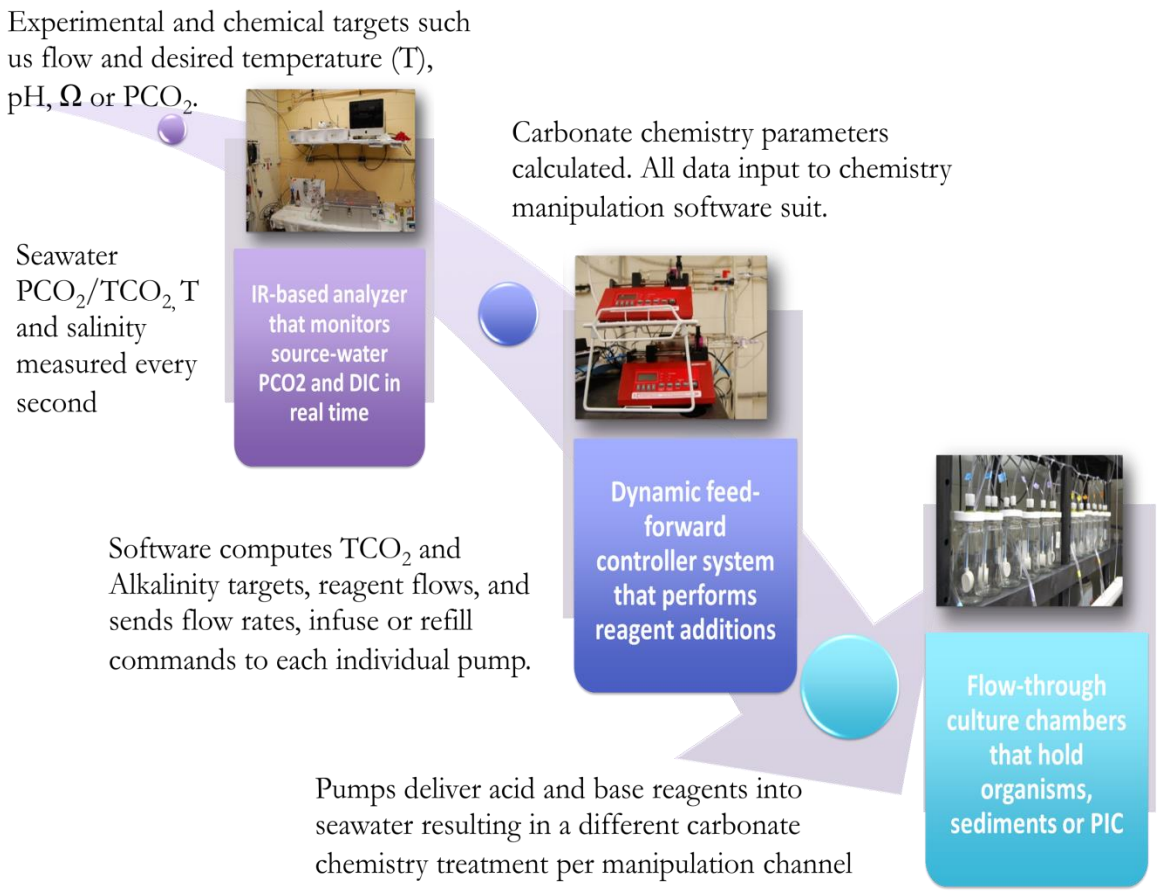

Figure 3.1. Step by step description of the DOAMES manipulation protocol and components.

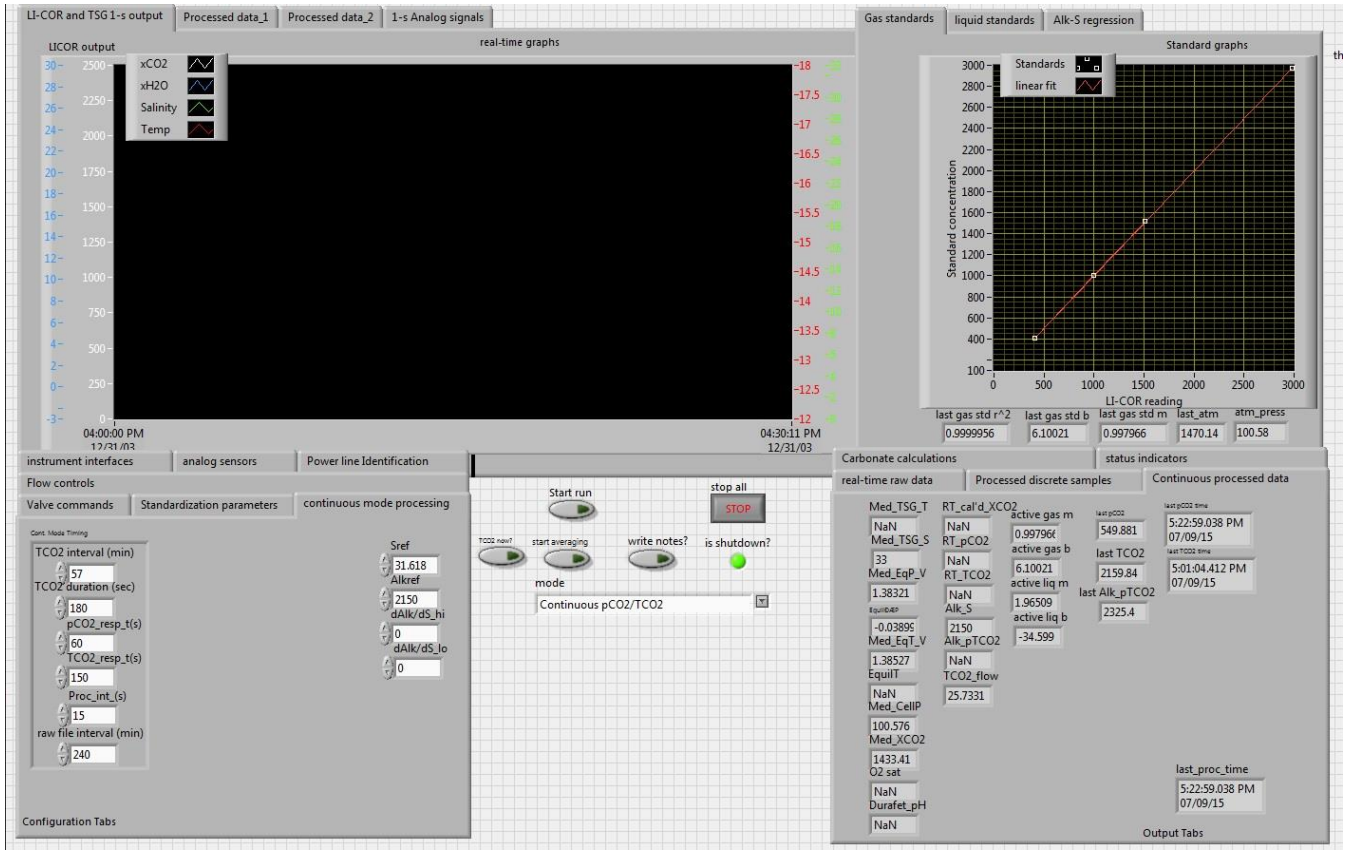

Figure 3.2. PCO_2/TCO_2 analyzer control panel. The main screen includes the monitoring mode selection and real-time graphical representation of sensor output and processed data (center), configuration and control parameters defined by user (bottom left), real-time measurements and automatically calculated carbonate chemistry system parameters (bottom right), and PCO_2 and TCO_2 calibration and alkalinity-salinity regressions (upper left).

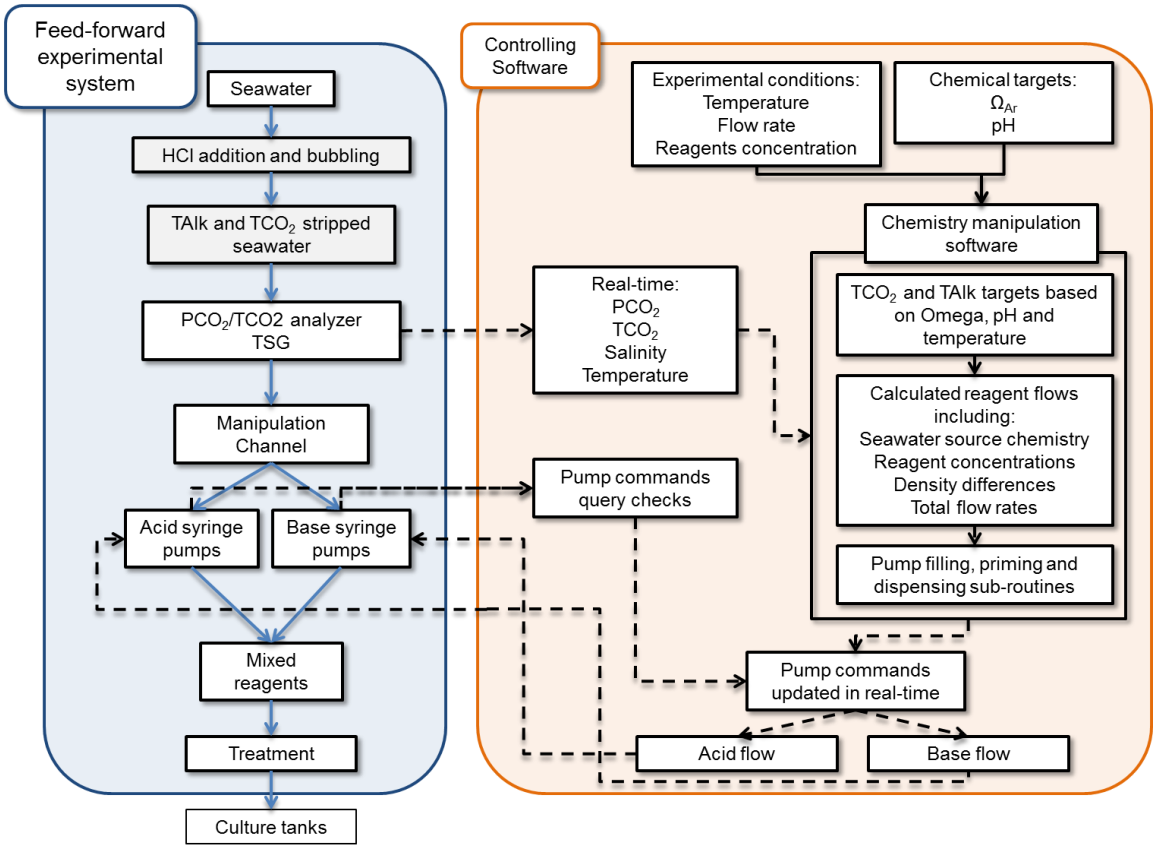

Figure 3.3. DOAMES conceptual diagram. In blue, the hardware components of the experimental system. In orange, the controller software architecture. Shaded boxes (e.g. "HCl addition and bubbling", and "TAlk and TCO_2 stripped water") show stages of the experimental system that are only included in some manipulation experimental designs. Solid, blue arrows represent the flow of seawater and manipulation reagents. Solid, black arrows represent static inputs of information set by the user. Dashed, black arrows represent dynamic inputs of information updated in real-time (<1 minute). Feedbacks within and across both components of the system are shown by dashed arrows crossing boxes.

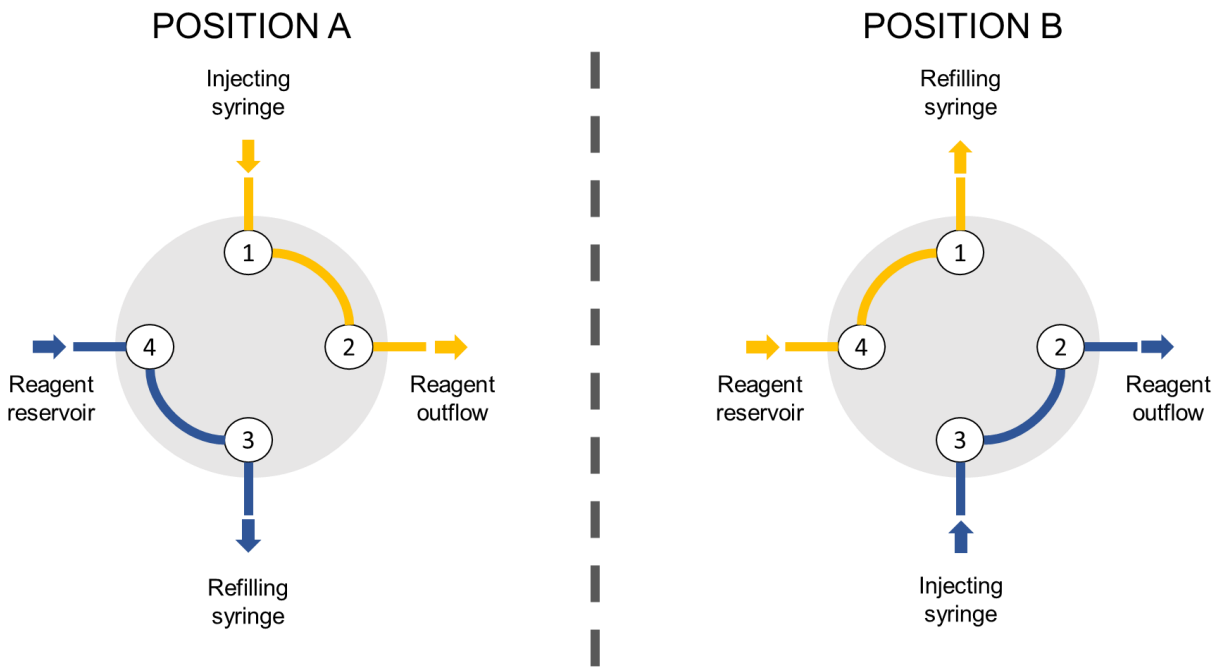

Figure 3.4. Schematic diagram of the two available positions of each reagent switch valve.

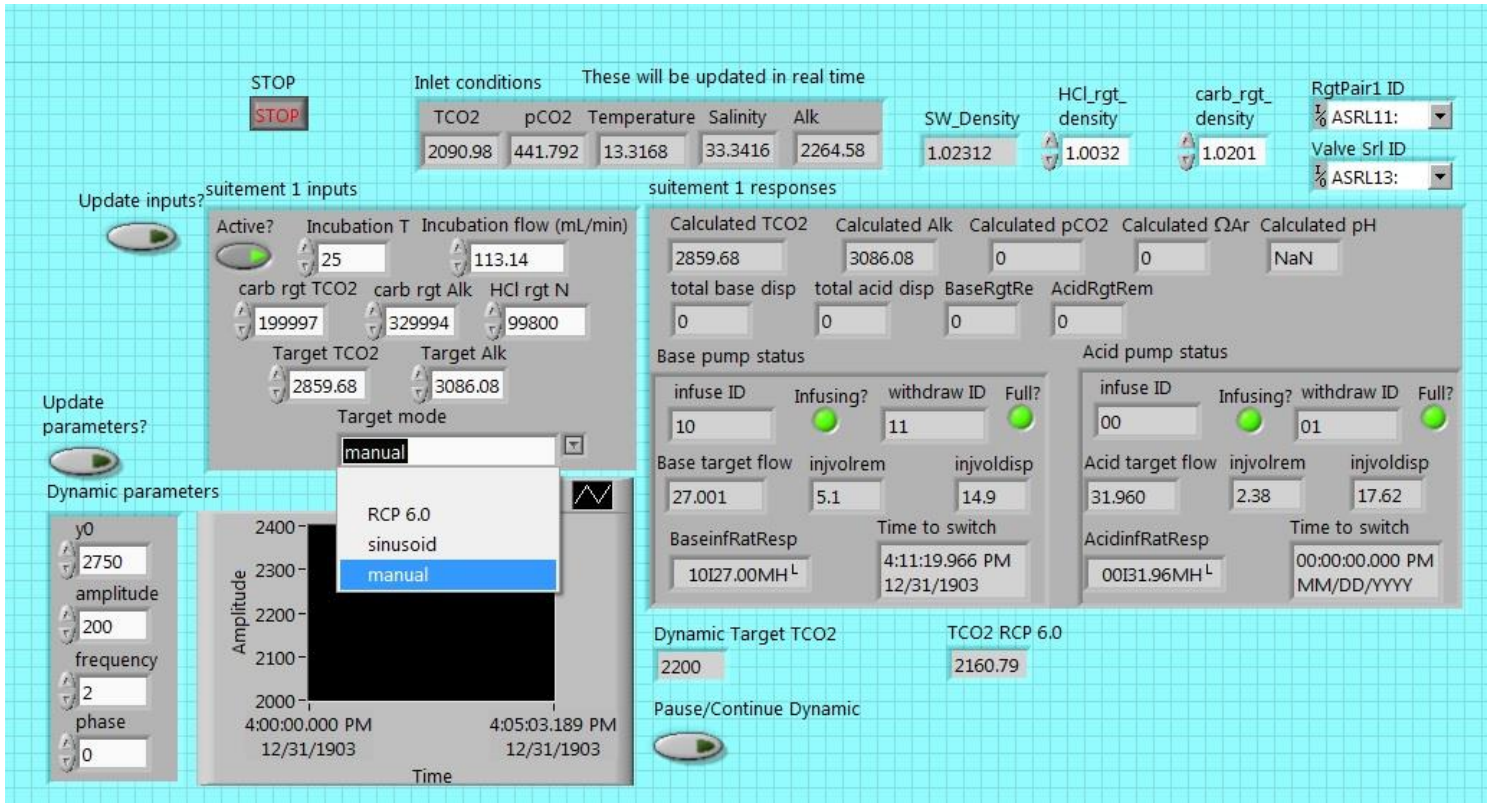

Figure 3.5. DOAMES software control panel .The main screen includes the source seawater (inlet) conditions (top center) and the user-defined manipulation parameters including temperature, flow, reagent concentrations, and TAlk and TCO_2 targets (center). The input tab box also includes the target mode drop-down menu, with the options of manual, dynamic or RCP 6.0 targets (see text). User-defined parameters for the dynamic manipulation mode, as well as a graphical time-series and instantaneous values of dynamic and RCP6.0 targets are shown at the bottom. The calculated TCO_2 and TAlk values, as well as the status and calculated target flow rates of reagent pumps are shown in the responses tab (center right).

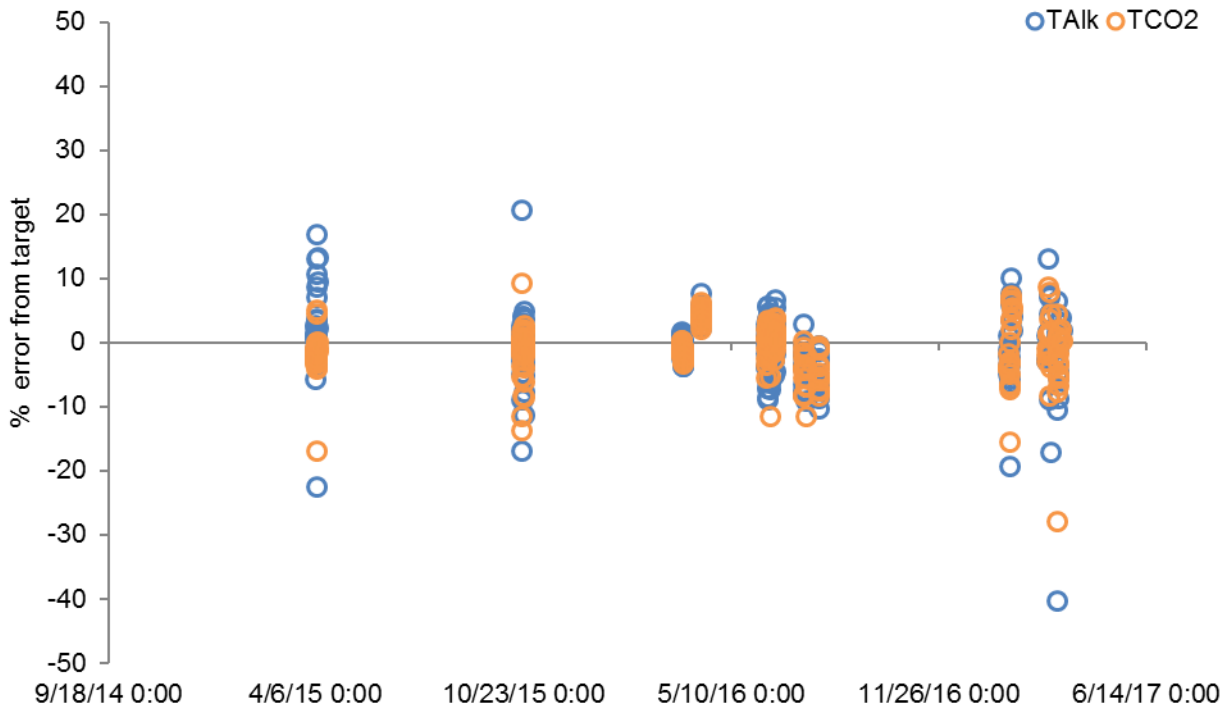

Figure 3.6. Timeline of multiple time-series of % signed relative error from targets from discrete samples of TAlk (blue) and TCO_2 (orange). Slight under-delivery of both chemical reagents were detected. Increased variability in 2017 trials was the result of mechanical fatigue of the reagent pumps (see assessment and discussion).

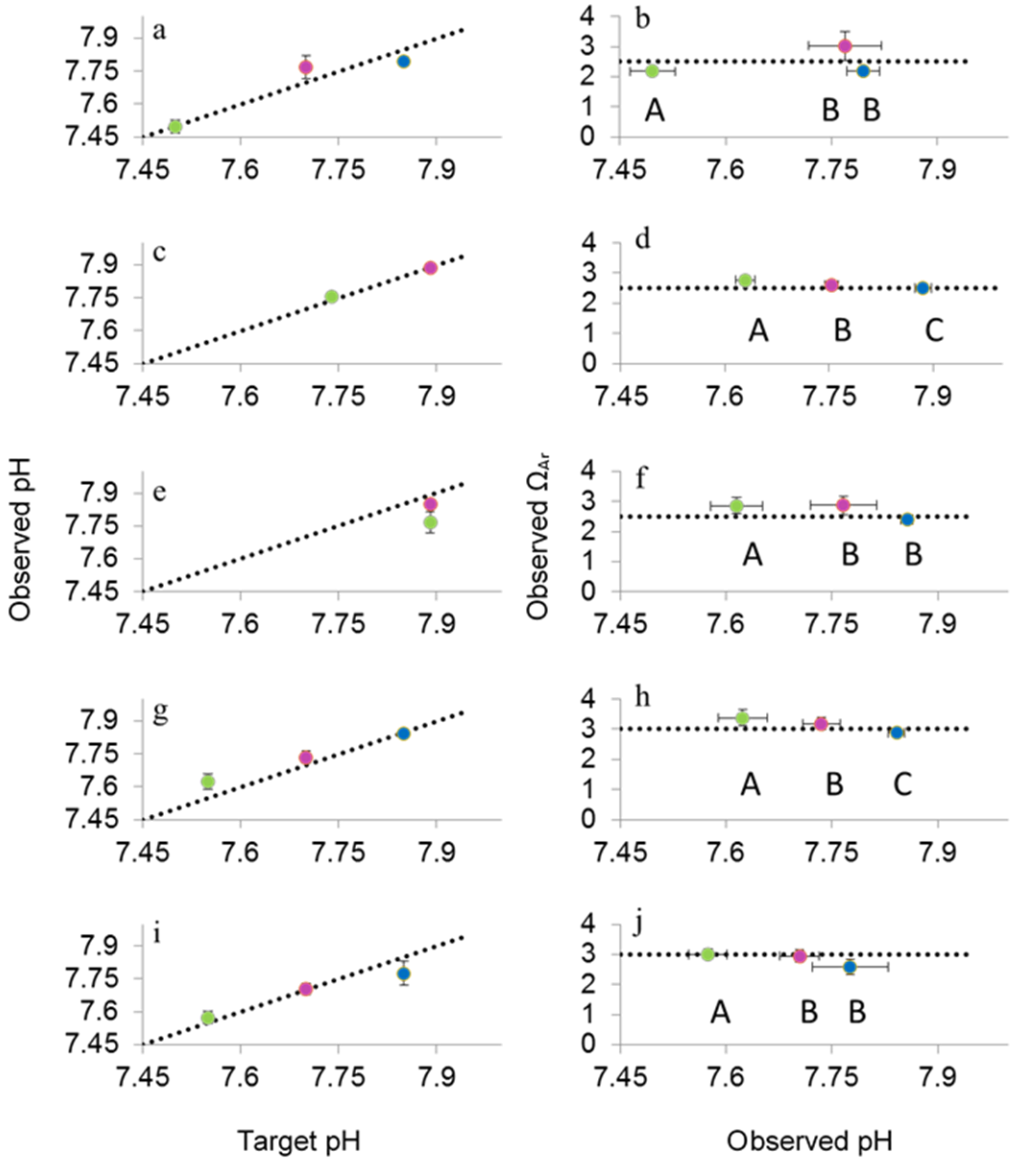

Figure 3.7. Examples of multiple manipulation experiments targeting constant Ω_{Ar} and varying pH levels. Each color corresponds to one manipulation channel. Error bars are Standard Errors (SE). Dotted line represents complete agreement between target and observations on $pH_{observed}$ versus pH_{target} plots (i.e. left panels), and target Ω_{Ar} in observed Ω_{Ar} versus observed pH plots (i.e. right panels). a-b) Experiment conducted in October 2015; c-d) Experiment conducted in March 2016; e-f) Experiment conducted in April 2016. g-h) Experiment conducted in July 2016; i-j) Experiment conducted in August 2016. Capital letters correspond to Tukey multiple comparisons on arcsine square root transformed proportions, p-value <0.1.

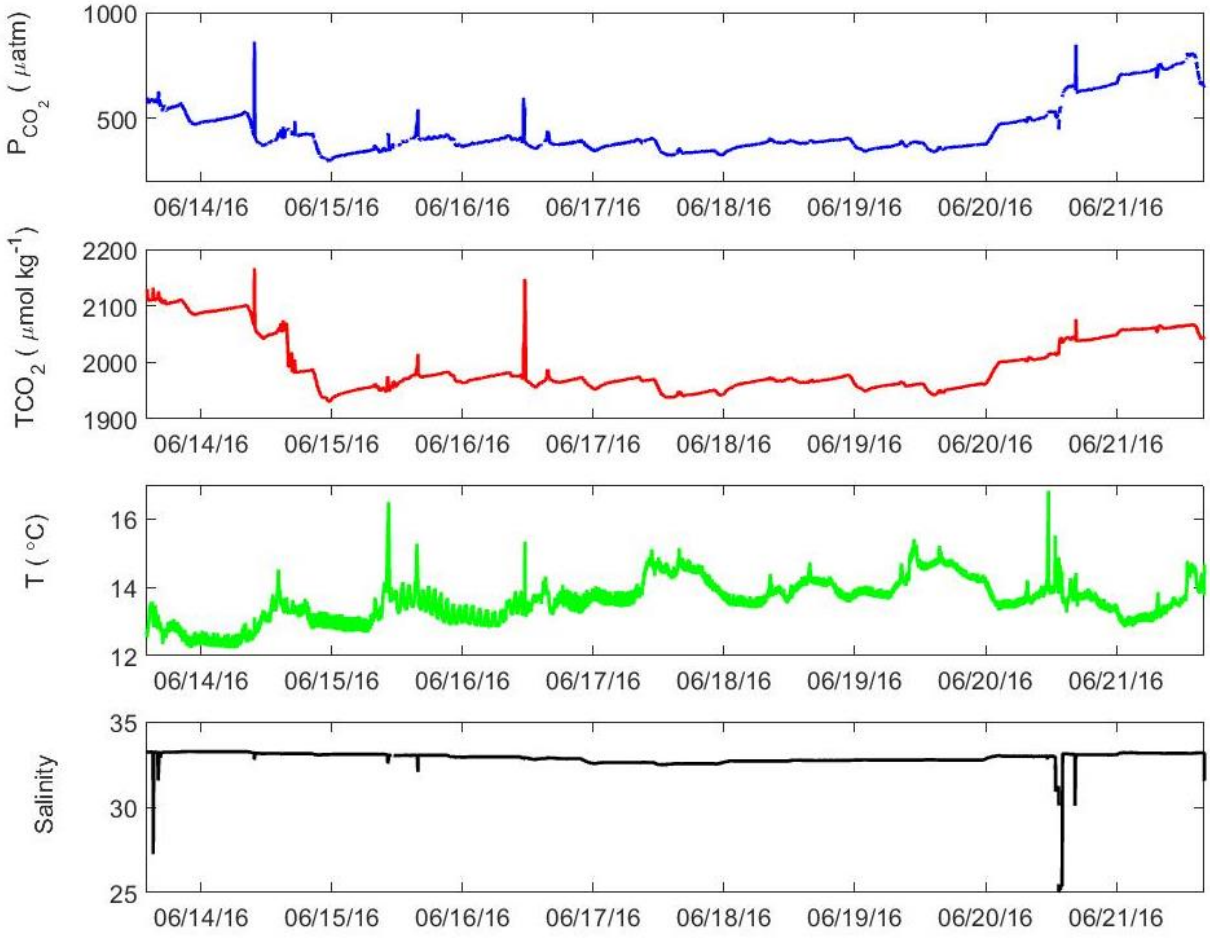

Figure 3.8. Time-series of source seawater conditions during the experiment with stable, dynamic and off-set simultaneous target manipulations.

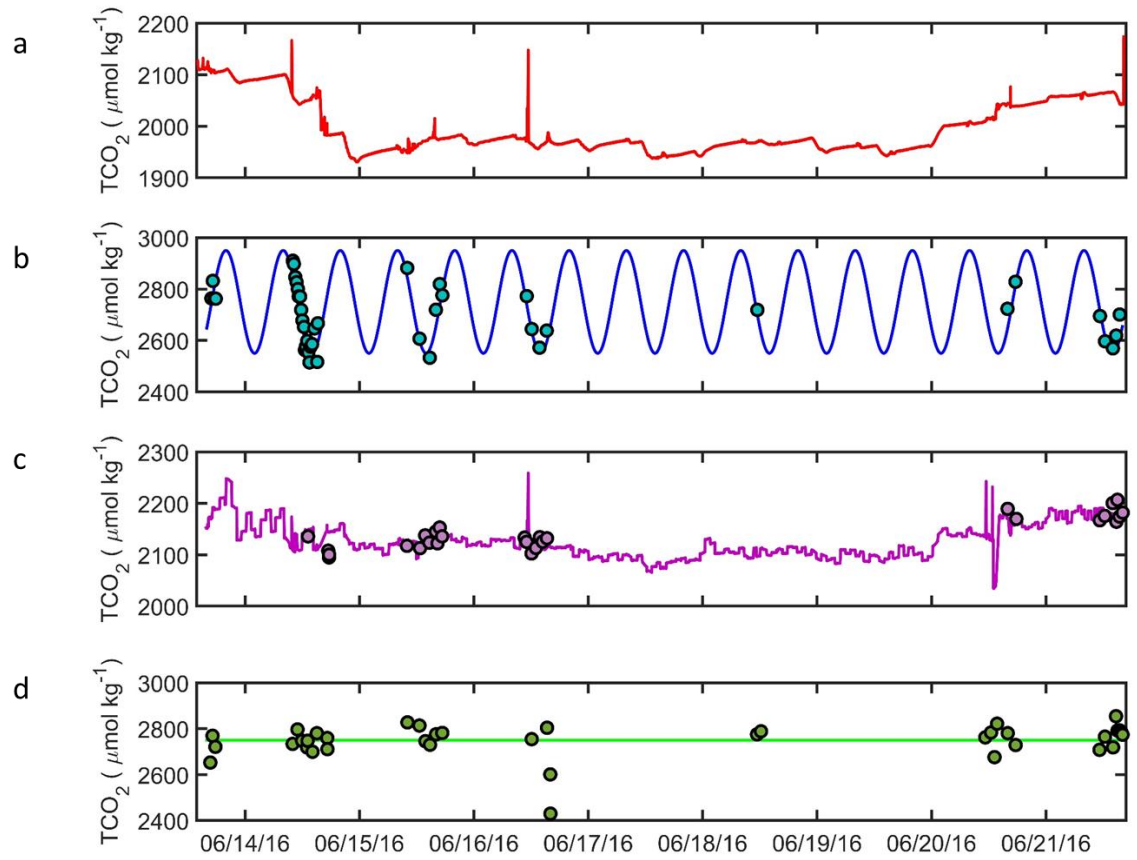

Figure 3.9. Stable, dynamic and off-set TCO_2 manipulations with moderately dynamic source seawater input. a) In red, time-series of three simultaneous carbonate chemistry manipulation treatments. b) In solid blue, idealized sinusoidal TCO_2 target for dynamic manipulation treatment. Blue dots are discrete samples from this dynamic treatment. c) In solid pink, offset TCO_2 target based on ΔPCO_2 projections for 2100 under RCP6.0. Pink dots are discrete samples from this offset treatment. d) In solid green, TCO_2 target for stable manipulation treatment. Green dots represent discrete samples from this stable treatment.

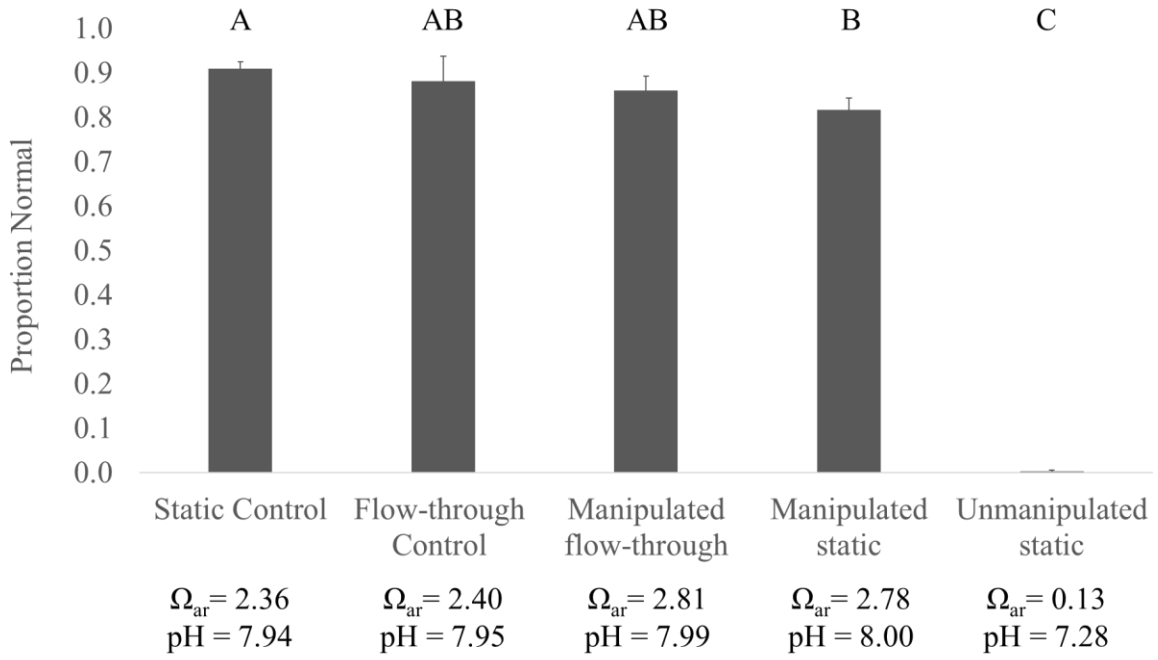

Figure 3.10. Proportion of normally developed Pacific oyster (Crassostrea gigas) at 48 hours post-fertilization. Error bars are Standard Deviations (SD) of replicate culture chambers per treatment (n=5, except for Manipulated Static n=4). Carbonate chemistry parameters correspond to the carbonate chemistry conditions for each treatment shown in Table 3.3. Letters correspond to Tukey multiple comparisons on arcsine square root transformed proportions, p-value <0.1.

4. CHAPTER IV.- Alkalinity fluxes from natural and restored oyster reef intact cores under normal and moderately acidified experimental conditions

4.1 Abstract

Many bivalve species form shell aggregations in temperate, coastal estuarine environments. Oyster reefs, a type of bivalve aggregation, have long been recognized as important agents in benthic-pelagic coupling and nutrient recycling in coastal areas; however, their biogeochemical feedbacks concerning inorganic carbon cycling have not been well constrained. Bivalve species have been generally identified as sensitive to ocean acidification (OA) and most studies have focused on organismal responses in isolation, thus habitat responses at the reef-level are poorly understood. We measured alkalinity and other geochemical fluxes under varying PCO_2 conditions on intact cores from a restored Eastern oyster (*Crassostrea virginica*) reef in Harris Creek, MD, USA. The measured net alkalinity effluxes from the oyster reef to the overlying water averaged 117 ± 44 mmol m^{-2} d^{-1}, varying among cores from 57 to 230 mmol m^{-2} d^{-1}. These fluxes exceed most of the published values for coastal sediments and match or exceed those of coral reefs. Alkalinity fluxes were not significantly different across PCO_2 treatments corresponding to moderate OA conditions (PCO_2 from ~800 to 1,250 µatm). Calcium (Ca^{2+}), ammonium (NH_4^+), nitrate-nitrite (NO_x), soluble reactive phosphorous (SRP), and silicate (Si) were also measured to constrain sources of alkalinity. We also estimated solid-phase material budgets down core from Computed Tomography (CT)-scan images. Alkalinity generation was correlated with Ca^{2+} production, presumably from shell dissolution, a

relationship further reinforced with the correlation between alkalinity fluxes and estimated % shell volume. Additionally, we found that non-carbonate, inorganic sources of alkalinity, likely the result of high rates of organic matter respiration associated with net denitrification and precipitation of sulfide (H_2S) produced from sulfate reduction as iron-sulfide minerals, accounted from negligible up to 70% of the total alkalinity net flux. Our results suggest that for shell aggregations to be most effective at buffering microenvironments they need both calcium carbonate and deposition of organic matter, so both carbonate and non-carbonate alkalinity generating processes can contribute to the overall alkalinity production. Ultimately, sustainable shell aggregations might generate chemical refugia for larval settlement and juvenile recruitment, alleviating bottleneck effects on oyster populations and providing a local mitigation strategy to increasing ocean acidification.

4.2 Introduction

Multiple shell-aggregating bivalves have been shown to be vulnerable to ocean acidification (OA), with observed adverse biological responses spanning larval to adult life stages (see reviews in Kroeker et al., 2010; Gazeau et al., 2013). Recent evidence suggests that OA might be narrowing the optimal environmental "windows-of-opportunity" for sensitive life-history stages, leading to population bottlenecks (Barton et al., 2012; Walbusser et al. 2013a; Hales et al. 2017). Most of the accumulated evidence, however, has been collected in laboratory experiments examining physiological responses at the organismal level. While very valuable in identifying sensitivity mechanisms, organismal based studies preclude the evaluation of any

potential effects of bivalve aggregations in mitigating or exacerbating OA responses as a result of habitat level biogeochemical properties and feedbacks.

Bivalves have long been recognized as “ecosystem engineers” (Jones et al., 1997; Gutiérrez et al., 2003; Gutiérrez et al., 2011), as they fundamentally alter the physico-chemical structure and function of their habitat. These changes are largely the result of feeding strategies that generally couple pelagic and benthic processes (Newell et al., 2005) and bivalves’ production and concentration of shell material (Gutiérrez et al., 2003). Living and dead bivalve shells accumulate and serve as substrate for newly settled bivalves and other organisms, therefore resulting in a positive feedback loop whereby more “shelliness” attracts more shell-building organisms, elegantly described as the “taphononic feedback” by Kidwell and Jablonski, (1983).

Relatedly, bivalve aggregations have also been recognized as providers of important ecosystem services (Newell, 2004; Coen et al., 2007; Coen et al., 2011; Grabowski et al., 2012), including improving water quality through filtration, enhancing nutrient cycling due to their coupling of benthic-pelagic processes, and helping to stabilize the shoreline, mostly due to the tridimensional aggregation structures they form.

The co-location of labile, reactive organic C and $CaCO_3$ within a bivalve aggregation framework and sediment (Hargis Jr and Haven, 1999; Waldbusser et al., 2013) is likely to result in high rates of alkalinity cycling within these systems (Waldbusser et al., 2013). Shell production consumes alkalinity and produces CO_2, while shell burial “sequesters” alkalinity in the sediment that can be released back to the overlying water column if shell dissolution is

thermodynamically favored (Morse et al., 2007), metabolically-enhanced (Hales and Emerson, 1997; Jahnke and Jahnke, 2004; Burdige et al., 2008), or driven by bioeroders (Carriker et al., 1978; Carver et al., 2011; Dunn et al., 2014; Carroll et al., 2015). Shell precipitation/dissolution dynamics can therefore act as an analogous to the ocean's "carbonate pump" within the aggregation (Waldbusser et al. 2013b). Aerobic respiration of biodeposits located in close proximity to shells will likely result in increased shell dissolution and, ultimately, partial buffering of metabolic acids (Waldbusser et al., 2013), as observed in other sediment environments (Hales and Emerson, 1997; Burdige et al., 2008).

If calcification and dissolution were the only processes affecting alkalinity cycling within shell aggregations, however, a mass balance would need to be achieved over long temporal and spatial scales. An accreting reef would result in a net sink of alkalinity, while a degrading reef would represent an alkalinity source to the overlying water. There are, however, other biogeochemical processes that can affect alkalinity dynamics within coastal sediments, including shell aggregations.

The primary and secondary biogeochemical processes contributing to alkalinity generation and consumption in coastal sediments are complex and dependent on the predominant anaerobic remineralization pathway (e.g. denitrification, iron-manganese reduction or sulfate reduction) and the net system-loss of reduced by-products of anaerobic respiration of organic matter either due to, for instance, outgassing (N_2 loss due to denitrification or anaerobic ammonium oxidation) or precipitation (HS^- or S^{2-} precipitation in the form of iron oxides such as pyrite) (Hu and Cai, 2011).

Nitrogen loss from the system as the result of denitrification increases alkalinity in a 1 NO_3^-:1 alkalinity molar ratio (Soetaert et al., 2007; Krumins et al., 2013). Some authors have questioned the overall effect of denitrification as contributor to global alkalinity (Hu and Cai, 2011), as a global N-cycle in steady-state requires a mass-balance between nitrogen fixation (-1 mol of alkalinity per mol of NO_3^- fixed, assuming fixation and nitrification) and denitrification (+1 mol of alkalinity per mol of NO_3^- consumed) (Wolf-Gladrow et al., 2007). Whether the global N cycle is in steady-state (Deutsch et al., 2007), or unbalanced (Hulth et al., 2005), the spatial decoupling of nitrogen fixation and denitrification in the global oceans results in the potential for denitrification to significantly affect alkalinity fluxes at local and regional spatial scales (Wolf-Gladrow et al., 2007; Hu and Cai, 2011).

A triumvirate of biogeochemical properties associated with oyster reefs have been proposed as the combined drivers of observed enhanced denitrification (Kellogg et al., 2014). First, elevated deposition of labile organic matter in the sediment, the result of production of biodeposits (i.e. oyster feces and pseudofeces) and physical retention of particulate organic carbon (POC) by the reef structure (Newell et al., 2005). Second, the presence of suboxic conditions near the sediment-water interface and the absence of significant microphytobenthos primary producers (Newell et al., 2005). Third, the provision of increased surface area in the form of calcium carbonate ($CaCO_3$, shell) for denitrifying microorganisms. Recently, living oyster shells have also been identified as potential hotspots for denitrification (Jackson et al., in prep; Kellogg et al., 2013; Smyth et al., 2013; Caffrey et al., 2016; Arfken et al., 2017).

The accumulation of organic carbon within the oyster reef framework as biodeposits and trapped allochthonous POC can also lead to high rates of anaerobic sulfate reduction. Sulfate reduction is the most important pathway of organic matter remineralization in organic-rich sediments like those found in oyster reefs, where oxygen is restricted to the top few centimeters of the sediment layer (Jørgensen, 1982; Burdige, 2006). Net precipitation of iron-sulfide minerals, through the intermediate production of sulfide as sulfate reduction by-product, would result in additional production of alkalinity in oyster reefs (Hu and Cai, 2011) in a 1:2 molar ratio of SO_4^{2-} consumed (or HS^- precipitated) per alkalinity produced.

Despite the multiple biogeochemical processes likely affecting alkalinity dynamics in bivalve aggregations, alkalinity and other relevant biogeochemical fluxes in these habitats have not been well constrained. From a physico-biogeochemical prospective, most studies on bivalve aggregations have focused on oyster reefs and have investigated their role in pelagic-benthic coupling and the associated effects in organic carbon and nutrient cycling (Dame et al., 1989; Newell et al., 2005). Nitrogen removal processes, mainly the result of enhanced organic matter burial and denitrification (Newell et al., 2005), have received particular attention in recent years (Kellogg et al., 2014).

In spite of the significant role that nearshore habitats potentially play in regional and global carbon cycles, there are significant knowledge gaps in the quantification of benthic alkalinity fluxes in these environments (Hu and Cai, 2011; Krumins et al., 2013). Before the global decline of oyster reefs due to disease and overharvesting (Beck et al., 2011; Zu Ermgassen et al., 2012), oysters reefs were ubiquitous in coastal, temperate habitats, and the focus of many

active restoration strategies (Luckenbach, M. W.; Mann, R.; And Wesson, J. A., 1999). Their ecological importance, therefore, further warrants the investigation of their potential role in alkalinity and inorganic carbon cycling in shallow, coastal environments (e.g. Waldbusser et al., 2013), particularly considering that the global carbonate budget has yet to be fully balanced (Milliman, 1993; Milliman and Droxler, 1996; Smith, 2013).

Understanding the alkalinity cycling within oyster reefs is also necessary to understand the impacts of OA on individual oysters living within the reef. We hypothesize that net alkalinity fluxes from oyster reefs to the overlying water might be affected by OA and, potentially, could transiently buffer corrosive conditions within the oyster reef, as suggested by Waldbusser et al., 2011 and Waldbusser et al., 2013. The goals of this study, consequently, were to evaluate biogeochemical fluxes between the overlying water on oyster reefs under different PCO_2 levels.

Despite the impacts of oyster reefs in biogeochemical cycling, direct measurement of biogeochemical fluxes are scarce and logistically challenging (Dame et al., 1984; Boucher and Boucher-Rodoni, 1988; Dame et al., 1989; Humphries et al., 2016). Previous oxygen, nitrogen and phosphorous flux measurements on restored oyster reef assemblages by Kellogg et al., 2013; and Jackson et al. in prep. demonstrated that high oxygen demand results in overlying O_2 saturation levels reaching severe hypoxia or even anoxic conditions in less than three hours in incubations. Short incubations (<2 hours) prevent the measurement of meaningful alkalinity fluxes due to the small signal-to-background ratio achieved during such brief periods. Thus, exploring the effects of altering the carbonate chemistry conditions of the overlying water to the

alkalinity fluxes in oyster reefs required a different methodological approach than traditional, sealed incubations.

In order to bridge the insight to be gained from performing direct measurements of biogeochemical fluxes in oyster reefs and the need to experimentally manipulate the incubation conditions, we: 1) implemented a vibracoring system to obtain intact, oyster reef cores and to incubate them in laboratory controlled settings; 2) developed an experimental system that allowed us to manipulate PCO_2 conditions of the overlying water while maintaining oxygenated conditions during core incubations; 3) evaluated alkalinity fluxes under different ocean acidification scenarios on intact cores from a restored Eastern oyster (*Crasoostrea virginica*) reef in Harris Creek, MD; and 4) attempted to discern or differentiate alkalinity derived from shell dissolution and other biogeochemical processes.

4.3 Materials and Methods

4.3.1 Study area

We chose three sampling sites within Harris Creek (38°45’12.46” N, 76°18’27” W), a tidal-dominated tributary to the Choptank River located in the mesohaline, mid-bay region of Chesapeake Bay, on the eastern shore of Maryland, USA (Figure 4.1). Harris Creek is also the location for the subtidal Harris Creek Oyster Sanctuary, a large-scale oyster reef restoration effort completed in 2015 that has restored more than 140 ha of suitable oyster reef habitat by out-planting oyster seed and additional substratum (i.e. shell) (National Oceanic and Atmospheric Adminisitration (NOAA), 2016). Six cores were collected across the three sites as follows. Core

1 was collected in June 2nd, 2017 within restored Reef #9 (38°45'43.8" N, 76°18'23.4" W; Figure 4.1), a 4.97 ha reef seeded with 47.23 millions of seed (oyster spat) in 2012 (NOAA 2016), and with an average density of live oysters of 32.18 oyster m^{-2} as of 2015 (NOAA 2016). Cores 2 and 3 were also collected on June 15th, 2017 at a site not subjected to restoration efforts (38°44'9.82" N, 76°18'24.84" W; Figure 4.1). Cores 4, 5 and 6 were obtained on June 15th, 2017 within Reef #11 (38°45'8.53" N, 76°18'37.51" W; Figure 4.1), a 2.64 ha reef seeded in 2012 with 28.19 millions of oyster spat, and with an average density of live oysters of 20.39 oysters m^{-2} as of 2015 (NOAA 2016).

At each site, bottom water temperature and salinity were measured using a handheld multiparameter sensor (YSI 600XLM). Bottom water temperatures ranged between 23°C and 28°C, while salinity values reached between 11 and 13 psu at the time of collection across all sites and dates. All sites were shallow, with water depths varying from 2.2 to 2.4 m, and bottom water oxygen saturation ranging from 72% to 99%, similar to monitoring data recorded by the Harris Creek Profiler (Maryland Department of Natural Resources, 2018).

4.3.2 Oyster reef core collection

Undisturbed, intact oyster reef cores were obtained by operating a customized, portable vibracoring system deployed from a small oceanographic vessel. Briefly, the vibracoring head is powered by a 5.5 hp gasoline engine (Honda GX160) connected through a flexible cable. The vibracoring head is housed inside a steel pipe cylindrical holder and attached to a steel, vertical pipe coring guide or hoisting mast. This vibracoring structure was then directly

attached to rigid, polyvinyl chloride (PVC) core tubes (50 cm long, 15.5 cm inside diameter) through two stainless steel clamps welded to the vibracoring holder. The core tubes were fitted with a PVC core cap with an associated ball valve. The valve was kept open during coring to allow free flush and minimal sample disturbance and remotely closed before core recovery to induce a partial vacuum pressure to retain the sediment. Additionally, each core tube bottom was fitted with a customized, stainless steel core-catcher to further mitigate the loss of sample upon core recovery.

After collection, each core was capped and kept partially submerged in unfiltered water to limit warming and light exposure while transported to Horn Point Laboratory, Cambridge, MD. Upon arrival to the laboratory, all cores were uncapped and submerged in a flow-through water bath with filtered Choptank River water until incubations were conducted. The water bath was gently aerated and kept at similar environmental conditions found in Harris Creek (Salinity of 11.0 – 11.7 psu, temperature between 22.5°C and 25°C).

4.3.3 Acidification experimental treatment design

It was determined in pilot studies that the metabolic rates of the cores would extinguish oxygen in closed core incubations before we anticipated measurable alkalinity fluxes. We therefore designed an incubation system that would allow us to maintain O_2 saturation levels above 50% for a minimum of 10 hours and impart various PCO_2 treatments in the overlying water. Surface PCO_2 values below atmospheric levels (~390 μatm) and significantly above (~700 μatm) have been measured in the mesohaline, mid-bay region of Chesapeake Bay (Cai et

al., 2017). Furthermore, greater PCO_2 values should be expected near the sediment-water interface, where under-saturation of O_2 has been measured (Cai et al., 2017), likely the result of aerobic respiration of organic matter and, therefore, associated with the production of metabolic CO_2. We chose, therefore, three PCO_2 levels: low, ambient PCO_2 (target: 400 μatm PCO_2; $\Omega_{Ca} \sim 1.7$), medium (target: 800 μatm; $\Omega_{Ca} \sim 0.97$), and high (target: 1,600 μatm; $\Omega_{Ca} \sim 0.5$), likely representative of conditions already occurring in the sediment-interface of Harris Creek restored oyster reefs and expected to become more frequent (i.e. medium and high) in future scenarios caused by the combination of anthropogenic induced OA and eutrophication. Treatments were applied to the individual cores in a cross-over design (low-medium-high-medium-high-low) resulting in a minimum of two measurements per treatment per core.

4.3.4 Core incubation system

Our incubation system is shown in Figure 4.2. For each incubation, cores were sealed by affixing lids, modified polypropylene rubber expansion plug fitted with two sampling ports: one for sample withdrawal and another for water replacement during sampling. Additionally, each lid was fitted with a suspended, submerged coated magnet. Cores were then arranged around a central rotating magnetic stirrer to mix the core's overlying water and prevent stratification. A closed, overlying water recirculating loop was set-up for each core during incubations to reestablish gas partial pressures. Antimicrobial tubing (Tygon S3^{TM}, Saint-Gobain Performance Plastics) was connected to both each core inlet and outlet and the overlying water was recirculated at a constant flow rate of 60 mL min^{-1} through the lumsenside of a membrane

contactor (3M™ Liqui-Cel™ MM-1.0x5.5 Series Membrane Contactor, Liqui-Cel). To achieve each target PCO_2 treatment, we stripped CO_2 from dry, ambient air with reagent grade soda lime (CaO/NaOH), and mixed it with pure CO_2 at the desired mass ratios by means of paired mass flow controllers (MFC): one for the zero-CO_2 air (2 standard L min^{-1}, Alita) and a second one for pure CO_2 gas (0.002 standard L min^{-1}, Alita). The resulting mixed gas stream was then circulated through the shellside of each membrane contactor at flow rate of 500 mL min^{-1}. Both liquid and gas flows were maintained separately by two multichannel peristaltic pumps (Masterflex series, Cole-Parmer™), with each pump controlling liquid or gas flows, and one channel per pump corresponding to each core. A flow-through cell equipped with an oxygen sensor (FireSting O_2-Mini oxygen meter) was installed immediately before the inlet of each membrane contactor to monitor changes of oxygen saturation in each core's overlying water over time. The oxygen sensors were calibrated daily by applying a two-point calibration curve consisting of seawater treated with sodium sulfite (Na_2SO_3) and seawater heavily aerated to achieve 0% and 100% O_2 saturation, respectively.

4.3.5 Biogeochemical flux measurements

The experimental system could only accommodate four cores at a given time, thus experiments were conducted on up to three oyster reef cores at a time, in addition to one blank core containing only water from the water bath. All incubations were conducted between June 9th and July 3rd, 2017. Prior to flux incubations, cores were allowed to fully re-oxygenate for a minimum of 24 hours in between experimental incubations.

Discrete overlying water samples were collected for alkalinity, dissolved inorganic Carbon (DIC), calcium, sulfate (SO_4^{2-}), ammonium (NH_4^+), nitrate-nitrite (NO_x), soluble reactive phosphorous (SRP, or ortophosphate), and silicate (Si) four times during each incubation, approximately every two hours after the start of the experiment. Samples were collected by briefly interrupting the closed, recirculating loop of each core's overlying water and fitting a sampling tube to the lid while allowing water from the incubating tank to replace the volume sampled. The approximate total sample volume collected at each sample point was 100 mL, or less than five percent of the total overlying water. No corrections for dilution were made.

Samples for alkalinity, DIC, and calcium were immediately preserved with saturated $HgCl_2$ (approximately 0.03% final concentration) and tightly sealed. Calcium samples were then filtered through a 0.45 μm nylon or poly-sulfonated syringe filter prior to analysis. Samples for SO_4^{2-}, NH_4^+, NO_x, SRP, and Si were filtered through a 0.45 μm nylon or poly-sulfonated syringe filter and immediately frozen until analysis.

Alkalinity was measured in an automated, open-cell titrator (Apollo SciTech, Cai and Wang, 1998), while DIC was measured using an infrared-based analyzer (Apollo SciTech; Cai and Wang 1998). Both analyzers were calibrated with Certified Reference Materials (CRM batch #146, Andrew Dickson's laboratory, Scripps Institution of Oceanography). Combined analytical uncertainty was estimated as 2% for alkalinity and 0.7% for DIC based on the reproducibility (coefficient of variation) of independent measurements of CRMs. Paired alkalinity and DIC values for each sampling point, core, and incubation experiment were then used to calculate all carbonate chemistry parameters using CO2SYS (version 1.1, MATLAB) following carbonic acid

equilibration constants from Millero (2010), Dickson (1990) constants for sulfate and total boron from Uppstrom (1974). Calcium samples were diluted 100-fold and measured on an inductively coupled plasma-optical emission spectrometer (ICP-OES Arcos, Spectro). Analytical uncertainty of calcium was estimated as 1.5% based on reproducibility of independent measurements of reference standard seawater (IAPSO Standard Seawater, OSIL). SO_4^{2-} samples were thawed, diluted 100-fold and analyzed by ion chromatography (HPIC Integrion, Thermo Integrion). Analyses of NH_4+, NO_x, SRP, silicate, were performed on a Smartchem discrete chemical analyzer (Westco Scientific, Danbury, CT). Ammonium was analyzed using a modification of the phenol method as outlined by Koroleff (1976). NO_x was measured following a modification of EPA method 353.2. Dissolved Inorganic Nitrogen (DIN) was computed as the sum of NH_4^+ and NO_x. SRP analysis followed a modification of the EPA method 365.2 and Si was analyzed according to Strickland and Parsons (1972).

Fluxes were determined as the slope of robust linear regressions (Jajo, 2005) of concentration over time. Only slopes statistically different from zero and regressions with adjusted coefficient of determination (i.e. adj-R^2) greater than 0.5 were considered as significant fluxes. Core fluxes were corrected by subtracting associated blank fluxes if the latter were deemed significant.

4.3.6 Computed tomography (CT) scans, material budget estimates and 3-D reconstructions

On July 7th, 2017, following completion of flux measurements, all oyster reef cores were stabilized for transport following previously described practices (Rosenberg et al., 2007; Davey

et al., 2011). Briefly, overlying core water was carefully drained and the sediment surface was covered with several layers of medical gauze and either sand or a mixture of Cream of Wheat (Nabisco) and seawater was poured over to completely cover the space. Finally, core tops were sealed with expansion plugs.

Stabilized cores were transported to Memorial Hospital (Easton, MD) to be scanned via computed tomography (CT-scan, LightSpeed16 multi-detector, General Electric). The parameters of all CT-scans were constant for all cores and consisted in slice thickness of 0.625 mm and power settings of 120 kV and 98-106 mA. The resultant pixel size was 0.703 mm x 0.703 mm, with an associated pixel area of 0.494 mm^2 and a voxel volume of 0.309 mm^3. The raw images from each CT-scan contained core cross-sections corresponding to the slice thickness and each pixel returned a CT-number or intensity number, a function of material density and atomic number.

We calibrated the obtained CT-numbers to reflect sediment materials with the use of calibration standards that were scanned in conjunction with the cores. The calibration standards included a glass rod, and plastic pipettes containing seawater and air. Based on the calibration standards CT-numbers and previous published results (Rosenberg et al., 2007), we binned the intensity results into five categories corresponding to five sediment materials: air (CT-numbers ranging from -1,055 to -400), water (-400 to 300), high porosity sediment (300 to 900), low porosity sediment (900-1,200), and calcium carbonate shells (1,200 to 2,500).

We reconstructed proportional volume material budgets vertical profiles on each core based on the proportion of pixels corresponding to each of the five materials in each CT scan

image. We first applied a Gaussian blur filter to all selected images to reduce noise and streaking due to beam hardening. Subsequently, we excluded an area of 4 pixels around the edges of all images to exclude potential sediment disturbances along the core walls derived from sampling and we omitted core bottom cross-sections that included the metal core-catcher.

Previously described shell CT-number threshold was also used to perform particle analysis on core sections and extract estimates of shell surface area and shell perimeters on all images. Image processing and analysis was conducted with ImageJ (v. 1.52d). We used unedited images to reconstruct the 3-D internal structure of the cores using the software 3D Slicer (v. 4.8.1).

4.3.7 Statistical analysis

We computed robust regressions of solute concentrations over time to calculate biogeochemical fluxes, which are particularly suited for datasets with outliers and unequal variances. We then evaluated the successful separation of experimental treatments through one-way analysis of variance (ANOVA) with manipulation treatment as a factor. We analyzed the effect of experimental treatments on computed fluxes by ANOVA on fitted mixed linear models with treatment as a fixed factor and experiment date and core as random factors. Normally distributed residuals were checked by visual inspection of Q-Q plots. We then performed ANOVA to evaluate if the models containing treatment were explaining more variance in the results by comparing fitted nested, reduced models without treatment and reduced models excluding the fixed factor. We explored correlations between alkalinity fluxes and solid phase

core characteristics estimated from analyses of CT-scan data through the non-parametric correlation Spearman coefficient. All statistical analyses were conducted on Rstudio (version 1.1.456).

4.4 Results

4.4.1 Sample collection

Some collected cores contained a visible mixture of living oysters and dead shells at the sediment-water interface, however live oysters were partially buried by fine sediments (Figure 4.3), as has been previously observed on assembled trays collected in the same area (Jackson et al., in prep.). Sediment samples obtained from the maximum core penetration depths (approximately 38 cm) showed a dense matrix of shell and degraded shell material (i.e. shell hash) (Figure 4.3)

4.4.2 Experimental conditions

While the experimental system succeeded in maintaining oxygen saturation levels greater than 50% during the 10-hour core incubations, the calculated PCO_2 values did not achieve the experimental targets, resulting in inadequate separation of treatments (Table 4.1). Although there was a nearly significant effect of treatment on PCO_2 values (ANOVA, $F_{35,2} = 3.138$; $p = 0.056$), post-hoc Tukey pairwise comparisons demonstrated that only the Low and Medium treatment were significantly different from each other.

Incubations for the Medium and High treatments performed at earlier dates showed overall greater mean PCO_2 values, at times displaying greater variability within replicate incubations of same cores than across treatments (Figure 4.4, Top). Conversely, the Low treatment incubations displayed the reverse pattern (Figure 4.4, Top), with greater PCO_2 values at later incubations.

Overall mean saturation states for calcite (Ω_{Ca} = 0.98-1.19) were close to the threshold of thermodynamic solubility stability (Ω_{Ca} = 1), while closer examination of individual core computed values showed earlier incubations for both the Medium and High treatments resulted in undersaturated values with respect to calcite, with particularly corrosive conditions for the Medium treatment (Figure 4.4, Bottom).

4.4.3 Biogeochemical fluxes

Despite the difficulties in maintaining separation of experimental treatments, there was a large net release (positive flux) of alkalinity from the oyster reef cores to the overlying water and under all experimental conditions. Calcium and silicate fluxes were generally out of the oyster reef to the overlying water, while SRP, NH_4^+, NO_x, and DIN (i.e. $NH_4^+ + NO_x$) fluxes were mixed but generally into the oyster reef (Table 4.2, 4.3, Figure 4.5). Alkalinity fluxes were nearly always significantly different from zero and linear with respect to time (95% of the measurements) (Table 4.2), however some flux estimates for other solutes resulted in non-significant or non-linear flux estimates, even after omitting statistical outliers, and were therefore excluded from further analyses. The percentage of omitted computed fluxes ranged from 37%

(Ca^{2+}) to 58% (NH_4^+). We excluded all SO_4^{2-} flux results after more than 70% of the regressions were considered non-significant or non-linear and the remaining estimates presented concerns regarding their validity, as they seemed abnormally high and analytical issues were suspected (Table 4.2).

The overall average alkalinity flux was 117 ± 44 mmol m^{-2} day^{-1} across all cores and experimental treatments, with a minimum of 57 and a maximum of 230 mmol m^{-2} day^{-1} (Table 4.3). Ca^{2+} average flux was 65.6 ± 40.3 mmol m^{-2} day^{-1}, with 11.7 and 89.7 mmol m^{-2} day^{-1}, as minimum and maximum values, respectively. NH_4^+ average flux was 5.46 ± 5.47 mmol m^{-2} day^{-1}, whereas NO_x was estimated to be 1.45 ± 2.60 mmol m^{-2} day^{-1}, and the combination of measured N-species (i.e. DIN; $NH_4^+ + NO_x$) resulted in an average of 7.28 ± 5.71 mmol m^{-2} day^{-1}. SRP average flux was -0.06 ± 0.30 mmol m^{-2} day^{-1}, whereas Si estimated value was 12.38 ± 7.50 mmol m^{-2} day^{-1}.

Differences among replicate core treatments (i.e. same experimental date and treatment) were the greatest source of variance in results (53% of variance), suggesting core-core heterogeneity was significant relative to experimental treatment. Comparison of treatment flux averages also indicated notable variability (27% of variance) within replicate measurements (i.e. same core and treatment, different date) (Figure 4.5). Analysis of variance demonstrated no significant effect of treatment when date of experiment and core were included as random effects in the model for all solutes except DIN ($F_{26,2} = 7.01$, $p = 0.0053$). Further demonstrating the lack of effect of the experimental treatments, a post-hoc analysis of variance comparison showed no statistically significant improvement on the variance explained by models including treatment as

a parameter when compared to a reduced model without treatment, except for a mild improvement in the case of DIN ($X^2_{6,4}$ = 8.43, p = 0.0148).

Alkalinity fluxes were correlated with other biogeochemical fluxes (Figure 4.6). We found highly significant robust linear relationships between alkalinity and Ca^{2+} fluxes (Figure 6a, Adjusted R^2=0.686, p <0.001), combined NH_4^+ and NO_x fluxes (Figure 4.6d, Adjusted R^2 = 0.418, $p<0.001$), and silicate fluxes (Figure 4.6e, Adjusted R^2 = 0.686, $p = 0.001$). We also found statistically significant regressions between alkalinity fluxes and NH_4^+ fluxes (Figure 4.6b) and NO_x fluxes (Figure 4.6c) individually, but we cautiously interpret the validity of these models due to the poor fit of linear regressions to the data (Adjusted R^2 < 0.3).

4.4.4 CT-scan material budgets

An example of a CT image of a cross section of a core, and the associated estimated material budget is shown in Figure 4.7, while the total estimated material budgets for all cores are shown in Table 4.4. Although the oyster reef cores showed an heterogenous inner composition of materials, and there was variability among cores in the relative contribution of the assessed materials to the overall composition of each core, sediment, including both low and high porosity sediment types, was the dominant component relative to total volume for all cores, ranging from 65.1% (Core 5) to 74.5% (Core 3). The volumetric contribution of shell ranged from 20.8% for Core 3 to 28.1% for Core 6. There was a statistically significant effect of collection site in the percentage of shell ($F_{6,2}$ = 11.61, p = 0.0387), but post-hoc Tukey comparisons demonstrated that there was only significant differences in the amount of shell

present between cores 2, 3 (i.e. non-restored site) and cores 4, 5, 6 (restored site), with greater shell content for the restored site. Shell content for core 1 (another restored site) fell in between and was not statistically different from any of the other cores.

Shell surface area and shell perimeter, secondary shell parameters derived from shell particle analysis, were not statistically different across sites. The estimated shell surface area was significant and negatively correlated with the volumetric percentage of shell (Figure 4.8f, R = -0.66, $p = 0.003$), whereas shell perimeter was not correlated with percentage of shell (R = -0.2, $p = 0.430$).

CT-scan cross-sections of each core and the associated 3-D reconstructions of the internal structure of the oyster reefs help to visualize differences in material spatial distributions across cores (Figure 4.8). Overall, the size of the shell fragments seems to decrease with depth, although there is variability across cores. For instance, Core 6 seems to show the most degradation of shell particles (Figure 4.8f), compared to relatively large shell fragments found at depth in Core 1 and 3 (Figure 4.8a, 4.8d). Similarly, Core 5 and 6 show substantial pockets of interstitial water down core and at the sediment-water interface, respectively (Figure 4.8e, 4.8f), compared to Core 4 (Figure 4.8d).

4.4.5 Alkalinity fluxes and estimated material budgets and shell characteristics

Alkalinity fluxes were correlated with estimated core material budgets (Figure 4.9). There was a strong positive correlation between alkalinity fluxes and volumetric percentage of shell (Figure 4.9a, R=0.61, p = 0.007). Alkalinity fluxes did not seem to be associated with shell

perimeter (Figure 4.9b, R= -0.38, p = 0.120), but they were strongly negatively correlated with shell surface area (Figure 4.9c, R= -0.75, p <0.001). Shell surface area is significantly correlated with percentage shell content (Figure 4.9e), complicating the interpretation of these results.

4.5 Discussion

We present, to our knowledge, the first measurements of alkalinity fluxes from intact oyster reef cores. Our data suggest significant alkalinity fluxes from oyster reefs to the overlying water (average of 117 ± 44 mmol m^{-2} d^{-1}), and while there is wide variability across cores, the range (57 to 230 mmol m^{-2} d^{-1}) is greater than most estimates of alkalinity fluxes in coastal habitats. A range of 0.5 – 6.5 mmol alkalinity m^{-2} d^{-1} has been proposed for coastal and shelf sediments based on modeling efforts (Hu and Cai, 2011; Krumins et al., 2013; Gustafsson et al., 2014), while incubations of intact cores of a very shallow mudflat ranged from 12-42 mmol m^{-2} d^{-1} (Gazeau et al., 2014). Cores from an intertidal sandflat resulted in an average alkalinity flux of 33 mmol m^{-2} d^{-1} (Rao et al., 2014). Carbonate-rich sediments displayed greater variability, and ranged from non-significant fluxes to 36 mmol m^{-2} d^{-1} for incubations of shallow sediments (Cyronak et al., 2013; Rassmann et al., 2018), to 12 and 52 mmol m^{-2} d^{-1} for core incubations and modeled advective fluxes, respectively, in sediments associated with seagrass beds (Burdige et al., 2008). Perhaps the most applicable comparison to an oyster reef habitat would be their tropical counterpart of dense aggregations of calcifiers: coral reefs. Lisle et al., 2014 estimated a range of 1 to 400 mmol m^{-2} d^{-1} in alkalinity diffusive fluxes for several coral reefs located in the Florida Keys, while Krumins et al. 2013 modeled the average net alkalinity efflux from coral

reefs as 5 mmol m^{-2} d^{-1}. Our results reveal the potential significant role of oyster reefs in alkalinity and inorganic C cycling in coastal areas when compared to alkalinity fluxes in other environments.

Our average NH_4^+ flux result (5.46 ± 5.47 mmol m^{-2} d^{-1}) is within the range of previous *in situ* estimates of NH_4^+ release (2.4-10.2 mmol m^{-2} d^{-1}) conducted utilizing a flow-through tunnel directly over subtidal oyster reefs by Dame et al., 1984. Comparing our estimates of nutrient biogeochemical fluxes to previous work in oyster reefs, however, warrants caution as, to our knowledge, this is the first time that intact cores from an oyster reef have been incubated. It is, however, informative to compare our results to estimates of biogeochemical fluxes in Chesapeake Bay measured in assembled trays, albeit these assemblages do not entirely represent the internal structure of the reef and might not accurately reflect the magnitude of all biogeochemical processes occurring within this system, particularly within the sediment. Kellogg et al. 2013 measured biogeochemical fluxes in assembled trays in the restored oyster reefs in the Choptank River, Chesapeake Bay and recorded NH_4^+ fluxes of 24-96 mmol m^{-2} d^{-1}, NO_x fluxes of 12-48 mmol m^{-2} d^{-1}, and 2.4-14.4 mmol m^{-2} d^{-1} fluxes of SRP, with lowest biogeochemical fluxes in November and April, intermediate values in June, and highest in August. It is worth noting, however, that the average density of oysters in Kellogg et al. 2013 (131 individuals m^{-2}) was more than 4-fold the density found in Harris Creek restored reefs reef (20-33 oysters m^{-2}, NOAA 2016). Jackson et al. in prep., measured a range of NH_4^+, NO_x and SRP on assembled trays of varying oyster densities in the Harris Creek restored reef. The flux measurements on

assembled trays with similar densities to the natural restored reef (33 oysters m^{-2}) showed average DIN fluxes of 24-96 mmol m^{-2} d^{-1} and SRP fluxes of 0.24-2.4 mmol m^{-2} d^{-1}.

Our measured fluxes (5.46 ± 5.47 mmol NH_4^+ m^{-2} d^{-1}; 7.28 ± 5.71 mmol DIN m^{-2} d^{-1} ; -0.06 ± 0.30 mmol SRP m^{-2} d^{-1}) are substantially lower than those measured by both Kellogg et al. 2013 and Jackson et al. in prep., likely the result of the differences between incubation techniques described above. Another possible, non-mutually exclusive explanation for the variance in biogeochemical fluxes lies on the spatial scale covered by each experimental technique. The reef area contained in our cores was small (0.019 m^2) and more than five times smaller than the assembled reefs trays (0.1 m^2, Kellogg et al. 2013, Jackson et al. in prep). Considering the heterogeneous and patchy distribution of living oysters within Harris Creek's restored reefs (NOAA, 2016), it is possible that some of our collected cores contained few or no living oysters, likely biasing down respiration rates and, therefore, nutrient fluxes, and potentially up-biasing alkalinity and Ca^{2+} fluxes.

The overall average alkalinity (117 ± 44 mmol m^{-2} d^{-1}, Table 4.3) and Ca^{2+} fluxes (65.6 ± 40.3 mmol m^{-2} d^{-1}, Table 4.3) strongly suggest that $CaCO_3$ shell dissolution is the dominant biogeochemical process responsible for observed alkalinity efflux, assuming a 2:1 molar ratio between alkalinity and Ca^{2+} (e.g. Zeebe and Wolf-Gladrow, 2001; Wolf-Gladrow et al., 2007). Indeed, comparing the average alkalinity and Ca^{2+} fluxes among treatments indicates roughly 74-105% of the alkalinity fluxes would be due to $CaCO_3$ dissolution (Table 4.3). The major contribution of shell dissolution to the measured net alkalinity fluxes is also supported by the highly significant positive correlation between shell content and alkalinity fluxes (Figure 4.9a).

Shell dissolution is expected to be a function of substrate availability (i.e. reactive surface area) (e.g. Hales and Emerson, 1997), therefore the observed strong positive relationship of total alkalinity fluxes with shell volume is expected. The overlying water average saturation state was near the thermodynamic equilibrium of $CaCO_3$ mineral calcite (Table 4.1), the dominant mineral phase in the sediment in the form of oyster shells. The magnitude of the observed fluxes, therefore, reveals the importance of metabolic-enhanced shell dissolution in lowering the saturation state in the top layers of sediment and, ultimately, leading to shell dissolution (e.g. Hales and Emerson, 1997; Burdige et al., 2008). The negative correlation between shell surface area and alkalinity fluxes (Figure 4.9c) is puzzling, as it would be expected greater shell surface area would lead to more exposed substrate for shell dissolution (Morse et al., 2007). It is possible, however, that the surface area estimates are biased, as the particle analysis spatial resolution was coarser than the pixel-resolution used for the estimate of overall shell content, thus underestimating the available surface area for small size shell fragments as compared to shell volume (e.g. Core 6).

A more nuanced inquiry into observed patterns of alkalinity and Ca^{2+} flux measurements revealed a more complex picture than just shell dissolution, however. When all disaggregated alkalinity and Ca^{2+} (i.e. without averaging replicates and cores) significant fluxes are compared (Table 4.2, Figure 4.5), the slope of the regression is 0.955 (Figure 4.6a), approximately half of the expected theoretical molar ratio of 2.00 if all the alkalinity flux was the result of shell dissolution. It is arguable that, given the high heterogeneity of oyster reefs, and the significant

variability among cores, analysis of only average flux values would preclude the evaluation of secondary processes contributing to alkalinity production.

The observed pattern in alkalinity fluxes might indeed reflect a more complex system with multiple sources and sinks of alkalinity, as it is common in shallow, coastal environments (Krumins et al., 2013). Ultimately, the result is a net flux that, although dominated by shell dissolution, cannot be entirely explained by this process. It is worth noting, however, that Ca^{2+} fluxes were less consistent compared to alkalinity, with more instances of non-significance or non-linearity (Table 4.2). Analytical precision errors in the Ca^{2+} measurements (1.5%) could result in some discrepancy between alkalinity and calcium fluxes. The expected small changes in Ca^{2+} concentrations compared to seawater's background levels result in a relatively high signal-to-background ratio that, ultimately, could lead to a lack of analytical sensitivity. It is, however, unlikely that poor precision Ca^{2+} measurements would have resulted in a systematic bias towards greater Ca^{2+} flux values that could explain the observed alkalinity regression slope of 0.955. Ca^{2+} measurements could also be biased towards lower numbers due to precipitation of non-calcium carbonate minerals (e.g. micrite). Precipitation of $CaCO_3$, besides also resulting in a net loss of alkalinity, is unlikely given the presence of inhibitors such as high concentrations of dissolved organic matter (Morse et al., 2007), commonly found in areas of Chesapeake Bay (Burdige, 2001). Collectively, these results indeed suggest that other biogeochemical processes besides shell dissolution might be affecting the net observed alkalinity fluxes.

Aerobic remineralization of organic matter generally consumes alkalinity, with all SRP species, NO_3^- and NO_2^- all reducing alkalinity in a 1:1 molar ratio (sensu Wolf-Gladrow et al.,

2007). NH_4^+ is a notable exception as it increases alkalinity in a 1:1 molar ratio, although in aerobic environments most of the produced NH_4^+ is ultimately oxidized to NO_3^- through nitrification, decreasing alkalinity in a 1:2 ratio (sensu Wolf-Gladrow et al., 2007). We applied a published overall nutrient-alkalinity factor based on Redfield ratios (i.e. -0.68 ΔNO_3^-; Wolf-Gladrow et al., 2007) to our overall average alkalinity fluxes, with the assumption that the DIN flux is a proxy for ultimate overall NO_3^- production. The net alkalinity flux can then be described as follows:

$$Alkalinity\ flux = 2Ca^{2+} - 0.68DIN \quad \text{Eq (1)}$$

Applying this correction, however, resulted in a marginal change of previous results, whereby the average alkalinity fluxes now represent 75-113% of the expected fluxes based on shell dissolution and aerobic remineralization of organic matter. The slope of the statistically significant regression between alkalinity fluxes and DIN fluxes (Figure 4.6d) is 4.6 (i.e. alkalinity *increases* 4.6 moles per mol of DIN produced), however, questioning the validity of the used 0.68 correction factor and, ultimately, suggesting that other nitrogen cycling processes might be contributing to the overall alkalinity fluxes.

Further evidence of the importance of other biogeochemical pathways that produce alkalinity is found if we disaggregate the alkalinity fluxes per core and treatment. Removing the effect of shell dissolution and aerobic remineralization of nutrients results in residual alkalinity fluxes with negative values (i.e. the measured alkalinity flux is lowered than modelled including only shell dissolution and nutrient release) up to more than 70% of the total net alkalinity flux attributable to inorganic non-carbonate alkalinity sources.

Inorganic non-carbonate alkalinity sources are, therefore, significant in oyster reefs, and are likely associated with anaerobic pathways of organic matter remineralization. Anaerobic pathways of early diagenesis of organic matter in the sediment generally result in the production of alkalinity, however, only significant sources of net alkalinity are observed if there is uncoupling of nitrification/denitrification processes or if there is net sulfate reduction (i.e. sulfate reduction is greater than hydrogen sulfide re-oxidization) (Hu and Cai, 2011; Krumins et al., 2013). Indeed, high rates of both of these processes are measured or predicted to be important within oyster reefs (Kellogg et al., 2014; Malkin et al., 2017).

Significant denitrification rates in oyster reefs were first proposed by conceptual frameworks suggesting enhanced nutrient cycling and benthic-pelagic coupling facilitated by bivalve aggregations (Newell et al., 2005), and subsequently confirmed by multiple experimental measurements, albeit with significant variability (see review in Kellogg et al., 2014). The potential for denitrification in regulating production of alkalinity is even more important when the source of substrate NO_3^- is considered (Hu and Cai, 2011). In Chesapeake Bay, a heavily eutrophied system (Kemp et al., 2005), terrestrial inputs of NO_3^- are significant (Hagy et al., 2004; Kemp et al., 2005). Denitrification of allochthonous NO_3^- would result in net production of alkalinity, rather than alkalinity regeneration as in the case of shell dissolution. Even if the net contribution of denitrification to the total alkalinity fluxes might be small, its role can result in a net gain for the system, thus warranting future investigation.

The accumulation of organic carbon within the oyster reef framework as biodeposits and trapped allochthonous POC can also lead to high rates of sulfate reduction. Sulfate reduction is

the most important pathway of organic matter remineralization in organic-rich environments like salt-marshes (Lord and Church, 1983) and, by extension, oyster reefs, where oxygen is restricted to the top few centimeters of the sediment layer (Jørgensen, 1982; Burdige, 2006). Sulfate reduction produces hydrogen sulfide, which if removed via mineral precipitation (e.g. pyrite formation or other iron-sulfide minerals, see review by Morse et al., 1987) or other means to prevent its reoxidation to sulfate, results in the production alkalinity in a 2 Alkalinity : 1 HS^- ratio (Hu and Cai, 2011). Holyoke, 2008 suggested observed and enhanced production of iron-sulfide minerals in shallow Chesapeake Bay sediments as a response of increased biodeposit deposition, therefore suggesting that iron is not limiting in this environment, thus, hydrogen sulfide precipitation in the form of iron complexes is favored. The lack of iron limitation claim is further supported by measurements of elevated dissolved Fe^{2+} (>800 µM) in top sediment layers from sediments collected in the mesohaline portion of Chesapeake Bay (Burdige, 1993). The above biogeochemical processes linked to the sulfur cycle represent, therefore, additional non-shell-based sources of alkalinity in oyster reefs are possible (Waldbusser et al. 2013b) and warrant further exploration.

Although our experimental design was insufficient to significantly increase the overlying water PCO_2 across experimental treatments, it did allow us to extend the core incubation times to ten hours by partially re-oxygenating the overlying water, thus allowing for the quantification of alkalinity fluxes in oyster reef intact cores for the first time. Gas exchange is a function of the gas concentration gradient and its transfer velocity. In our case, the concentration gradient was presumably much greater for O_2 than for CO_2, due to the redistribution of CO_2 gas into other

species part of the seawater DIC system. Furthermore, while CO_2 gas is more permeable than O_2 in polymer membranes like the one used in our experimental system (Waack et al., 1955), O_2 has a greater diffusion coefficient and, therefore, lower Schmidt numbers, than CO_2 (Wanninkhof, 2014), therefore contributing to a net slower gas transfer for CO_2 compared to O_2. Future experimental incubations designed to assess potential effects of OA in oyster reef alkalinity fluxes will benefit from pre-equilibration of the overlying water of the cores to achieve PCO_2 targets before the start of each experimental incubation (Gazeau et al., 2014; Rassmann et al., 2018). Reduced liquid flow rates would maximize contact time and, thus result in greater gas transfer which, ultimately, would contribute to maintain experimental treatments throughout core incubations. Smaller liquid flow rates will also result, however, in increased overlying water residence times, therefore potentially resulting in an increased incubation container effect.

While the lack of experimental treatment separation hinders our ability to make robust predictions of the potential effects of OA in oyster reef alkalinity fluxes, no difference in flux averages across a PCO_2 range of ~800 to 1,250 μatm (Ω_{Ca} = 0.98-1.20) suggest a relatively insensitive system to moderate acidification conditions, or an insufficiently long experimental exposure for the overlying PCO_2 conditions to penetrate into the biogeochemically active sediment layers. In a similar experiment conducted in Arctic sandy muds with ~ 20% $CaCO_3$, Gazeau et al. 2014 did not measure significant changes in alkalinity fluxes across a PCO_2 range of 317 to 1,256 μatm, corresponding to a range of Ω_{Ca} of 2.67 to 0.80, although a significant increase was measured at 3,169 μatm and a Ω_{Ca} value of 0.33. Conversely, Rassman et al. 2018 measured significant increases in alkalinity fluxes in cores incubated at PCO_2 2,020 μatm and

Ω_{Ca} of 1.25 when compared to the control (PCO_2 = 350 μatm; Ω_{Ca} = 5.00). These discrepancies may reflect differential sensitivities to acidified conditions by the main biogeochemical processes responsible for the generation of alkalinity in coastal zones: dissolution of calcium carbonate deposits, and alkalinity generated through anaerobic processes, primarily uncoupled nitrification/denitrification and net sulfate reduction associated with hydrogen sulfide precipitation (Hu and Cai, 2011; Krumins et al., 2013).

Carbonate dissolution is thermodynamically favored under Ω<1 and therefore expected to be enhanced during events of corrosive overlying water. The kinetics of this process, however, are slow (Morse et al., 2007). Waldbusser et al., 2011 measured oyster shell dissolution rates from -0.20% to 0.00% per day under Ω_{Ca} conditions ranging from 0.47 to 2.00 and for shells of various legacy states.

Sedimentary microbially-mediated redox processes, however, have been shown to display differential sensitivities to experimental or naturally acidified conditions. Some studies have suggested a decrease in nitrification and denitrification under increased PCO_2 (e.g. Widdicombe et al., 2009; Tait et al., 2014; Vopel et al., 2018), whereas others have suggested no significant responses to OA (Kitidis et al., 2011; Gazeau et al., 2014). In the case of sulfate reduction, studies have shown optimal rates over a range of 6-8 pH values (Kelly and Rudd, 1984), therefore encompassing the pH conditions encountered in most sediments (Soetaert et al., 2007) and, potentially, resulting in non-significant responses to OA. Regarding the potential key role of both denitrification and net sulfate reduction in the production of alkalinity in oyster

reefs, as previously discussed, their insensitivity to OA might also help to explain the observed non-response of alkalinity fluxes to moderate OA conditions.

Ultimately, even if the Harris Creek restored oyster reefs seem to be relatively insensitive to moderate acidification, measured large net alkalinity fluxes from these reefs to the overlying water suggest the potential of these habitats to act as buffering agents of transient corrosive conditions across small spatial scales, as first suggested by Waldbusser et al., 2013. This buffering effect might be particularly important in creating microenvironments of reduced corrosivity, likely providing a refugia for sensitive larvae and new oyster settlers. Multiple chemical cues have been suggested to explain marine bivalve settlement behavior (Pawlik, 1992; Hadfield and Paul, 2001b). Among them, calcium carbonate saturation state has been identified as a recruitment cue for multiple species of bivalves (Green et al., 2013; Clements and Hunt, 2014; Peng et al., 2017; Clements and Hunt, 2017).

In oysters, gregarious behavior, or preferential settlement on adult oyster shells has been described in numerous studies (Abbe, 1988; Luckenbach, M. W.; Mann, R.; And Wesson, J. A., 1999 and references therein), thus spurring shell planting as a key oyster reef restoration strategy (e.g. Nestlerode et al., 2007; NOAA, 2016; Hernández et al., 2018). Ultimately, sustainable shell aggregations can generate refugia for larval settlement and juvenile recruitment, alleviating bottleneck effects on oyster populations and providing a local mitigation strategy to increasing ocean acidification. We contend, however, that for shell aggregations to be most effective at buffering microenvironments through the production of alkalinity, they need both calcium carbonate (shell) and deposition of organic matter. A living oyster reef, therefore, would then

encourage the regeneration of alkalinity through the release of metabolic acids as byproducts of remineralization of organic matter (Waldbusser, Powell, et al., 2013), ultimately favoring shell dissolution, but also enhancing the production of inorganic non-carbonate alkalinity through denitrification and precipitation of sulfide minerals.

Acknowledgements.

This research was supported by the NOAA grant NA15NOS4780190 to GGW. The authors would like to thank Jack Seabrease for assistance in designing and customizing the vibracorer and Melanie Jackson for her significant assistance in conducting experiments and analyzing samples. We thank Brian Haley and the technicians at OSU's Keck Lab for guidance and assistance in performing ICP-OES measurements. Finally, the authors are grateful to Isaiah Kaela-Pacheco, Dave Edge, and Sally Albright for their collaboration in sample analysis and data processing.

Table 4.1. Mean experimental conditions for core incubations experiments. ± are Standard Deviations (SD).

Treatment	T (°C)	S	Alkalinity (μeq kg^{-1})	TCO_2 (μmol kg^{-1})	PCO_2 (μatm)	HCO_3^- (μmol kg^{-1})	CO_3^{2-} (μmol kg^{-1})	pH_t	Ω_{Ca}	Ω_{Ar}
Low	23.8 ± 0.7	11.4 ± 0.2	1448 ± 94	1422 ± 81	822 ± 169	1354 ± 74	41 ± 12	7.73 ± 0.10	1.19 ± 0.36	0.70 ± 0.21
Medium	23.6 ± 0.4	11.4 ± 0.3	1475 ± 95	1474 ± 100	1243 ± 668	1398 ± 95	34 ± 13	7.62 ± 0.20	0.98 ± 0.39	0.57 ± 0.23
High	23.7 ± 0.5	11.3 ± 0.2	1470 ± 74	1459 ± 76	1023 ± 205	1388 ± 74	34 ± 6	7.66 ± 0.07	1.01 ± 0.18	0.59 ± 0.11

Table 4.2. Calculated sediment-water biogeochemical fluxes for all intact oyster reef cores and experimental treatments. Positive values indicate flux from oyster reef to the overlying water, while negative represent fluxes into the oyster reef. n.s./n.l. designate fluxes that were non-significantly different from zero, or highly non-linear (adjusted-R^2<0.5).

Core	Treatment	Date (2017)	Biogeochemical fluxes (mmol m^{-2} d^{-1})						
			Alkalinity	Ca^{2+}	NH_4^+	NO_x	$NH_4^+ + NO_x^{\dagger}$	SRP	Si
1	Low	6/9	108.00	60.84	13.53	*n.s / n.l.*	12.78	0.26	*n.s / n.l.*
1	Low	7/2	*n.s / n.l.*	51.48	*n.s / n.l.*	*n.s / n.l.*	*n.s / n.l.*	*n.s / n.l.*	15.55
1	Medium	6/12	131.60	28.08	*n.s / n.l.*	*n.s / n.l.*	10.06	*n.s / n.l.*	*n.s / n.l.*
1	Medium	6/19	78.80	*n.s / n.l.*	*n.s / n.l.*	-2.14	-2.97	*n.s / n.l.*	*n.s / n.l.*
1	Medium	6/27	36.48	*n.s / n.l.*	*n.s / n.l.*	-2.56	*n.s / n.l.*	-0.29	13.02
1	High	6/13	117.78	51.48	*n.s / n.l.*	n.s / n.l.	7.61	*n.s / n.l.*	*n.s / n.l.*
1	High	6/25	85.60	*n.s / n.l.*	*n.s / n.l.*	0.19	1.40	-0.28	20.13
1	High	6/30	79.52	-28.08	*n.s / n.l.*	n.s / n.l.	2.98	*n.s / n.l.*	*n.s / n.l.*
2	Low	6/18	103.68	*n.s / n.l.*	5.86	-0.89	10.55	*n.s / n.l.*	*n.s / n.l.*
2	Low	7/3	*n.s / n.l.*	*n.s / n.l.*	0.77	*n.s / n.l.*	*n.s / n.l.*	*n.s / n.l.*	5.66
2	Medium	6/20	102.21	46.08	3.53	*n.s / n.l.*	4.10	*n.s / n.l.*	*n.s / n.l.*
2	Medium	6/29	48.23	43.2	*n.s / n.l.*	*n.s / n.l.*	*n.s / n.l.*	-0.07	*n.s / n.l.*
2	High	6/26	68.81	34.56	*n.s / n.l.*	*n.s / n.l.*	*n.s / n.l.*	*n.s / n.l.*	*n.s / n.l.*
2	High	7/1	44.46	77.76	*n.s / n.l.*	*n.s / n.l.*	1.53	*n.s / n.l.*	5.13
3	Low	7/5	107.84	59.28	4.25	1.05	11.50	-0.20	11.58
3	Low	6/18	104.53	62.4	*n.s / n.l.*	*n.s / n.l.*	*n.s / n.l.*	-0.23	*n.s / n.l.*
3	Medium	7/3	126.05	59.28	2.65	1.26	3.91	*n.s / n.l.*	*n.s / n.l.*
3	Medium	6/20	75.27	*n.s / n.l.*	*n.s / n.l.*	*n.s / n.l.*	*n.s / n.l.*	-0.07	9.67
3	High	6/29	99.25	-24.96	*n.s / n.l.*	*n.s / n.l.*	*n.s / n.l.*	*n.s / n.l.*	*n.s / n.l.*
3	High	6/26	79.58	115.44	*n.s / n.l.*	3.47	*n.s / n.l.*	*n.s / n.l.*	*n.s / n.l.*

Table 4.2. (Continued)

Core	Treatment	Date (2017)	Biogeochemical fluxes (mmol m^{-2} d^{-1})						
			Alkalinity	**Ca^{2+}**	**NH_4^+**	**NO_x**	**$NH_4^+ + NO_x$**	**SRP**	**Si**
4	Low	7/1	90.78	*n.s / n.l.*	*n.s / n.l.*	*n.s / n.l.*	6.64	*n.s / n.l.*	*n.s / n.l.*
4	Low	7/5	99.69	43.56	-0.92	1.93	-1.87	*n.s / n.l.*	4.26
4	Medium	6/18	97.93	*n.s / n.l.*	-4.04	0.08	-5.72	*n.s / n.l.*	*n.s / n.l.*
4	Medium	7/3	55.86	*n.s / n.l.*	*n.s / n.l.*	0.93	0.39	-0.24	1.73
4	High	6/20	99.07	*n.s / n.l.*	*n.s / n.l.*	0.48	n.s / n.l.	*n.s / n.l.*	*n.s / n.l.*
4	High	6/29	93.65	*n.s / n.l.*	5.83	*n.s / n.l.*	1.56	*n.s / n.l.*	*n.s / n.l.*
5	Low	6/26	208.18	61.20	15.62	-1.96	20.02	0.40	27.13
5	Low	7/1	131.11	*n.s / n.l.*	*n.s / n.l.*	-1.06	n.s / n.l.	*n.s / n.l.*	13.51
5	Medium	7/5	312.08	189.72	14.49	*n.s / n.l.*	13.41	1.17	*n.s / n.l.*
5	Medium	6/17	147.89	*n.s / n.l.*	8.89	-0.80	9.53	-0.20	25.55
5	High	7/2	204.26	85.68	*n.s / n.l.*	-2.10	3.68	-0.56	26.31
5	High	6/19	121.66	91.80	7.04	5.33	13.37	-0.15	23.28
6	Low	6/27	198.38	60.72	8.67	*n.s / n.l.*	13.59	0.10	*n.s / n.l.*
6	Low	6/25	98.69	71.76	*n.s / n.l.*	6.32	n.s / n.l.	*n.s / n.l.*	6.25
6	Medium	6/30	201.34	82.8	*n.s / n.l.*	*n.s / n.l.*	8.24	*n.s / n.l.*	*n.s / n.l.*
6	Medium	7/4	115.25	*n.s / n.l.*	1.18	4.73	5.96	*n.s / n.l.*	11.41
6	High	6/17	166.53	91.08	*n.s / n.l.*	4.26	9.47	-0.41	15.07
6	High	7/2	152.74	88.32	4.10	7.18	10.12	*n.s / n.l.*	6.17

†Combined NH_4^+ and NO_x are calculated by adding the concentration of both NH_4^+ and NO_x at each sampling point and performing robust regressions on the combined measurements, not by adding the calculated fluxes of each individual component.

Table 4.3. Mean sediment-water biogeochemical fluxes averaged across oyster reef cores for each experimental treatment and overall. Positive values indicate flux from oyster reef to the overlying water, while negative represent fluxes into the oyster reef. ± are Standard Deviations (SD). Values in brackets represent the range of minimum and maximum results.

Treatment	**Biogeochemical fluxes (mmol m^{-2} d^{-1})**						
	Alkalinity	**Ca^{2+}**	**NH_4^+**	**NO_x**	**$NH_4^+ + NO_x$†**	**SRP**	**Si**
Low	122 ± 30	57.6 ± 8.6	7.41 ± 6.37	1.38 ± 3.10	11.80 ± 5.69	0.14 ± 0.26	10.60 ± 6.38
Medium	121 ± 62	80.9 ± 64.1	3.00 ± 5.68	0.67 ± 2.65	4.58 ± 4.65	-0.04 ± 0.31	12.28 ± 8.60
High	110 ± 42	58.3 ± 32.6	5.66 ± 1.48	2.30 ± 2.31	5.08 ± 3.88	-0.35 ± 0.07	15.17 ± 8.92
All Combined	117 ± 44 (57 – 230)	65.6 ± 40.3 (11.7 – 189.7)	5.46 ± 5.47 (-4.05 – 15.62)	1.45 ± 2.60 (-2.35 – 6.32)	7.28 ± 5.71 (-2.67 – 20.02)	-0.06 ± 0.30 (-0.41 – 0.49)	12.38 ± 7.50 (1.73 – 25.55)

†Combined NH_4^+ and NO_x are calculated by adding the concentration of both NH_4^+ and NO_x at each sampling point and performing robust regressions on the combined measurements, not by adding the calculated fluxes of each individual component.

Table 4.4. Core characteristics and integrated material budgets for each core estimated from CT-scan images.

Core	Length (cm)	% Air (v/v)	% Water (v/v)	% Shell (v/v)	% High Porosity Sediment (v/v)	% Low Porosity Sediment (v/v)	% Total Sediment (v/v)	Shell surface area estimate (cm^2)	Shell perimeter estimate (cm)
1	30.5	4.0	4.8	24.1	31.1	36.0	67.1	24748.8	1743
2	38	2.7	2.8	23.3	38.7	32.5	71.2	27841.6	1803
3	37	1.1	3.5	20.8	44.8	29.7	74.5	19872.8	1537
4	33.5	1.3	1.9	26.5	31.7	38.6	70.3	22908.9	1481
5	24.5	1.6	6.0	27.3	30.7	34.4	65.1	18169.4	1410
6	38.5	2.2	2.9	28.1	27.3	39.4	66.7	9529.1	1773

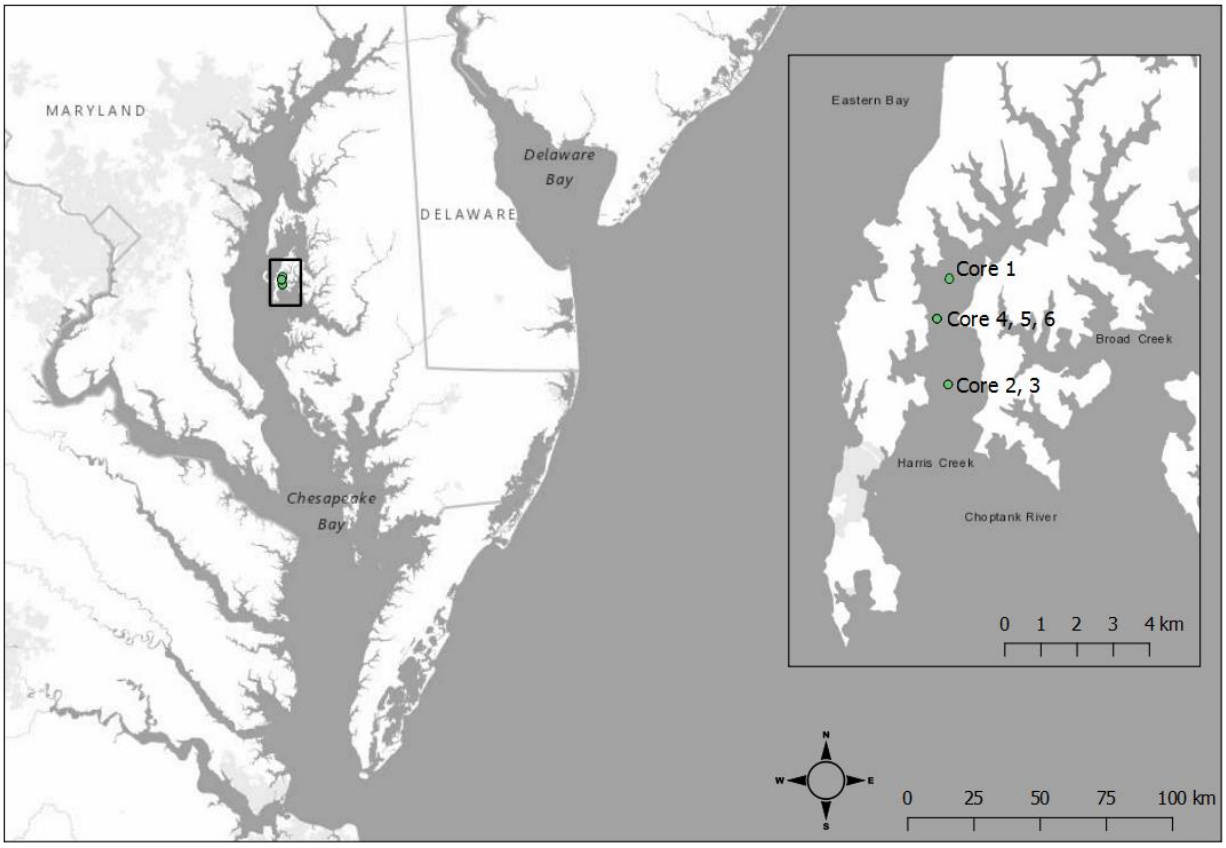

Figure 4.1. Map of study area showing the collection sites of oyster reef cores within Harris Creek, a tributary of Chesapeake Bay.

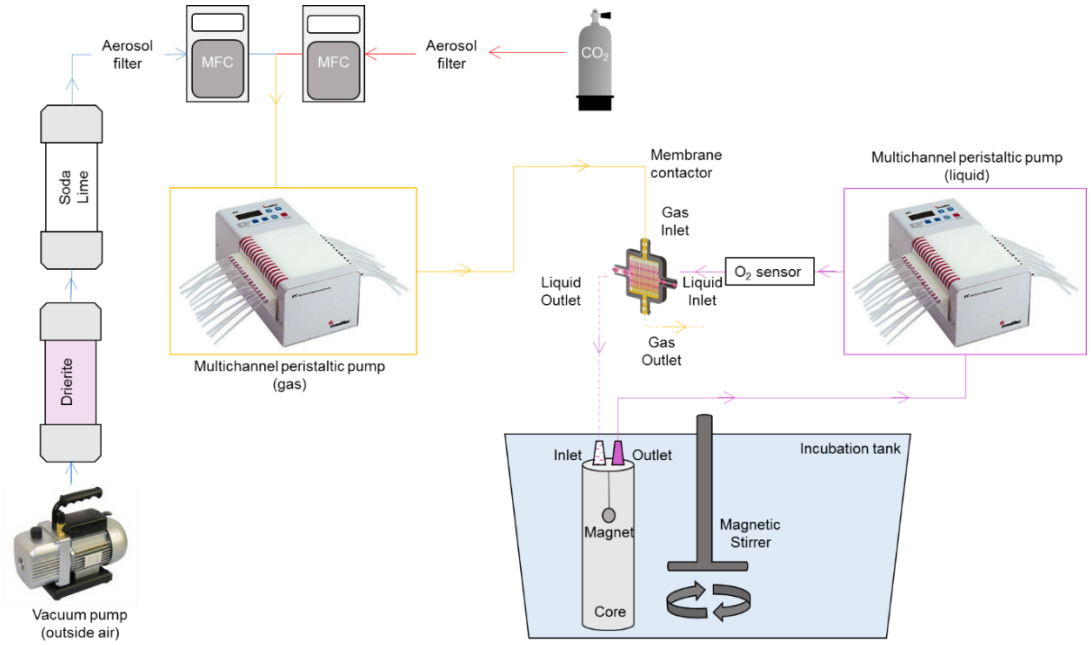

Figure 4.2. Schematic of the core incubation system utilized to maintain high levels of O2 saturation and impart different levels of core overlying water PCO2. This schematic represents just one core, but four cores (three oyster reef cores and one blank core with just water) were incubated simultaneously during experiment. In pink, closed, stream flow loop of each core's overlying water. Core overlying water flows through the inside (lumenside) of an individual membrane contactor at a flow rate of ~60 mL min^{-1}, while the gas stream counter-flows through the outside (shellside) of the membrane contactor at a flow of ~500 mL min^{-1}, maximizing surface area contact and gas transfer (i.e. absorption of O_2 and CO_2 equilibration). The gas stream flow is 100% saturated in O_2, while the CO_2 concentration is regulated by Mass Flow Controllers (MFC) and set to the treatments low, medium or high (see methods). In yellow, gas stream flow. In blue, outside, ambient air that is dried, stripped of CO_2 and filtered. In red, filtered, pure CO_2 gas. Solid lines represent flow towards the membrane contactor, while the dashed lines represent return water flow to the core or waste gas stream.

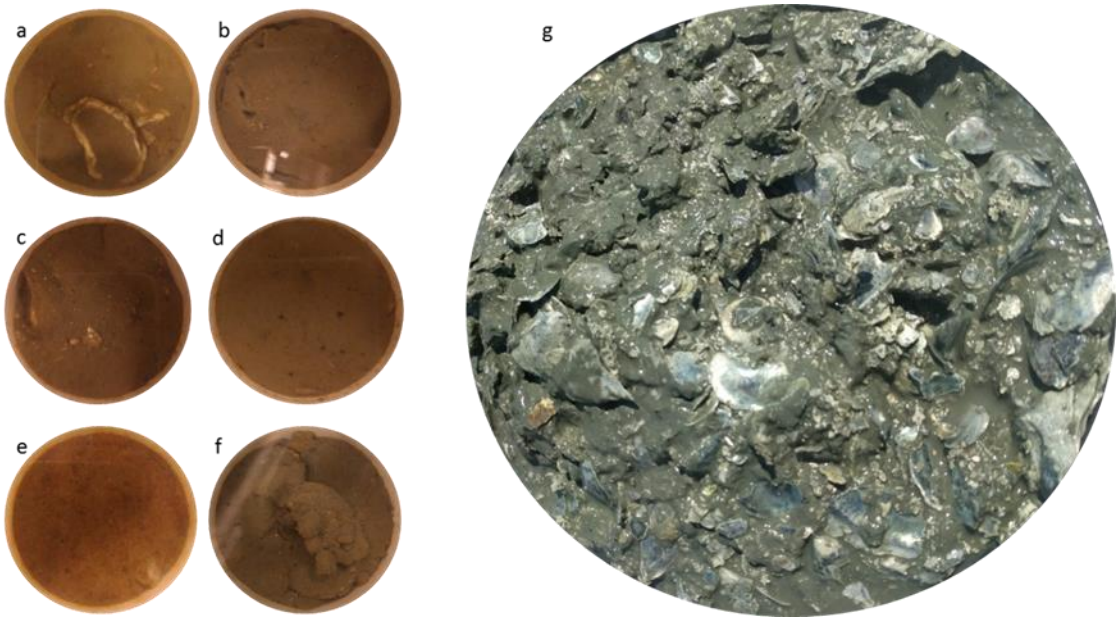

Figure 4.3. Images of oyster reef intact cores. a-f) Sediment-water interface. a) Core 1; b) Core 2; c) Core 3; d) Core 4; e) Core 5; f) Core 6. g) Representative example of oyster reef sediment matrix at maximum penetration of oyster reef cores.

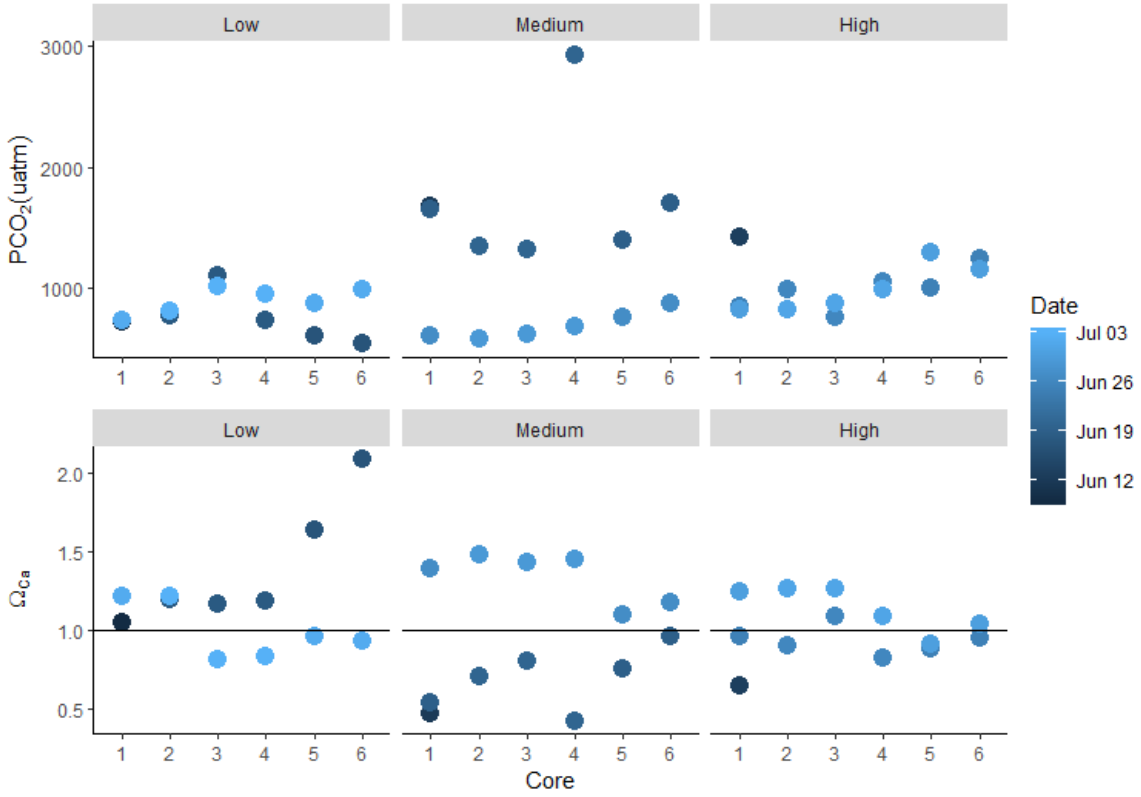

Figure 4.4. Experimental conditions for each core, sorted by treatment and incubation date. Top: PCO_2 computed values Bottom: Ω_{Ca} computed values. Horizontal line in bottom panel represents the threshold of thermodynamic stability for calcite mineral.

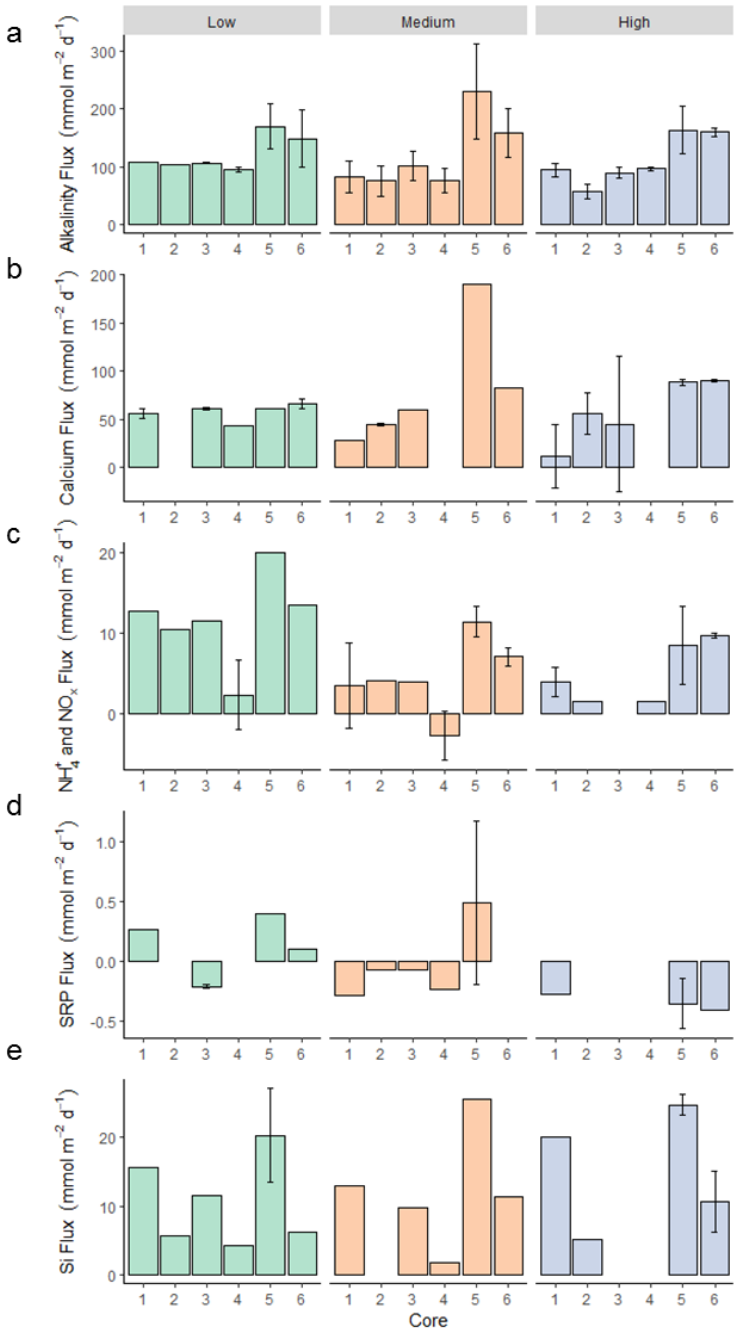

Figure 4.5. Average biogeochemical fluxes estimated from core incubations. (a) Alkalinity, (b) Calcium, (c) Combined NH4+ and NOx, (d) SRP, and (e) Silicate from individual cores and across experimental treatments. Error bars are Standard Deviations (SD).

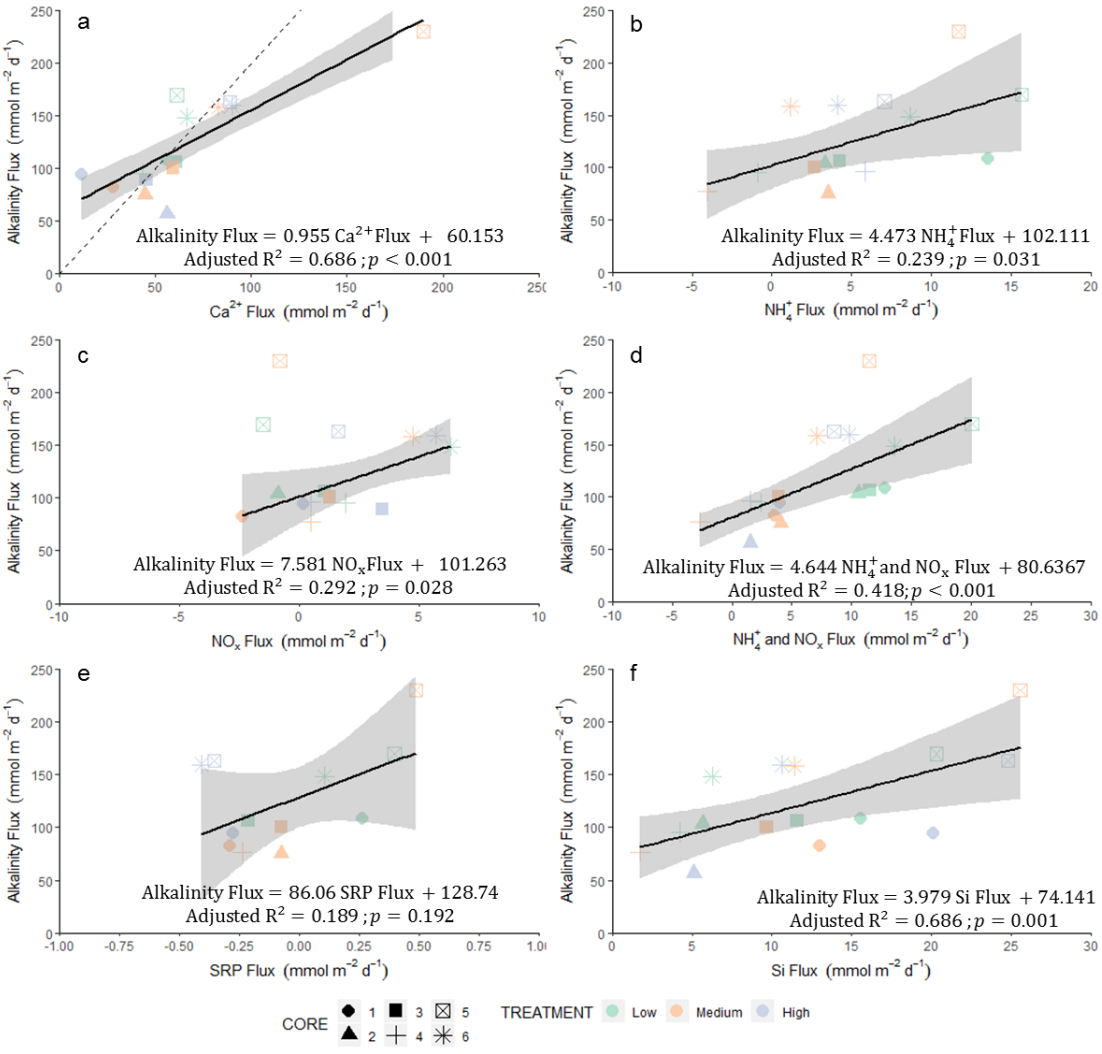

Figure 4.6. Robust linear regressions of average alkalinity fluxes as a function of average biogeochemical fluxes of other solutes. a) Ca^{2+}; b) NH_4^+; c) NO_x; d) NH_4^+ and NO_x; e) SRP; and f) Si. Dashed line in panel a represents a slope of 2 Alkalinity : 1 Ca^{2+}, the stoichiometric slope expected if fluxes were dominated by $CaCO_3$ dissolution.

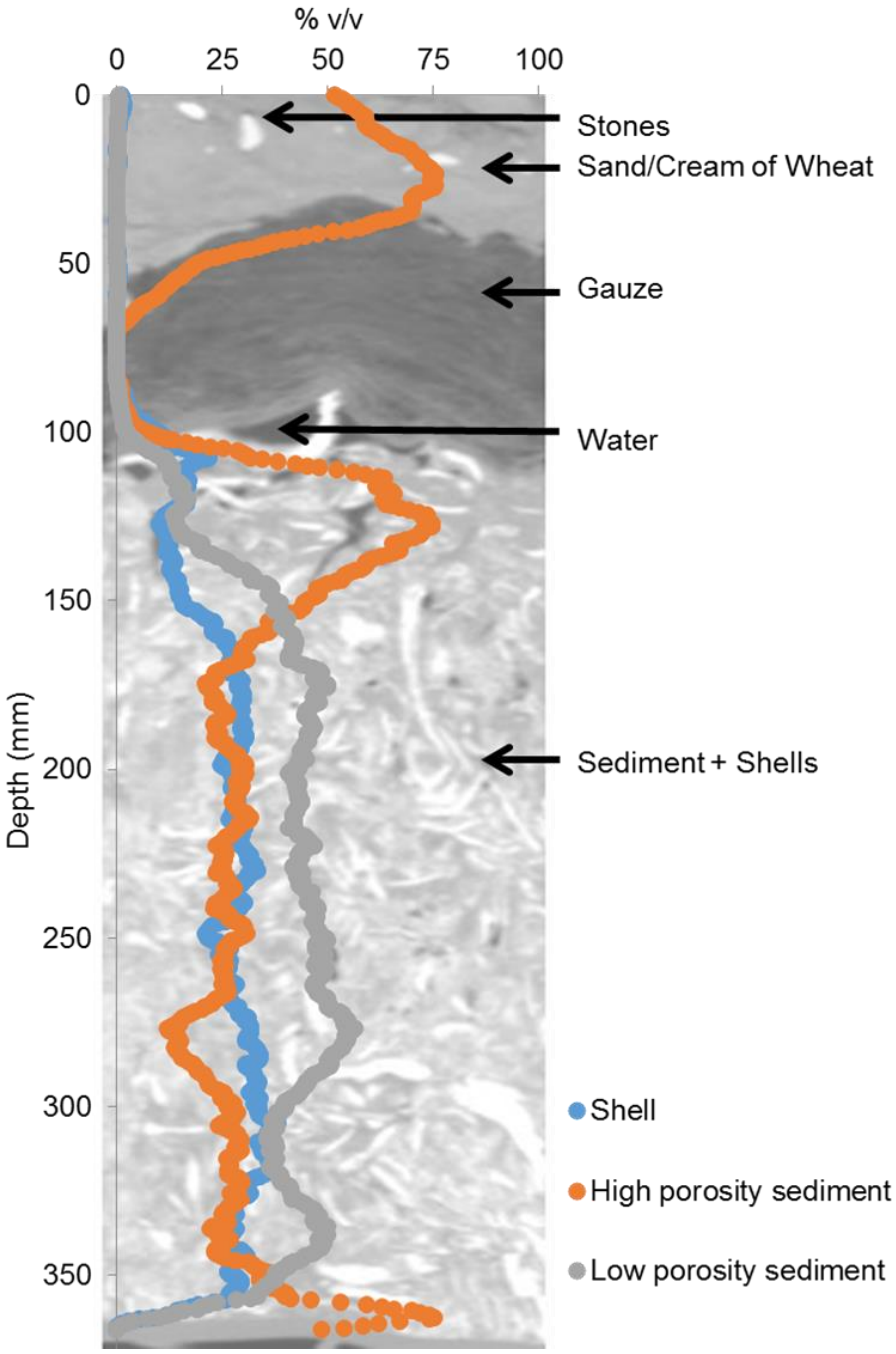

Figure 4.7. Example of reconstructed material budget over an annotated CT-scan composite image.

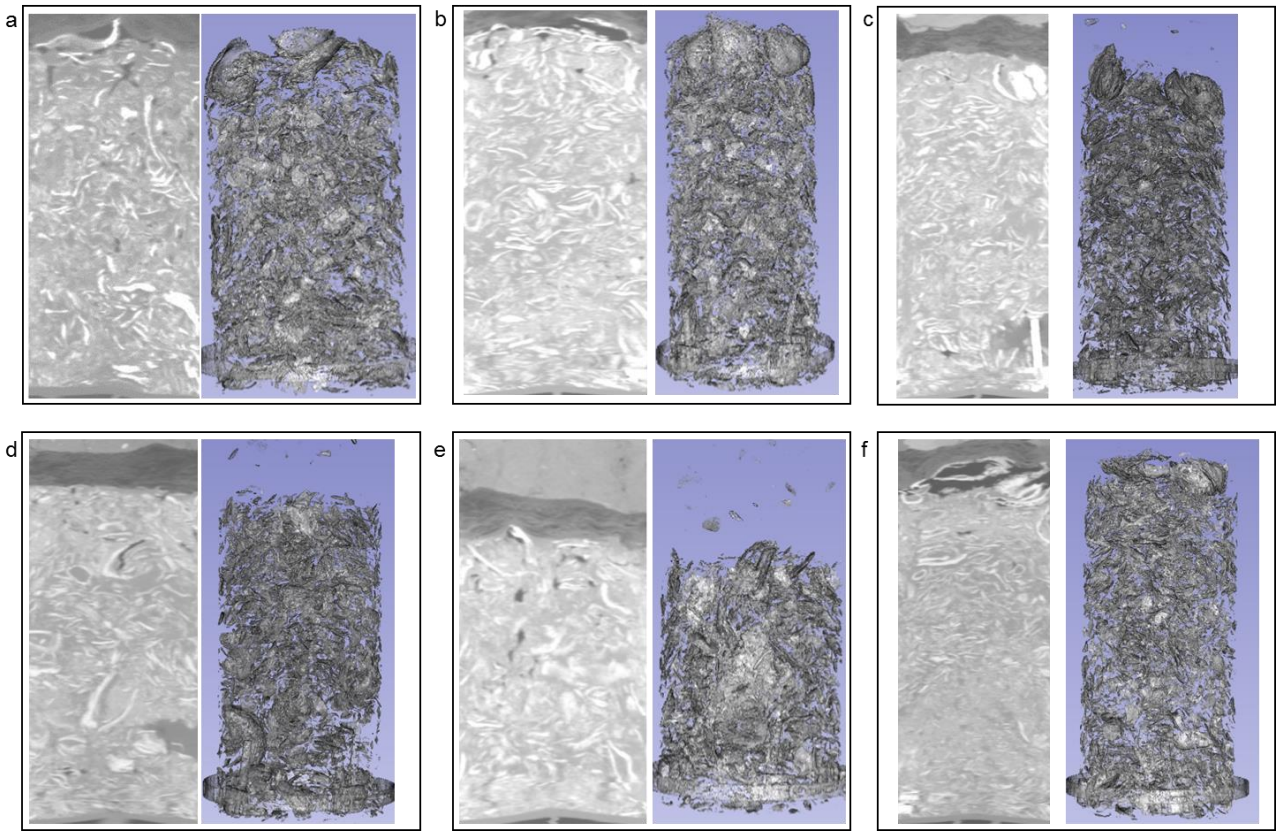

Figure 4.8. Composite of cores CT-scan images and reef 3-D reconstructions. Left) CT-Scan images of oyster reef intact cores. Right) Associated 3-D reconstructions of oyster reef cores. a) Core 1; b) Core 2; c) Core 3; d) Core 4; e) Core 5; f) Core 6.

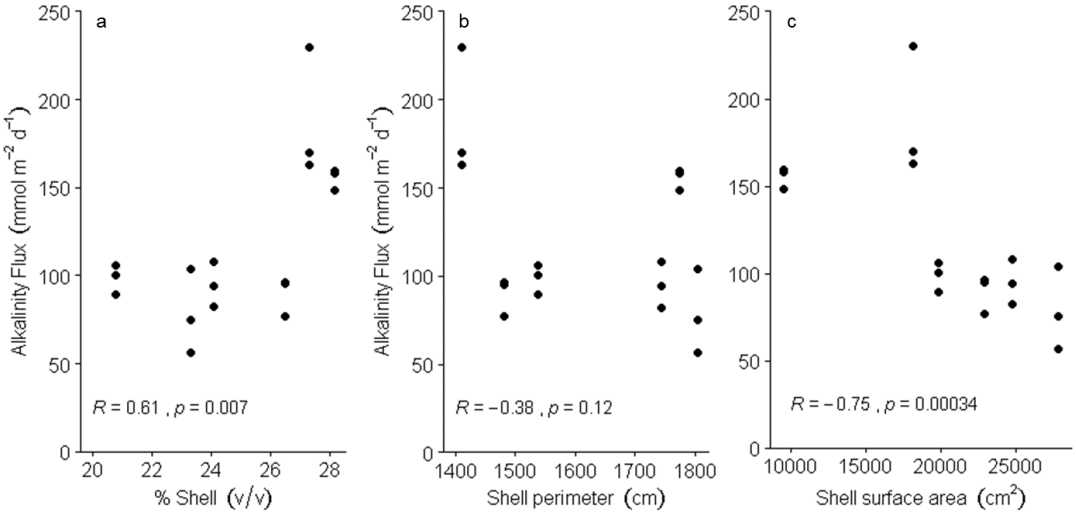

Figure 4.9. Spearman correlations between alkalinity fluxes and material budget and shell structure estimates. a) Average alkalinity fluxes and % shell, b) Average alkalinity fluxes and shell perimeter, c) Average alkalinity fluxes and shell surface area.

5. CHAPTER V.-Oyster reef biogeochemistry: An heterogeneous system dominated by early diagenetic processes and net production of alkalinity

5.1 Abstract

The internal biogeochemical structure and function of oyster reefs is not well constrained, thereby precluding the development of necessary functioning frameworks crucial to improve predictions regarding habitat-level responses to future scenarios such as climate conditions or management strategies. Bivalve species have been identified as sensitive to ocean acidification (OA), but the potential of shell aggregations like oyster reefs to provide buffering to transient corrosive conditions through the release of alkalinity has not been evaluated. We measured porewater distributions of alkalinity, dissolved inorganic carbon (DIC), pH, calcium (Ca^{2+}), sulfate (SO_4^{2-}), hydrogen sulfide (H_2S), ammonium (NH_4^+), nitrate-nitrite (NO_x), soluble reactive phosphorus (SRP), and silicate (Si) on intact oyster reef cores collected on a restored Eastern oyster (*Crassostrea virginica*) reef in Harris Creek, MD, USA. We also determined solid-phase components such as organic and inorganic C, shell content, and total reduced sulfur (TRS) to further characterize the dominant biogeochemical processes within the reef framework. The sediment was classified as coarse sand and dominated by the presence of oyster shell, as the average contribution of $CaCO_3$ was 87% by weight and the organic carbon represented an average of 1.25% of the sediment. Alkalinity, DIC and nutrient concentrations were elevated in porewaters and generally increased with depth, while Ca^{2+} concentrations decreased with respect

to overlying water, with moderate increases with depth. SO_4^{2-} decreased with depth, while H_2S and TRS showed the opposite pattern, although overall concentrations were low for H_2S and high for TRS when compared with other Chesapeake Bay sediments. Statistically significant regressions were found between alkalinity and DIC (1.10 molar ratio), alkalinity and SO_4^{2-} (-1.11) and alkalinity and Ca^{2+} (1.91). The observed porewater and solid-phase distributions, as well as the molar relationships between alkalinity and other solutes, support the production of alkalinity through metabolically-enhanced shell dissolution and net sulfate reduction, but the evidence suggests that the latter biogeochemical pathway is the dominant process generating alkalinity within oyster reef porewaters. These results indicate that alkalinity production is maximized when shell and organic carbon in the form of biodeposits are collocated, therefore suggesting that restoration and OA mitigation strategies should strive to maintain living reefs, where organic matter production rates are maximized.

5.2 Introduction

Despite the well-described key role of oyster reefs in coastal ecosystems (Dame, 2012) and the numerous ecosystem services they provide (Coen et al. 2007), the biogeochemical structure of these habitats is poorly constrained. To our knowledge, Bahr and Lanier 1981 provided the first detailed description of the inner structure of an oyster reef, though it was a qualitative description based on visual inspection of intertidal oyster reefs at Sapelo Island, GA, US. These authors identified three distinct depth “horizons” based on shell coloration patterns: 1) a top layer of mostly living oysters whose shells were displayed green-grey shades -likely the

result of epiphyte algae-; 2) a medium section of red-brown shells embedded within biodeposits and sediments; and 3) a bottom layer of silver-black shells, which the authors associate with precipitation of sulfide minerals and, therefore, as an indicator of anoxic sediment environments. This early work, therefore, suggests that oyster reefs are habitats where active redox diagenetic processes are occurring.

Since this seminal work, the most robust description of the likely biogeochemical structure of oyster reefs was provided by Hargis and Haven, 1999 and refined by Waldbusser et al. 2013. In this work, the authors proposed that the structure oyster reefs follows a tiered framework. First, a reef veneer that comprises the surficial layer of the oyster reef framework and where living oysters and recently dead shells are concentrated. This oyster reef layer is largely oxic and therefore subject to higher shell dissolution rates, thus its denomination as the taphonomically active zone (TAZ). Second, below the TAZ and above the seafloor bottom, lies a suboxic or anoxic layer labeled the reef core or framework, where shell fragments and biodeposits accumulate and were early diagenesis processes are largely associated with remineralization of organic matter. Finally, an anoxic reef-sub-bottom is found below the seafloor bottom and is composed of the same materials than the reef core.

Based on the co-location of calcium carbonate shells and biodeposits rich in organic C, Waldbusser et al. 2013 suggested that oyster reefs could act as “carbonate pumps”, sequestering carbonate -and thus, alkalinity- from the overlying water to form shells and burying this alkalinity into the reef upon their death. Regeneration of alkalinity would then occur as a result of shell dissolution, mostly within the TAZ and likely favored by the release of metabolic acids

as a result of the remineralization of organic matter (i.e. biodeposits) (e.g. Hales and Emerson, 1997; Jahnke and Jahnke, 2004; Burdige et al., 2008). Waldbusser et al. 2013 also suggested that additional alkalinity could also be produced within the suboxic and anoxic region of the oyster reef, though the exact biogeochemical pathways were not described.

We suggest that the most likely suboxic and anoxic processes affecting alkalinity dynamics within oyster reefs are net denitrification and/or sulfate reduction of organic matter, which can increase alkalinity in 1:1 or 2:1 molar ratios per NO_3^- and SO_4^{2-} consumed, respectively (Soetaert et al., 2007, Hu and Cai, 2011, Krumins et al. 2013). Elevated rates of denitrification have been reported within oyster reefs (see review in Kellogg et al. 2014), yet the overall effect of alkalinity production within the internal structure of the reef will depend on the spatial extent of the suboxic layer and the absence of nitrate substrate limitation (Newell et al. 2005). Sulfate reduction is the most important pathway of organic matter remineralization in organic-rich environments like oyster reefs, where oxygen is restricted to the top few centimeters of the sediment layer (Jørgensen, 1982; Burdige, 2006). Indeed, high rates of sulfate reduction have been measured in sediments collected from bivalve aggregations (Malkin et al. 2017). If sulfate reduction is decoupled from the reoxidation of the produced hydrogen sulfide (H_2S) then net alkalinity is generated.

Despite the hypothesized substantial role oyster reefs could play in the biogeochemical cycling of alkalinity and inorganic C within coastal habitats, the study of oyster reefs' effect on biogeochemical cycles is, to date, heavily focused on their influence in pelagic-benthic couple of organic C and nutrients (Newell et al., 2005). Recently, oyster reefs have received increased

attention due to their potentially significant role in removing nitrogen through burial and enhanced denitrification (see review in Kellogg et al., 2014), and carbon sequestration through burial of biodeposits (organic C) and calcium carbonate shells (inorganic C) (e.g. Fodrie et al. 2017).

Fodrie et al. 2017 provided, to our knowledge, the first rigorous description of organic and inorganic C solid-phase profile distributions within several natural and restored oyster reefs. These authors found that some reefs acted as net sinks of C over annual timescales, while other reefs resulted in net sources of C. These results highlight the complexity and heterogeneity of these habitats but porewater and solid-phase depth-distributions are both necessary to fully characterize the biogeochemical structure of these habitats. A solid understanding of biogeochemical structure and function of oyster reefs is necessary to improve our assessment regarding the potential biogeochemical responses of these habitats to environmental perturbations.

Multiple reef-building oyster species have been shown to be vulnerable to ocean acidification (OA) at the organismal level (see reviews in Kroeker et al., 2010; Gazeau et al., 2013). The responses of intact oyster reefs to OA are, however, largely unknown. The potential importance of alkalinity-producing biogeochemical processes within these habitats nevertheless warrants a rigorous biogeochemical characterization of these systems. Ultimately, a well-defined bigeochemical framework of shell aggregations is required in order to evaluate the potential habitat-level feedbacks that can alter the carbonate chemistry at local spatial scales and, likely, provide buffering against transient corrosive conditions, thereby indicating shell aggregations

can act as potential OA refugia for sensitive organisms - including the bivalves that build the reefs.

The goals of this work, therefore, were: 1) measure important porewater and solid-phase components and characterize their depth distributions; 2) evaluate the importance of alkalinity regeneration and production within the oyster reef framework; and 3) assess the relationships between alkalinity and other important solutes to elucidate what biogeochemical pathways are driving alkalinity generation, if present.

5.3 Materials and methods

5.3.1 Study area

We collected intact oyster reef cores in two restored oyster reefs within Harris Creek (38°45'12.46" N, 76°18'27" W) (Figure 5.1), a tidally influenced tributary to the Choptank River located in the mesohaline, mid-bay region of Chesapeake Bay, and where the Harris Creek Oyster Sanctuary is located (NOAA 2016). Harris Creek Oyster Sanctuary is a pilot, large-scale oyster reef restoration effort that restored more than 140 ha of suitable oyster reef habitat since 2011, largely through shell planting and the addition of live oyster seed (NOAA 2016).

All cores were collected in September 25th, 2017 (Table 5.1). Cores 2, 3 and 6 were obtained within restored Reef #9 (38°45'43.8" N, 76°18'23.4" W; Table 5.1, Figure 5.1), whereas cores 4 and 5 were obtained within Reef #11 (38°45'8.53" N, 76°18'37.51" W; Table 5.1, Figure 5.1). Both sites were subtidal, with depths of 1.8 and 2.1 m for reef #9 and #11,

respectively. Reef#9 is a 4.97 ha reef seeded with 47.23 million of seed (oyster spat) in 2012 (NOAA 2016), while reef #11 is a 2.64 ha reef seeded in 2012 with 28.19 million of oyster spat. As of 2015, the average density of live oysters was 32.18 oyster m^{-2} and 20.39 oysters m^{-2} for reef #9 and #11, respectively (NOAA 2016).

Physico-chemical conditions were very similar between sites (Table 5.1). Bottom water temperatures were 25.3 °C in both locations, while salinity was 15.3 psu at reef #9 and 15.5 psu at reef#11. Bottom water oxygen saturation varied from 69% to 72%, slightly lower values than monitoring data collected by the Harris Creek Profiler (average O_2 saturation 90%; range 80-99%) (Maryland Department of Natural Resources, 2018). All measurements were carried out using a handheld multiparameter sensor (YSI 600XLM).

At each site, surface water samples were collected for alkalinity, DIC, Ca^{2+}, SO_4^{2-}, Cl^-, and nutrients (i.e. NH_4^+, NO_x, SRP, and Si) analyses were collected. Alkalinity and DIC samples were preserved with concentrated $HgCl_2$ (final concentration ~0.03%). Ca^{2+}, SO_4^{2-} and Cl^- were filtered through a 0.45 μm filter and acidified to a pH below two, while nutrient samples were filtered, kept refrigerated and frozen upon arrival to the laboratory.

5.3.2 Oyster reef core collection

A customized, portable vibracorer was utilized to collect undisturbed, intact oyster reef cores at each sampling site. The methodology employed is described in detail in Chapter 4. Concisely, our coring system comprised a vibracoring head attached to a coring guide and powered by a 5.5 hp gasoline engine (Honda GX160), an attached polyvinyl chloride (PVC) core

tube (50 cm long, 15.5 cm inside diameter), and a core cap with a valve to minimize sample disturbance during sample collection. Each core was also fitted with a built-in core-catcher to reduce loss of sediment. Cores were sealed and kept partially submerged until arrival to Horn Point Laboratory, Cambridge, MD. Upon arrival to the laboratory, all cores were uncapped and submerged in a flow-through bath with filtered Choptank River water until sampled. All cores were sampled within less than a week from collection.

5.3.3 Core sampling

Cores were sectioned under an N_2 atmosphere inside a glove bag, with spatial resolution among sediment intervals ranging from 2.5 to 3.3 cm (Table 5.2). Large shell fragments were preserved in sample plastic bags and frozen, while sediment and small shell fragments were transferred to 50 mL centrifuge tubes. One centrifuge tube was immediately frozen for porosity and total reduced sulfur (TRS) analysis. The remaining tubes were centrifuged at approximately 12,000 rpm for 15 minutes. Porewater was siphoned off using acid-cleaned syringes and filtered through 0.2 μm or 0.45 μm Nylon syringe filters. About 8 mL were transferred to glass vials and immediately analyzed for alkalinity and pH. Samples for nutrients (i.e. NH_4^+, NO_x, SRP, and Si) were immediately frozen. DIC samples (roughly 4mL) were transferred to amber glass vials, preserved with saturated $HgCl_2$ (0.03% final concentration) and sealed for DIC analysis. Ca^{2+}, SO_4^{2-} and Cl^- samples (~1.5 mL) were acidified to a pH below two with trace metal clean concentrated hydrochloric acid. Samples for H_2S were preserved in vacutainers with equal

volumes of 20% ZnAc and immediately frozen. Centrifuge tubes containing sediment were immediately frozen upon porewater sampling.

5.3.4 Analytical methods

5.3.4.1 Solid phase

After thawed, sediment samples were dried at ~60°C until stable weight was achieved. Porosity was calculated as follows:

$$\varphi = \frac{V_{porewater}}{V_{porewater}+V_{sediment}} = \frac{m_{porewater}*\rho_{porewater}}{m_{sediment}*\rho_{sediment}}, \quad \text{Eq (1)}$$

where $m_{porewater}$ represents the mass difference between wet sediment and dry sediment, $m_{sediment}$ is the dry sediment mass, $\rho_{porewater}$ is the density of the porewater, assumed to be equivalent to the density of the overlying water (i.e. 1.0084 and 1.0086 g mL^{-1} for reef #9 and #11, respectively), and $\rho_{sediment}$ is the density of the sediment, assumed to be 2.65 g mL^{-1}, a published reference value for sandy mud sediments (Burdige, 2006). Total Reduced Sulfur (TRS; i.e. acid volatile sulfur (AVS) + chromium reducible sulfur (CRS)) was determined by following a 6 N HCl-extraction and $PbClO_4$ titration (Canfield et al., 1986; Cornwell and Morse, 1987).

Sediment samples were then sieved for 15 minutes on a sieve shaker and grain size distributions and associated statistics calculated using the software GRADISTAT (v.8.; Blott and Pye, 2001). Sediment sieves spanned 1 mm, 500 µm, 355 µm, 250 µm, 125 µm, and 90 µm. The fraction of sediment retained in 1 mm sieve was considered entirely composed of shell

fragments, thus combined with dried large shells from the same sample, weighted and photographed.

All sediment fragments smaller than 1 mm were combined and two aliquots were randomly selected, ground with a mortar and pestle and homogenized. Total carbon (%TC), organic C (%Org C) and Nitrogen (%N) were determined by high-temperature combustion on an elemental analyzer (NC2500, ThermoQuest, (Goñi et al., 2006). We measured %TC and %N in an unacidified sample, whereas an additional sediment aliquot was acidified by exposing it to concentrated HCl fumes and 10% aqueous HCl to remove inorganic C and measure organic C (%Org C). Inorganic C (%Inorg C) content was determined as the difference between %TC and % Org C. Total % $CaCO_3$ was estimated by assuming that all inorganic C in the <1mm sediment fraction corresponded to pure $CaCO_3$ and that oyster shell weights corresponded to 100% $CaCO_3$.

5.3.4.2 Porewater

Alkalinity and pH were measured within hours of sampling, while DIC and Ca^{2+} samples were measured within a month and SO_4^{2-}, Cl^-, nutrients, and H_2S within nine months post-collection. Alkalinity was determined in an automated, open-cell titrator (Apollo SciTech, Cai and Wang, 1998) calibrated with a custom-made $NaHCO_3$ standard and validate with Certified Reference Materials (CRM batch #146, Andrew Dickson's laboratory, Scripps Institution of Oceanography). Analytical uncertainty was estimated as 1.3% based on repeated measurements of CRM and internal standards. pH was measured with a combination micro-electrode (Orion

8220 BNWP, ThemoFisher) calibrated with three traceable NBS buffers. Analytical precision of the pH microprobe is ± 0.01 units.

DIC measurements were determined by coulometry (CO_2 Coulometer Model 5011; UIC, Inc.) calibrated with an internal standard independently validated against Certified Reference Materials (CRM, Andrew Dickson's laboratory, Scripps Institution of Oceanography). Analytical uncertainty was estimated as 2.2%. Calcium samples were diluted 200-fold and measured on an inductively coupled plasma-optical emission spectrometer (ICP-OES Arcos, Spectro). Analytical uncertainty of calcium was estimated as 1.6% based of the calculated coefficient of variance of repeated measurements of a seawater standard (IAPSO Standard Seawater, OSIL). SO_4^{2-} and Cl^- samples were diluted 100-fold and analyzed by ion chromatography (HPIC Integrion, Thermo Integrion). Analyses of NH_4^+, NO_x, SRP, and Si were performed on a Smartchem discrete chemical analyzer (Westco Scientific, Danbury, CT). NH_4^+ was measured following a modified method from Koroleff (1976) and NO_x was determined by a modified EPA method 353.2. SRP measurements were carried out by adapting EPA method 365.2, and Si analysis followed Strickland and Parsons (1972). H_2S samples were thawed, centrifuged and the precipitated ZnS was dissolved in deionized water to remove porewater matrix effects. The resulting sample was measured on an spectrophotometer (UV-1201S, Shimazdu) following Cline, 1969.

Paired alkalinity and DIC values, and DIC and measured pH values, together with H_2S, SRP, NH_4^+, and Si values were used to calculate all carbonate chemistry parameters. We used a modified version of CO2SYS (version 2.3, Excel; (Xu et al., 2017)) and carbonic acid equilibration constants from Millero (2010), Dickson (1990) constants for sulfate, and total

boron from Lee et al. (2010). The contribution of dissolved organic compounds to alkalinity (Cai et al., 1998; Hunt et al., 2011) was estimated as the difference between measured alkalinity and computed alkalinity ($Alk_{computed}$) based on measured DIC, pH, H_2S, SRP, NH_4^+ and Si values, as described in Hunt et al. 2011.

5.3.5 Statistical analysis

Relationships between porewater solutes were evaluated through the fitting of robust linear regression models. All statistical analyses were conducted on Rstudio (version 1.1.456).

5.4 Results

5.4.1 Sediment characteristics

Oyster reef sediments were classified as moderately sorted coarse sands, with average grain sizes ranging from 823 to 893 µm and mean porosities varying from 0.56 to 0.64 (Table 5.2). Organic C depth distributions remained relatively stable and displayed low variability among cores (Figure 5.2). The average content of organic C was 1.25 %, although maxima of 2.16 and 2.58 were measured in cores 5 and 6 at 6 and 28 cm depths, respectively. The average C:N value was 9.92, although after excluding four measurements with ratios greater than 18, the average value decreased to 8.85. Inorganic C profiles were relatively stable with depth, although average values differed among cores and ranged between 4.2% and 5.7% (Figure 5.2). Estimated total $CaCO_3$ averaged 86.6% of the total solid phase by weight, although values ranged between 76.7% and 94.3% (Figure 5.2), while it represented between 27.9% and 52.4% of the <1mm

sediment fraction. Shell fragment sizes generally decreased with depth, with predominantly intact shells in the upper cm of the oyster reef cores and small fragments showing boring pits and partial dissolution at greater depths (Figure 5.3)

5.4.2 Porewater carbonate chemistry and Ca^{2+} measurements

Porewater alkalinity and DIC were substantially elevated with respect to surface water measurements and generally increased with depth (Figure 5.4), despite notable variability in the depth distribution of both solutes among cores. Convergent alkalinity values between 4,000 and 4,500 µM among cores 2, 4, and 5 were found at depths greater than 15 cm. Similarly, DIC values for the same cores stabilized between 3,500 and 3,800 µM at the same depths. Cores 5 and 6 show maxima in alkalinity of 6,700 and 7,100 µM, respectively, at depths 11-13 cm. Only core 6, however, show a DIC maximum (6,170 µM) at the same depth. Global maxima of alkalinity and DIC, however, reached ~7330 µM and 6090 µM, respectively, and corresponded to depths greater than 30 cm (Figure 5.4, Core 3). The average contributions of non-carbonate alkalinity associated with dissolved organic compounds was 7.8%, though values ranged from negligible to 41% and did not display robust patterns with depth. In contrast to alkalinity and DIC, Ca^{2+} concentrations were generally lower than surface water measurements and show the strongest negative gradients in the upper 7.5 cm of oyster reef sediments while exhibiting relatively small increases in concentration at greater depths (Figure 5.4).

Measured pH values were only collected for four cores, and generally show decreased values with respect to surface waters and a pattern of decreasing values with depth (Figure 5.4),

with most values falling between 7.6 and 7.8 units. Computed pH showed lower values with respect to surface waters (Figure 5.5), though values span a wide range with a pH minimum of 6.67 and a maximum of 8.65 in the total scale. While patterns differ among cores, a common feature is the existence of a pH minimum ~5-10 cm and relatively stable values of pH ~7.9-8.3 at greater depths, with the exceptions of core 4, with a value of 7.2 at a depth of 15.8 cm, and core 5, which shows a maximum value of 9.3 at 11.5 cm, although this data point meets the criteria to be considered a statistic outlier.

Saturation states with respect to calcite (Ω_{Ca}) and aragonite (Ω_{Ar}) -calculated from measurements of alkalinity, DIC, Ca^{2+}, NH_4^+, SRP and Si- generally showed supersaturation at depths greater than 10 cm for all cores (Figure 5.5). In cores 4 and 6, the upper 5 cm are undersaturated with respect to both minerals, whereas between 5 and 16 cm depths only some isolated measurements of aragonite and calcite undersaturation are associated with cores 3, 4 and 5 (Figure 5.5). Core 5 shows a statistical outlier (Ω_{Ca} = 46.5 and Ω_{Ar} = 28.1) at depth 11.5 cm associated with the decoupling between alkalinity and DIC in this sample.

5.4.3 Sulfur compounds: Porewater and solid phase

SO_4^{2-} concentrations were lower than surface waters and generally decreased with depth (Figure 5.6), with depletions with respect to surface values reaching approximately Δ4 mM at 40 cm depth. SO_4^{2-} measurements normalized to porewater Cl^- concentrations showed the same general depth distributions (Figure 5.6). H_2S concentrations were below 1μM in the upper 4 cm of all cores, and overall increased at greater depths for all cores except core 2 (Figure 5.6).

Despite most H_2S measurements for cores 2, 4, 5 and 6 ranging between 0 and 15 µM, maximum concentrations of 39 µM (core 6) and 113 µM (core 5) were achieved at 15.5 – 16.5 cm depths (Figure 5.6). Core 3 stands out with H_2S concentrations at depths greater than 8 cm an order of magnitude greater than most measurements for cores 2, 4, 5, and 6 with a maximum of 304 µM at 32.8 cm. This pattern is reversed in sediment TRS measurements, which showed general increases with depth (up to 232 µmol g dry weight (DW) but substantially lower values for core 3 when compared to other cores (Figure 5.6).

5.4.4 Porewater nutrients: NH_4^+, NO_x, SRP, and Si

All nutrient concentrations except NO_x were substantially elevated in core porewaters with respect to surface water (Figure 5.7). While NH_4^+ profiles were variable, with some cores displaying a pattern of increasing concentrations with depth (i.e. core 6) and others the opposite trend (i.e. core 5), average concentrations of NH_4^+ were two orders of magnitude greater than surface waters (225 µM compared to <1 µM) and reached maxima ranging from 394 to 442 µM at a wide range of depths (8-38 cm, Figure 5.7). NO_x concentrations were low (< 5µM) but similar to measured surface water values (Figure 5.7). Core 3 NO_x values were distinctively higher when compared to other cores and reached a maximum of 3.6 µM at 17 cm depth. SRP concentrations were one order of magnitude greater than those measured at surface waters, and generally increased with depth in all cores (Figure 5.7). Cores 2, 4, and 5 showed a stabilization of concentrations ~55 µM at depths greater than 10 cm, while core 3 and 6 reached maxima of 90-105 µM at depths of 16 cm and 33 cm, respectively. Si depth distributions, although

concentrations were elevated with respect to surface water, did not show strong patterns with depth (Figure 5.7). The average concentration was approximately ~350 µM, although cores 4 and 5 presented a minimum of 175-200 µM at depths 7-9 cm, and core 3 showed consistently higher concentrations when compared to other cores and a maximum of >1 mM at ~28 cm.

5.4.5 Stoichiometric relationships among porewater solutes

Alkalinity porewater distributions were correlated with other solutes (Figure 5.8). Highly significant robust linear regressions were estimated between alkalinity and DIC (Figure 5.8a, adjusted $R^2 = 0.88$, $p < 0.001$), resulting in a molar ratio of 1.10. Similarly, alkalinity was negatively correlated with SO_4^{2-} (Figure 5.8b, adjusted $R^2 = 0.71$, $p < 0.001$), with a similar molar ratio of -1.11. Regressions between alkalinity and Ca^{2+}, or the difference between porewater concentrations with respect to surface water for both solutes, were statistically significant ($p \leq 0.02$) but not linear (adjusted R^2= 0.10 and 0.24, Figure 5.8c-d), and resulted in molar ratios of 1.84 and 1.91, respectively (Figure 5.8).

5.5 Discussion

5.5.1 Sediment structure

This work represents, to our knowledge, the most complete and rigorous description of the biogeochemical structure of an oyster reef – natural or restored – to date. While valuable contributions were provided by Bahr and Lanier (1981) and, more recently, by Foudrie et al.

2017, we believe this is the first time that a detailed examination of the solid-phase and porewater solute distributions has been achieved.

Our results confirm that oyster reefs are very heterogeneous habitats that, in some ways, defy traditional classifications associated with temperate coastal sediment systems (Burdige, 2006). Oyster reef sediments are classified as permeable, coarse sands based on our grain size analysis (i.e. mean grain size = 854.4 μm) and porosities (i.e. mean porosity = 0.59), thereby matching previously reported values (Kellogg et al., 2013; Humphries et al., 2016, although see Malkin et al., 2017). The solid phase is, however, very heterogeneous and dominated by shell fragments, with estimates of $CaCO_3$ representing ~87% of the total sediment by weight. This dominant contribution of solid carbonates vastly surpasses estimates of sedimentary carbonates measured for other nearshore systems (e.g. Aller, 1982; Green and Aller, 1998; D'Andrea et al., 2002; Rassmann et al., 2016) and shelf sediments (e.g. Marinelli et al., 1998; Rusch et al., 2003), although it is comparable to measurements carried out in tropical coral reefs (e.g. Erftemeijer and Middelburg, 1993). Permeable, coarse sediments, regardless of their $CaCO_3$ content, usually are low in % organic C. While our measured average of 1.25% is not as elevated as values described for organic-rich, fine-sediment environments (Burdige, 2006 and references therein), it is higher than usually expected in nearshore, permeable sediments (e.g. D'Andrea et al., 2002; Rao et al., 2014). Our results of relatively high content of organic C are within the lower range of previously measured organic contents in natural and restored oyster reefs (Kellogg et al., 2013; Humphries et al., 2016; Fodrie et al., 2017; Malkin et al., 2017). This triumvirate of sediment properties: coarse sediment size, significantly elevated concentrations of $CaCO_3$, and relatively

high content of organic C distinguishes oyster reefs as an anomaly within the usual classification of sedimentary systems.

Average organic C:N ratios (i.e. 9.92) are within the ranges of previously published results for biodeposits and sediments collected in oyster reefs (i.e. 7.76 – 12.8; Newell et al., 2005; Holyoke, 2008; Higgins et al., 2013; Humphries et al., 2016). The measured C:N ratios deviate from theoretical Redfield ratios (i.e. 6.65) and likely indicate carbon and nitrogen enrichment in biodeposits through the incorporation of more refractory carbon of terrestrial origin in the form of pseudofeces (Newell et al., 2005), or preferential preservation of the less labile fraction of organic C within the reef, as high rates of organic matter remineralization have been described for oyster reefs (Malkin et al., 2017) and other permeable sediment environments (Marinelli et al., 1998; D'Andrea et al., 2002).

5.5.2 Diagenetic processes responsible for porewater solute distributions.

Our results demonstrate significant alkalinity and DIC production within oyster reef sediments with respect to overlying waters. The statistically significant correlation between alkalinity and DIC porewater (Figure 5.8a) shows a slope of 1.1, close to the value of 1.0 predicted for sediments dominated by calcium carbonate dissolution enhanced by aerobic remineralization of organic matter, or sulfate reduction (Hu and Burdige, 2008; Burdige et al., 2010). Inquiry into the biogeochemical processes driving the observed results, therefore, involves disentangling the relative importance of these two major early diagenetic processes:

$CaCO_3$ (i.e. calcite, as oyster shell is mostly formed by this $CaCO_3$ mineral) dissolution or sulfate reduction of organic matter.

Sediment calcite dissolution is thermodynamically favored when porewater $\Omega_{Ca} < 1$. Our results show some instances of undersaturation with respect to calcite in the upper 10 cm, demonstrating that shell dissolution in the upper cm of the sediment could be an important driver of alkalinity generation (Figure 5.5); however, some cores showed saturation state measurements much greater than the thermodynamic dissolution threshold (Figure 5.5). Calcium carbonate dissolution potential key role, though, is suggested by the statistically significant linear regression found between alkalinity and Ca^{2+} (Figure 5.8d), though there is considerable scatter of values, as shown by the low value of the coefficient of determination (Adjusted $R^2 = 0.24$). The measured alkalinity:Ca^{2+} molar stoichiometry is 1.91, close to the theoretical value of 2.00 associated with $CaCO_3$ dissolution (Soetaert et al., 2007; Wolf-Gladrow et al., 2007).

Ca^{2+} porewater concentrations, however, are generally lower than those found in the overlying water, the opposite as expected if significant dissolution was taking place. Moreover, Ca^{2+}, albeit generally increasing with depth at depths greater than 10-15 cm, does not show profile patterns as consistent as those measured for alkalinity and DIC (Figure 5.4). Although it is always possible that the relatively low precision of our Ca^{2+} measurements could explain some of the variability in the Ca^{2+} data, back-of-the-envelope estimates of expected changes in Ca^{2+} based on ΔAlkalinity = 1mM, a conservative value applicable to all cores observed, should have resulted in changes in Ca^{2+} greater than 10%, much higher than the estimated 1.6 % uncertainty of our analytical techniques.

Porewater data, therefore, show conflicting evidence regarding the role of shell dissolution in the studied restored reef. We hypothesize that metabolically enhanced shell dissolution is, effectively, a key biogeochemical process responsible for some of the alkalinity produced. Its role is likely confined to the first cm of sediment, however, and the depth resolution of our sampling might not be able to fully capture the likely increase in Ca^{2+} concentrations expected in microzones found in that horizon. Resolving the mechanisms responsible for the observed decreased concentration of Ca^{2+} at depths greater than 10-15 cm is beyond the scope of this work. We speculate, however, that modest amounts of authigenic precipitation of calcium phosphate could be occurring, given the optimum conditions with regards to pH, abundance of porewater SRP, and decreased levels of Mg^{2+} compared to seawater with salinity > 30 psu (Berner, 1966; Van Cappellen and Berner, 1991).

In sediments with supersaturated overlying waters like the studied habitat, calcium carbonate undersaturation in porewaters is often the result of the production of metabolic acids as by-products of aerobic remineralization of organic matter (Green et al., 1993; Hales and Emerson, 1997; Burdige et al., 2008). While we lack O_2 measurements to empirically define the depth of the redox boundary layer, visual inspection of the sediment during sampling revealed black mineral deposits very close to the sediment-water interface. These observations suggest that the taphonomically active zone (TAZ), the oxic portion of the oyster reef framework, is in this case a relatively thin, surficial layer. Nevertheless, important bioturbating macrofauna are associated with oyster reefs (e.g. Kellogg et al., 2013), and could periodically re-oxygenate

deeper sections of the sediment, thus stimulating metabolically enhanced shell dissolution (e.g. Green et al., 1993).

The hypothesis of a relatively thin TAZ in the analyzed cores is supported, however, by the consumption of SO_4^{2-} with depth - indicative of sulfate reduction- and by elevated concentrations of reduced nitrogen (i.e. NH_4^+) compared to the oxidized nitrogen species NO_x, which are severely depleted (Figure 5.7). Alternatively, it is possible that depletion of NO_x is evidence of denitrification, a suboxic process prevalent in surficial oyster reef sediments (Kellogg et al., 2014). The low values of NO_x in the overlying water and the lack of correlation between alkalinity and DIN (data not shown), however, suggest low rates of denitrification within these cores, likely due to NO_x substrate limitation.

Among the anaerobic pathways for remineralization of organic matter, sulfate reduction is a dominant one in organic-rich sediments (Jørgensen, 1982). This pathway has indeed been described as prevalent in sediments collected within oyster reefs (Malkin et al., 2017). High rates of organic matter remineralization are supported by the elevated concentrations of inorganic nutrients (Figure 5.7) and their increase with depth. Furthermore, our results indicate that sulfate reduction is the dominant remineralization pathway in our system as consumption of SO_4^{2-} with depth is apparent and patterns are maintained after normalizing SO_4^{2-} concentrations to Cl^- to eliminate changes related to porewater salinity variations (Figure.5.6).

Alkalinity is generated through net sulfate reduction in a 2 alkalinity: $1SO_4^{2-}$ molar ratio (Soetaert et al., 2007) if reoxidation of the produced hydrogen sulfide (H_2S) is not complete and, instead, is precipitated in the form of iron-sulfide minerals (Hu and Cai, 2011). Alkalinity

production through sulfate reduction requires the coupling of iron and manganese oxide reduction and the formation of iron-sulfide such as pyrite (see discussions in Hu and Cai, 2011; Krumins et al., 2013). The net effect of all coupled reactions, however, is an increase of two moles of alkalinity per mole of sulfide produced that it is not reoxidized (Soetaert et al., 2007; Hu and Cai, 2011; Krumins et al., 2013).

Our results indicate very low concentrations of H_2S but values of precipitated TRS comparable to measurements carried out on mid-bay Chesapeake Bay sediments (Marvin-DiPasquale and Capone, 1998; Marvin-DiPasquale et al., 2003). There is no significant correlation, however, between ΔSO_4^{2-} and TRS (even after multiple corrections were applied to transform TRS to a comparable concentration metric), suggesting that most of the produced H_2S might be reoxidized or, alternatively, that unidentified sinks for SO_4^{2-} might be present, such as SO_4^{2-} adsorption to shell surfaces (e.g. Millero et al., 2001).

The key role of SO_4^{2-} reduction in producing alkalinity in the investigated oyster reef sediments is further demonstrated by the highly significant and predictive regression between alkalinity and SO_4^{2-} (Adj-R^2 = 0.71, Figure 5.8b). The slope of this regression is -1.11, however, far from the theoretical value of -2.00 (Soetaert et al., 2007; Hu and Cai, 2011; Krumins et al., 2013), thus indicative of some loss of alkalinity through reoxidation of reduced compounds (including H_2S) or abiotic precipitation of $CaCO_3$ (i.e. micrite). Precipitation of $CaCO_3$, although thermodynamically favored in depths > 10 cm, is unlikely, however, given the observed high concentrations of dissolved organic matter (DOM)- a well-known abiotic precipitation inhibiting factor (Morse et al. 2007)- in Chesapeake Bay sediment porewaters (Burdige, 2001), likely

further elevated within the first cm of oyster reef framework. At greater depths, however, reprecipitation of $CaCO_3$ could occur, as observed by Waldbusser et al. 2011 in dredged shells.

Finally, we estimated generally a small contribution of non-carbonate organic alkalinity to the total alkalinity (mean of 7.8%), likely associated with dissolved organic anions such as humic substances (Cai et al., 1998; Cai and Wang, 1998). However, the magnitude of the contribution to alkalinity might display temporal variability associated with the seasonality of terrestrial inputs of humic substances to the estuary and thus warrants further exploration.

Collectively, these observations amount to evidence for both metabolically-enhanced shell dissolution and net sulfate reduction in these sediments, and though we hypothesize that both processes are partially responsible for the production of alkalinity in these systems, the present evidence suggest that sulfate reduction might be the dominant biogeochemical pathway responsible for the observed increase in alkalinity and DIC porewater. From a mass-balance prospective, in an oyster reef in steady-state, the overall net production of alkalinity through shell dissolution over annual or interannual timescales must be balanced by calcification. The production of inorganic alkalinity through non-carbonate pathways like SO_4^{2-} reduction or that associated with organic compounds, however, could result in a net subsidy of alkalinity to the system if a significant percentage of the organic matter fueling this production is not recycled within the reef but imported from external terrestrial or oceanic sources.

5.5.3 Implications of habitat-level biogeochemical processes for individual bivalves

Our biogeochemical exploration of this restored oyster reef demonstrates the tight links between alkalinity and organic C in the form of biodeposits. Organic carbon likely regulates the production of alkalinity either through metabolically-enhanced shell dissolution, production of inorganic non-carbonate alkalinity associated with anaerobic respiration or organic matter, or, directly, through the contribution of dissolved organic compounds to alkalinity.

Alkalinity releases from the reef could play an important role as settlement cue for settling larvae and newly metamorphosed post-larvae and as local buffering against corrosive conditions (Waldbusser et al. 2013), thereby enhancing survival at this stage. Calcium carbonate saturation state has been identified as an important chemical cue for some bivalves (Green et al., 2013; Clements and Hunt, 2014; Peng et al., 2017; Clements and Hunt, 2017) and bivalve juveniles have also been identified as sensitive to OA (e.g. Green et al. 2004, 2009; Beniash et al. 2010; Waldbusser et al. 2011; Hettinger et al., 2012; Bressan et al. 2014; Clements and Hunt, 2014; Miller and Waldbusser, 2016) The negative impacts of acidification at this life-stage, however, seem to be temporally restricted to the initial post-metamorphosis stages in clams (Green et al. 2009; Miller and Waldbusser, 2016), thus could potentially be buffered at small and short spatial and temporal scales (e.g. Green et al. 2009).

While any significant effect on the overlying water carbonate chemistry will depend on local hydrodynamics within the oyster reef, microscale observations of oyster reef circulation support the existence of local retention areas (Whitman and Reidenbach, 2012). These areas with relatively long water residence times could display transient significantly increased alkalinity due to efflux from the oyster reef framework, thereby affecting calcium saturation state

Thus, the observed alkalinity production within the reef could have important implications in oyster restoration management and OA mitigation strategy planning. Ultimately, our results suggest that to maximize alkalinity production within an oyster reef, both shell substrate and organic matter deposition are necessary, thereby suggesting that restoration strategies that solely focus on shell planting might not be as effective as those that encourage the growth of living oyster reefs or shell planting in organically-rich sediments.

Table 5.1. Core sampling dates, and spatial coordinates and environmental conditions for collection sites.

	Site	Date (2017)	Lat	Long	Site depth (m)	T (°C)	S
Core 2	1	9/25	38.76186°	-76.30663°	2.13	25.3	15.25
Core 3	1	9/25	38.76186°	-76.30663°	2.13	25.3	15.25
Core 6	1	9/25	38.76186°	-76.30663°	2.13	25.3	15.25
Core 4	2	9/25	38.75232°	-76.31049°	1.83	25.3	15.48
Core 5	2	9/25	38.75232°	-76.31049°	1.83	25.3	15.48

Table 5.2. Cores penetration depths, profile sampling resolution, grain size analysis results, and average porosities.

	Penetration depth (cm)	Sampling resolution (cm)	Mean grain size (μm)	Mean grain size (descript)	Sorting	Average Φ
Core 2	19	3.2	846	Coarse sand	Moderately sorted	0.59
Core 3	42	2.6	893	Coarse sand	Moderately sorted	0.56
Core 6	17	2.8	863	Coarse sand	Moderately sorted	0.58
Core 4	23	3.3	847	Coarse sand	Moderately sorted	0.59
Core 5	20	2.5	823	Coarse sand	Moderately sorted	0.64
Average	-	-	854.4	Coarse sand	Moderately sorted	0.59

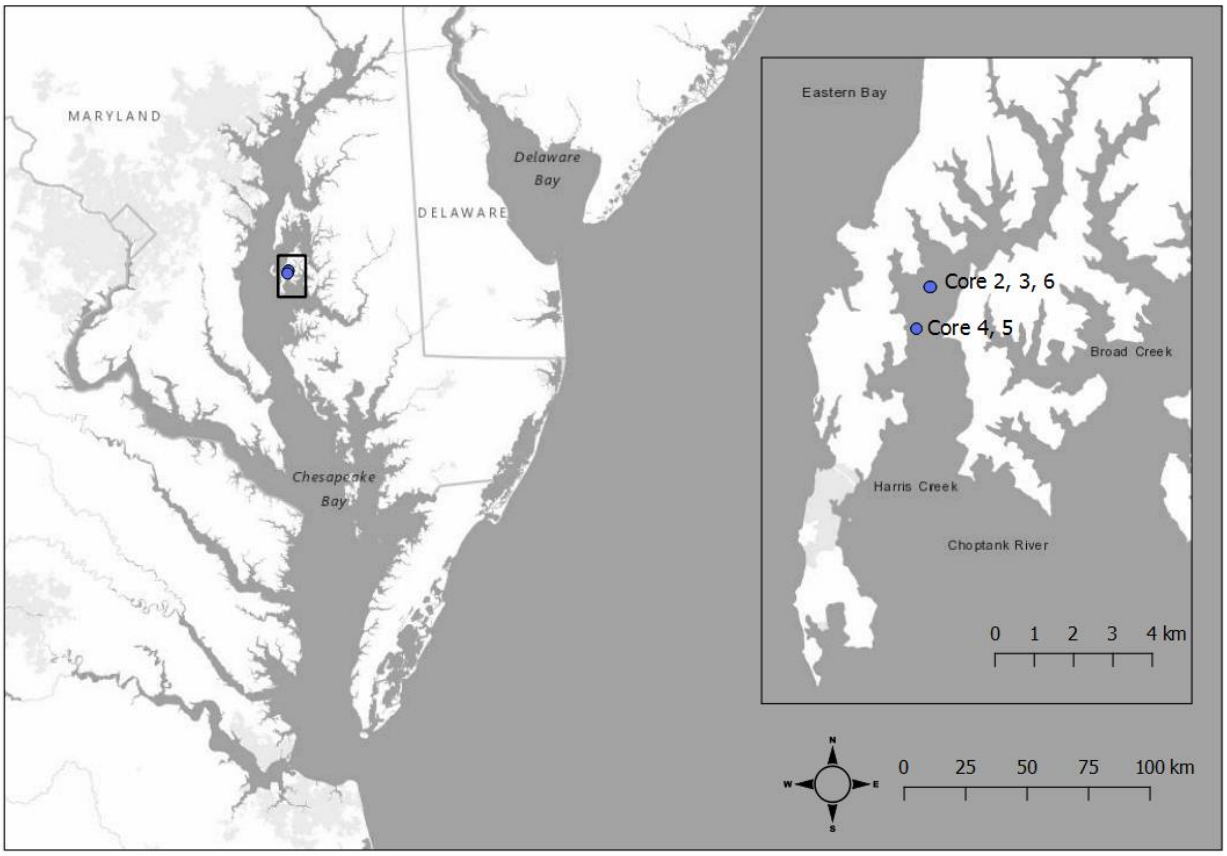

Figure 5.1. Map of study area showing the collection sites of oyster reef cores within Harris Creek, a tributary of Chesapeake Bay.

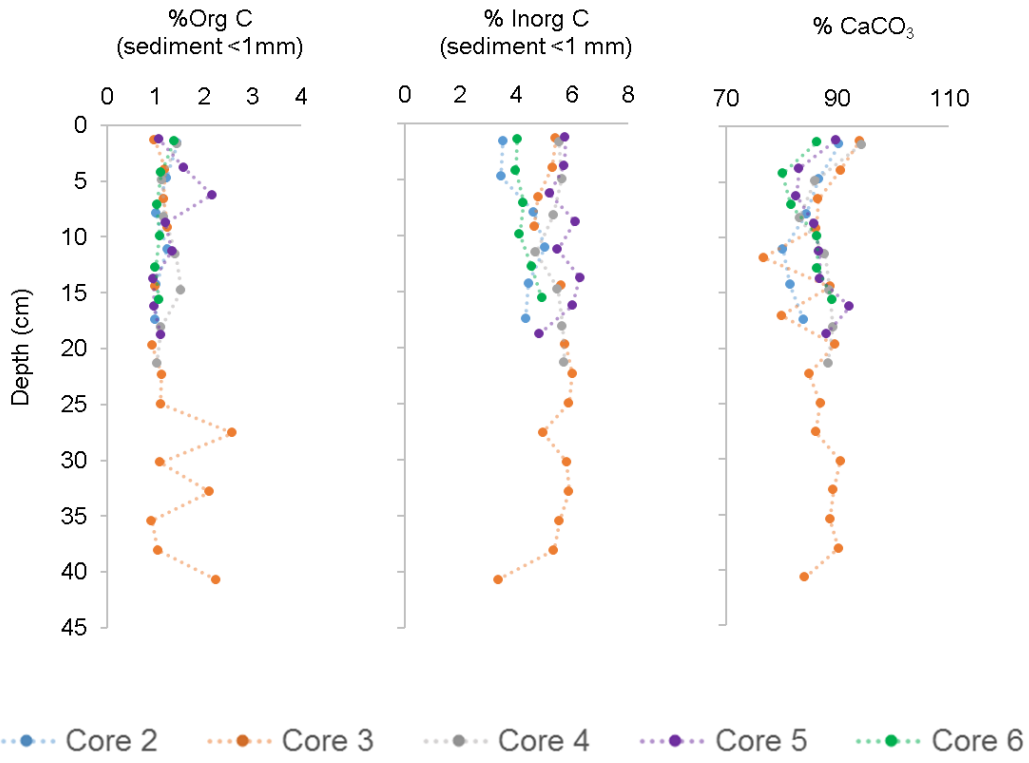

Figure 5.2. Solid phase depth profiles of measured % Org C, % Inorganic C in the sediment fraction < 1mm, and estimated total % of $CaCO_3$ in intact oyster reef cores.

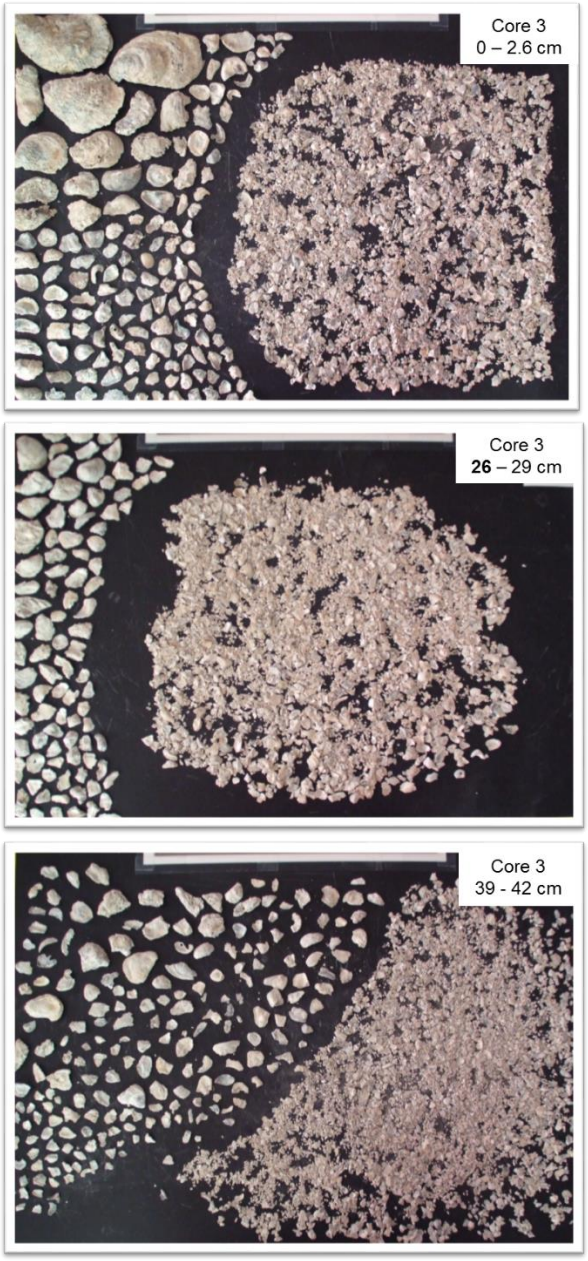

Figure 5.3. Example images of the type and size of shell fragments found at three different depths within the oyster reef framework.

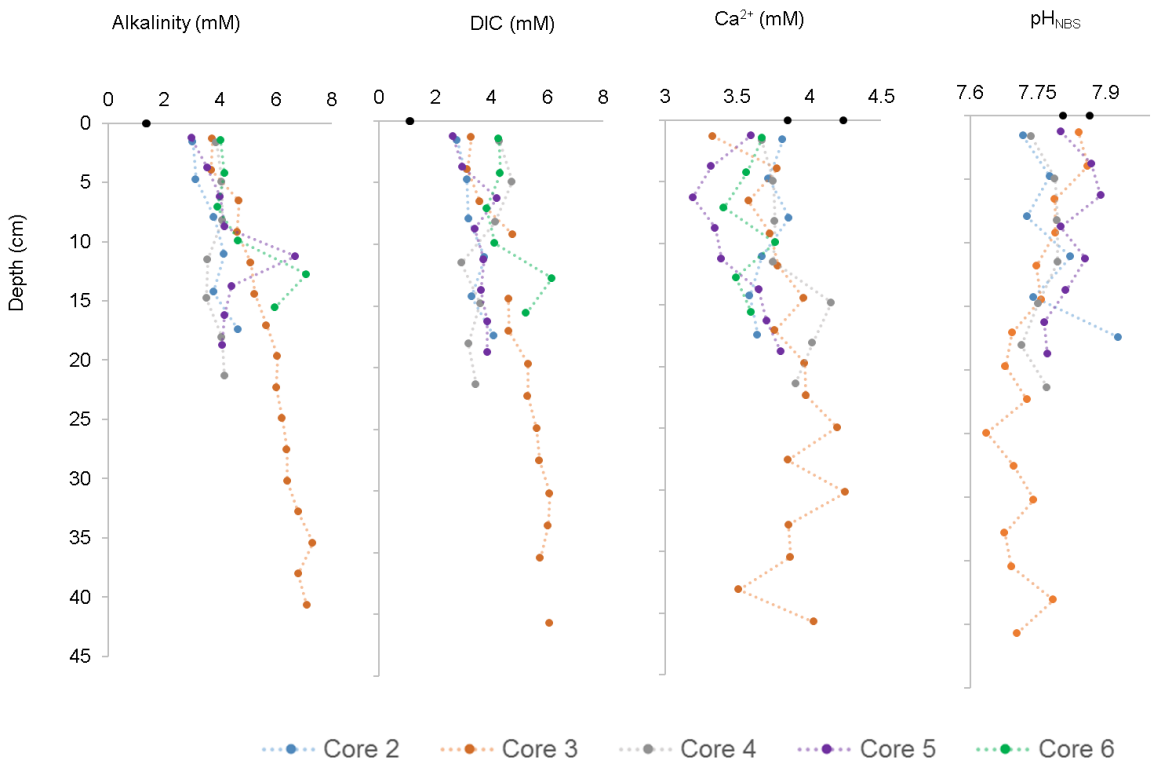

Figure 5.4. Porewater depth profiles of measured Alkalinity, DIC, Ca^{2+} and pH_{NBS} in intact oyster reef cores. Black dot indicates surface water concentration. Color dots are centered discrete measurements and color dashed lines represent linear interpolations.

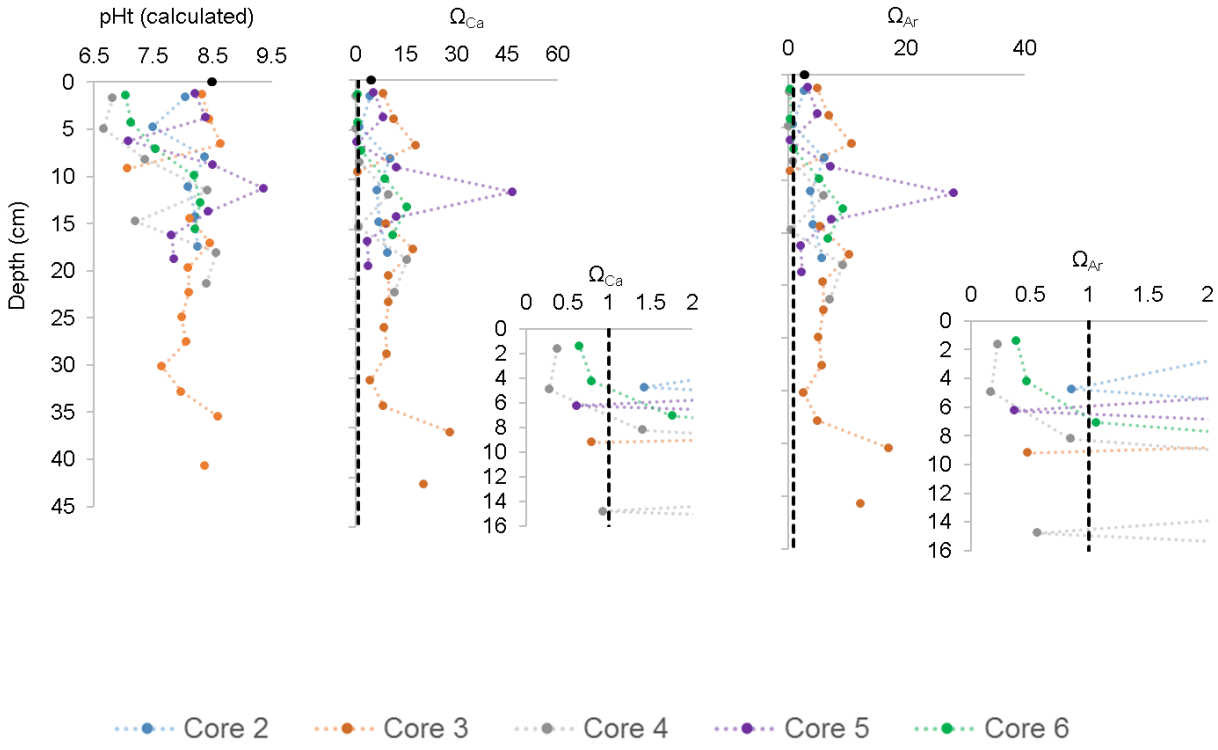

Figure 5.5 Porewater depth profiles of calculated pH_t, Ω_{Ca} and Ω_{Ar} in intact oyster reef cores. Inserts are magnified porewater depth profiles of Ω_{Ca} and Ω_{Ar} in the first 16 cm depth. Black dot indicates surface water concentration. Black dashed line represents Ω=1, or the saturation thermodynamic threshold. Color dots are centered estimates and color dashed lines represent linear interpolations. Note that Core 5 data point at 11.5 cm is a statistical outlier.

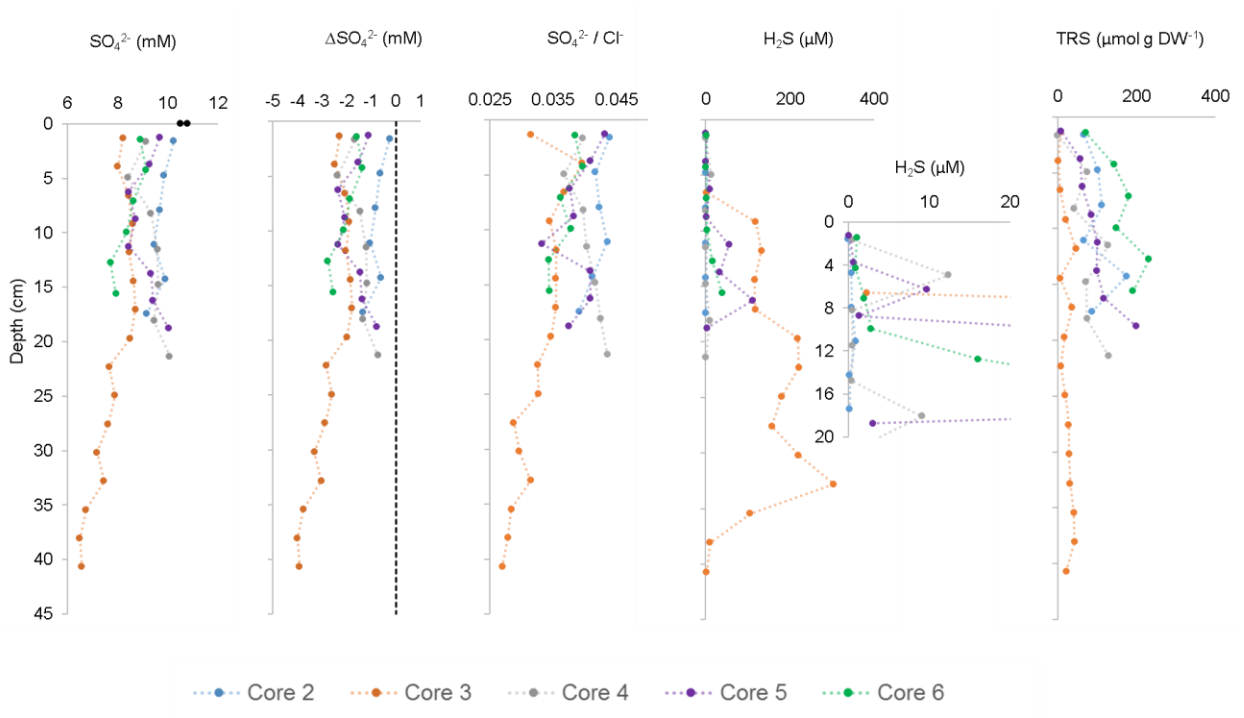

Figure 5.6. Porewater depth profiles of measured SO_4^{2-}, ΔSO_4^{2-} (i.e. $SO_4^{2-}{}_z$ - $SO_4^{2-}{}_{surface\ water}$), H_2S and TRS in intact oyster reef cores. Inserts is magnified porewater depth profiles of H2S in the first 20 cm depth. Black dot indicates surface water concentration. Black dashed line corresponds to $\Delta SO_4^{2-} = 0$. Color dots are centered discrete measurements and color dashed lines represent linear interpolations.

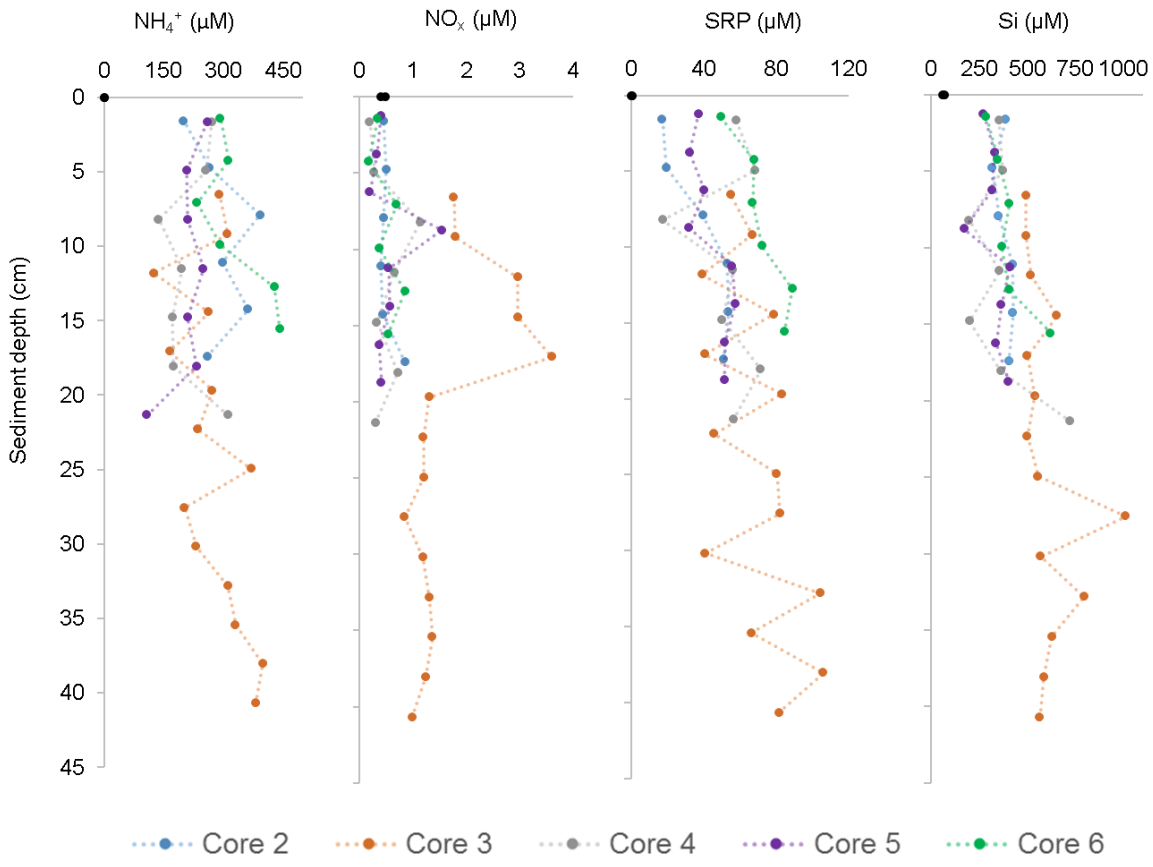

Figure 5.7. Porewater depth profiles of measured NH_4^+, NO_x, SRP, and Si in intact oyster reef cores. Color dots are centered discrete measurements and dashed lines represent linear interpolations.

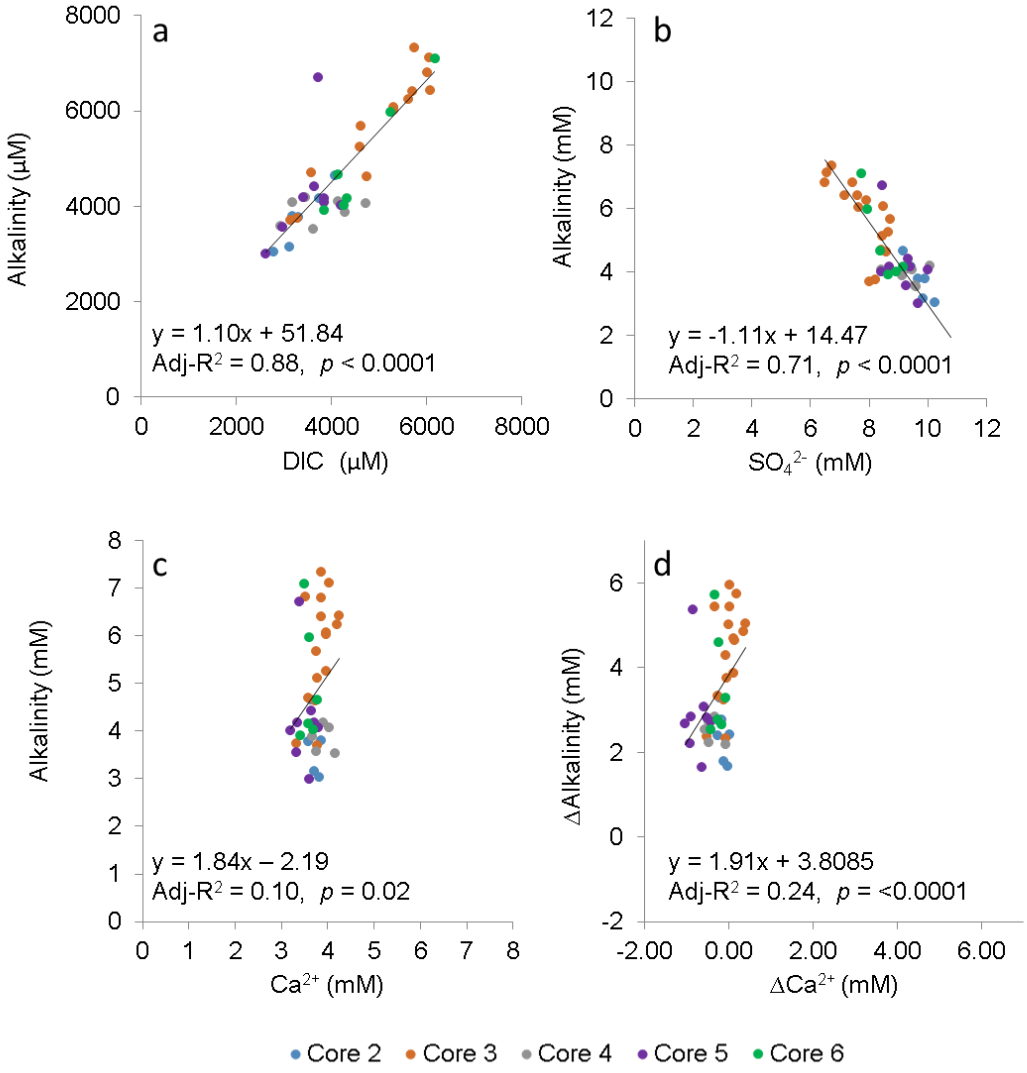

Figure 5.8. Robust linear regressions of porewater alkalinity as a function of other solutes. a) DIC; b) SO_4^{2-}; c) Ca^{2+}; d) ΔCa^{2+} (i.e. $Ca^{2+}{}_z$- $Ca^{2+}{}_{surface\ water}$)

6. CHAPTER VI.- Conclusions

While a growing body of experimental work has advanced our understanding of the effects of ocean acidification on marine bivalves (Gazeau et al., 2013; Kroeker et al., 2013), a key vulnerable taxa, important questions remain regarding the effects of highly variable carbonate chemistry commonly found in bivalve habitats (e.g. Hofmann et al., 2010; Barton et al., 2012; Hauri, Gruber, Vogt, et al., 2013; Evans et al., 2015; Hales et al., 2017; Pacella et al., 2018). The majority of work exploring OA impacts on bivalves in the last decade has focused on isolated laboratory experiments with constant acidification treatments, conditions that do not match those experienced by organisms in natural environments (Boyd et al., 2016; Dillon et al., 2016). Similarly, there are vast gaps in knowledge regarding the biogeochemical processes potentially regulating carbonate chemistry conditions at smaller scales within bivalve aggregations (i.e. oyster reefs).

The principal goal of this dissertation was, therefore, to advance the current understanding of OA effects on bivalves through the incorporation of carbonate chemistry variability at physiologically relevant temporal and spatial scales (*sensu* Helmuth et al., 2014; Waldbusser and Salisbury, 2014). This overarching objective was achieved through two sub-goals: 1) the study of the effects of high-frequency temporal variability on carbonate chemistry conditions in OA-sensitive bivalve larvae; 2) the characterization of the biogeochemical structure of oyster reefs, focusing on alkalinity production dynamics and habitat-level responses to moderate OA conditions.

The first sub-goal is the subject of both chapter 2 and 3, and was accomplished through 1) the development of a new acidification stress metric (OASIS) that empirically accounts for natural high-frequency temporal variability of carbonate chemistry conditions on Pacific oyster larvae survival; and 2) the design and validation of a new experimental system (DOAMES) capable of decoupling carbonate chemistry parameters, often occurring in coastal areas, and of creating dynamic environmental treatments to mimic natural variability found in bivalve habitats.

The second sub-goal was carried out by describing the biogeochemical structure and function of an Eastern oyster restored-reef in Harris Creek, MD, US and its responses to moderate perturbations of overlying PCO_2. This research focused on the alkalinity dynamics within the reef and attempted attribution of biogeochemical processes responsible for the measured large alkalinity fluxes from the oyster reef to the overlying water and their potential as small-scale buffering agents to local, transient corrosive conditions.

The primary conclusion of this research is that incorporating temporal and spatial carbonate chemistry variability into experiments is crucial to accurately predict important organismal outcomes such as oyster larvae survival and can be achieved through relatively simple modeling techniques, new experimental systems and closer examination to the bivalve habitat-level carbonate chemistry dynamics. These findings are not new, as the crucial role of environmental variability has been well-documented regarding other physico-chemical parameters such as temperature (e.g. Helmuth and Hofmann, 2001; Helmuth et al., 2010; Helmuth et al., 2014). The effects of carbonate chemistry variability in bivalves are however not

well constrained and divergent responses to variable OA have been reported (e.g. Frieder et al., 2014; Griffith and Gobler, 2017).

This research demonstrates that relatively simple stress models such as OASIS can accurately predict bivalve larval survival under fluctuating, natural carbonate chemistry conditions. Metrics like OASIS are of particular importance in order to transform high-frequency monitoring data into relevant metrics for stakeholders and managers and, relatedly, to incorporate biological meaning to increasingly complex mechanistic models that forecast future carbonate chemistry conditions at the regional and local scale (e.g. Hauri, Gruber, Vogt, et al., 2013; Siedlecki et al., 2016; Pacella et al., 2018).

Similarly, the development DOAMES allows for the simultaneous recreation of complex coastal carbonate chemistry dynamics and to mimic realistic future conditions following state-of-the-art forecasting techniques that do not neglect inherent environmental variability in nearshore environments (see Pacella et al. 2018 and references therein). DOAMES is also relatively flexible to implement by other interested researchers, thereby exponentially expanding its potential to generate critical insight into OA impacts on organisms. DOAMES therefore provides improved predictions of the fate of bivalves and other sensitive taxa under future OA system-specific conditions and at the relevant physiological temporal and spatial scales, thereby generating crucial information for managers and stakeholders.

The second major conclusion of this work is that habitat-level responses to OA and organism-habitat interactions between organisms need to be assessed to better predict responses to future climate scenarios. This work demonstrates that there are large alkalinity effluxes from

oyster reefs to the overlying water, a previously unknown biogeochemical feature of these habitats, although the magnitude of these fluxes seems unaffected by moderate increases in overlying PCO_2. Furthermore, the results of this work suggest that the release of alkalinity is largely the result of anaerobic processes within the anoxic sediment framework and metabolically enhanced- dissolution of dead oyster shells, indicating feedbacks between the organic and inorganic carbon pools beyond burial within the oyster reef framework.

These results can have wide-ranging implications if alkalinity releases from the oyster reef significantly modify carbonate chemistry at micro spatial scales, even if the effects are transient. Both larval and juvenile bivalve stages are sensitive to OA, and calcium carbonate saturation state has been identified as a settlement cue for some species. Thus, alkalinity fluxes from the reef, although seem to be relatively insensitive to moderate increases in overlying water PCO_2, might have a key role in contributing to positive recruitment if they significantly ameliorate the carbonate chemistry conditions at local spatial scales, as first hypothesized by Waldbusser et al. 2013. The importance of this effect will likely be enhanced if large alkalinity effluxes coincide with the timing of larval and juvenile “windows-of-sensitivity”.

Consequently, as both the larval and habitat-level work demonstrate, differential sensitivities across life-stages need to be included in the parameterization of predictive models such as OASIS, as well as in understanding the potential habitat-level effects of OA on the alkalinity cycling within shell aggregations.

In summary, this dissertation suggests that relatively simple modeling and laboratory tools can successfully incorporate temporal variability naturally experienced by bivalves and

provide adequate predictions of survival. It further provides first evidence that reef-level biogeochemical feedbacks derived from the collocation of calcium carbonate shell and labile organic matter result in the production of large alkalinity fluxes that, while not very sensitive to increased moderate PCO_2, could indeed buffer corrosive conditions at local spatial scales, providing microrefugia to sensitive larval and juveniles.

Ultimately, this body of work is proof of the need to shift from an OA open-ocean paradigm based on stable carbonate chemistry conditions to improve our understanding regarding OA impacts on sensitive coastal organisms exposed to dynamic carbonate chemistry conditions.

Bibliography

Abbe G. 1988. Population structure of the American oyster on an oyster bar in central Chesapeake Bay: Changes associated with shell planting and increased recruitment. Journal of Shellfish Research 7(1): 33–40.

Aller RC. 1982. Carbonate Dissolution in Nearshore Terrigenous Muds: The Role of Physical and Biological Reworking. The Journal of Geology 90(1): 79–95.

Amaral V, Cabral HN, Bishop MJ. 2012. Moderate acidification affects growth but not survival of 6-month-old oysters. Aquat Ecol 46(1): 119–127. doi: 10.1007/s10452-011-9385-5

Arfken A, Song B, Bowman JS, Piehler M. 2017. Denitrification potential of the eastern oyster microbiome using a 16S rRNA gene based metabolic inference approach. PLOS ONE 12(9): e0185071. doi: 10.1371/journal.pone.0185071

Bach, L. T., L. C. M. Mackinder, K. G. Schulz, G. Wheeler, D. C. Schroeder, C. Brownlee, and U. Riebesell. 2013. Dissecting the impact of CO2 and pH on the mechanisms of photosynthesis and calcification in the coccolithophore Emiliania huxleyi. New Phytol. 199: 121–134. doi:10.1111/nph.12225

Bahr LM, Lanier WP. 1981. The ecology of intertidal oyster reefs of the south Atlantic coast: A community profile. Report No.: FWS/OBS-81/15.

Bandstra L, Hales B, Takahashi T. 2006. High-frequency measurements of total CO2: Method development and first oceanographic observations. Mar Chem 100(1–2): 24–38. doi: 10.1016/j.marchem.2005.10.009

Barros P, Sobral P, Range P, Chícharo L, Matias D. 2013. Effects of seawater acidification on fertilization and larval development of the oyster Crassostrea gigas. J Exp Mar Biol Ecol 440: 200–206. doi: 10.1016/j.jembe.2012.12.014

Barton A, Hales B, Waldbusser GG, Langdon C, Feely RA. 2012. The Pacific oyster, Crassostrea gigas , shows negative correlation to naturally elevated carbon dioxide levels: Implications for near-term ocean acidification effects. Limnology and Oceanography 57(3): 698–710. doi: 10.4319/lo.2012.57.3.0698

Barton A, Feely R, Weisberg S, Newton J, Hales B, Cudd S, Eudeline B, Langdon C, Jefferds I, King T, et al. 2015. Impacts of coastal acidification on the Pacific Northwest shellfish industry and adaptation strategies implemented in response. Oceanography 25(2): 146–159. doi: 10.5670/oceanog.2015.38

Bates, N. R., M. H. P. Best, K. Neely, R. Garley, A. G. Dickson, and R. J. Johnson. 2012. Detecting anthropogenic carbon dioxide uptake and ocean acidification in the North Atlantic Ocean. Biogeosciences Discuss. 9: 989–1019. doi:10.5194/bgd-9-989-2012

Bates, N., Y. Astor, M. Church, and others. 2014. A Time-Series View of Changing Ocean Chemistry Due to Ocean Uptake of Anthropogenic CO2 and Ocean Acidification. Oceanography 27: 126–141. doi:10.5670/oceanog.2014.16

Beck MW, Brumbaugh RD, Airoldi L, Carranza A, Coen LD, Crawford C, Defeo O, Edgar GJ, Hancock B, Kay MC, et al. 2011. Oyster Reefs at Risk and Recommendations for Conservation, Restoration, and Management. BioScience 61(2): 107–116. doi: 10.1525/bio.2011.61.2.5

Beniash E, Ivanina A, Lieb N, Kurochkin I, Sokolova I. 2010. Elevated level of carbon dioxide affects metabolism and shell formation in oysters Crassostrea virginica (Gmelin). Marine Ecology Progress Series 419: 95–108. doi: 10.3354/meps08841

Berner RA. 1966. Chemical diagenesis of some modern carbonate sediments. American Journal of Science 264: 1–36.

Blott SJ, Pye K. 2001. GRADISTAT: a grain size distribution and statistics package for the analysis of unconsolidated sediments. Earth Surface Processes and Landforms 26(11): 1237–1248. doi: 10.1002/esp.261

Bochenek E, Klinck J, Powell E, Hofmann EE. 2001. A biochemically based model of the growth and development of Crassostrea gigas larvae. J Shellfish Res 20(1): 243–265.

Bonhomme R. 2000. Bases and limits to using ‘degree. day’units. Eur J Agron 13(1): 1–10.

Boucher G, Boucher-Rodoni R. 1988. In situ measurement of respiratory metabolism and nitrogen fluxes at the interface of oyster beds. Marine Ecology Progress Series: 229–238.

Boyd PW, Cornwall CE, Davison A, Doney SC, Fourquez M, Hurd CL, Lima ID, McMinn A. 2016. Biological responses to environmental heterogeneity under future ocean conditions. Global Change Biology 22(8): 2633–2650. doi: 10.1111/gcb.13287

Bozinovic F, Pörtner H-O. 2015. Physiological ecology meets climate change. Ecol Evol 5(5): 1025–1030. doi: 10.1002/ece3.1403

Breese WP, Malouf RE. 1975. Hatchery manual for the Pacific oyster. Corvallis, OR: Sea Grant College Program - Oregon State University. Agricultural Experiment Station - Special Report no. 443 Report No.: ORESU-H-75-002. Available at

http://ir.library.oregonstate.edu/xmlui/bitstream/handle/1957/6637/?sequence=1. Accessed 2015 May 13.

Bressan M, Chinellato A, Munari M, Matozzo V, Manci A, Marceta T, Finos L, Moro I, Pastore P, Badocco D, et al. 2014. Does seawater acidification affect survival, growth and shell integrity in bivalve juveniles? Marine Environmental Research 99: 136–148.

Buckley LB, Waaser SA, MacLean HJ, Fox R. 2011. Does including physiology improve species distribution model predictions of responses to recent climate change? Ecology 92(12): 2214–2221.

Burdige DJ. 1993. The biogeochemistry of manganese and iron reduction in marine sediments. Earth-Science Reviews 35(3): 249–284. doi: 10.1016/0012-8252(93)90040-E

Burdige DJ. 2001. Dissolved organic matter in Chesapeake Bay sediment pore waters. Org Geochem 32(4): 487–505. doi: 10.1016/S0146-6380(00)00191-1

Burdige DJ. 2006. Geochemistry of Marine Sediments. Princeton, New Jersey: Princeton University Press.

Burdige DJ, Zimmerman RC, Hu X. 2008. Rates of carbonate dissolution in permeable sediments estimated from pore-water profiles: The role of sea grasses. Limnology and Oceanography 53(2): 549–565. doi: 10.4319/lo.2008.53.2.0549

Burdige DJ, Hu X, Zimmerman RC. 2010. The widespread occurrence of coupled carbonate dissolution/reprecipitation in surface sediments on the Bahamas Bank. American Journal of Science 310(6): 492–521. doi: 10.2475/06.2010.03

Burrell, R. B., A. G. Keppel, V. M. Clark, and D. L. Breitburg. 2016. An automated monitoring and control system for flow-through co-cycling hypoxia and pH experiments: Automated co-cycling DO and pH system. Limnol. Oceanogr. Methods 14: 168–185. doi:10.1002/lom3.10077

Caffrey JM, Hollibaugh JT, Mortazavi B. 2016. Living oysters and their shells as sites of nitrification and denitrification. Mar Pollut Bull 112(1–2): 86–90. doi: 10.1016/j.marpolbul.2016.08.038

Cai W-J, Wang Y. 1998. The chemistry, fluxes, and sources of carbon dioxide in the estuarine waters of the Satilla and Altamaha Rivers, Georgia. Limnol Oceanogr 43(4): 657–668. doi: 10.4319/lo.1998.43.4.0657

Cai W-J, Wang YA, Hodson REA. 1998. Acid-Base Properties of Dissolved Organic Matter in the Estuarine Waters of Georgia, USA. Geochimica et Cosmochimica Acta 62(3): 473–483. doi: 10.1016/S0016-7037(97)00363-3

Cai, W.-J., X. Hu, W.-J. Huang, and others. 2011. Acidification of subsurface coastal waters enhanced by eutrophication. Nat. Geosci. 4: 766–770. doi:10.1038/ngeo1297

Cai W-J, Huang W-J, Luther GW, Pierrot D, Li M, Testa J, Xue M, Joesoef A, Mann R, Brodeur J, et al. 2017. Redox reactions and weak buffering capacity lead to acidification in the Chesapeake Bay. Nat Commun 8(1). doi: 10.1038/s41467-017-00417-7

Caldeira K, Wickett ME. 2003. Anthropogenic carbon and ocean pH. Nature 425: 365.

Canfield DE, Raiswell R, Westrich JT, Reaves CM, Berner RA. 1986. The use of chromium reduction in the analysis of reduced inorganic sulfur in sediments and shales. Chemical Geology 54(1–2): 149–155. doi: 10.1016/0009-2541(86)90078-1

Carriker MR, Van Zandt D, Grant TJ. 1978. Penetration of molluscan and non-molluscan minerals by the boring gastropod Urosalpinx cinerea. The Biological Bulletin 155(3): 511–526.

Carroll JM, O'Shaughnessy KA, Diedrich GA, Finelli CM. 2015. Are oysters being bored to death? Influence of Cliona celata on Crassostrea virginica condition, growth and survival. Diseases of Aquatic Organisms 117(1): 31–44. doi: 10.3354/dao02928

Carver CE, Thériault I, Mallet AL. 2011 Feb 1. Infection of Cultured Eastern Oysters Crassostrea virginica by the Boring Sponge Cliona celata, with Emphasis on Sponge Life History and Mitigation Strategies. http://dx.doi.org/10.2983/035.029.0423. doi: 10.2983/035.029.0423

Chan F, Barth JA, Blanchette CA, Byrne RH, Chavez F, Cheriton O, Feely RA, Friederich G, Gaylord B, Gouhier T, et al. 2017. Persistent spatial structuring of coastal ocean acidification in the California Current System. Scientific Reports 7(1). doi: 10.1038/s41598-017-02777-y

Chezik KA, Lester NP, Venturelli PA, Tierney K. 2014. Fish growth and degree-days I: selecting a base temperature for a within-population study. Can J Fish Aquat Sci 71(1): 47–55. doi: 10.1139/cjfas-2013-0295

Cigliano, M., M. C. Gambi, R. Rodolfo-Metalpa, F. P. Patti, and J. M. Hall-Spencer. 2010. Effects of ocean acidification on invertebrate settlement at volcanic CO2 vents. Mar. Biol. 157: 2489–2502. doi:10.1007/s00227-010-1513-6

Clark, H., and C. Gobler. 2016. Diurnal fluctuations in CO2 and dissolved oxygen concentrations do not provide a refuge from hypoxia and acidification for early-life-stage bivalves. Mar. Ecol. Prog. Ser. 558: 1–14. doi:10.3354/meps11852

Clements JC, Hunt HL. 2014. Influence of sediment acidification and water flow on sediment acceptance and dispersal of juvenile soft-shell clams (Mya arenaria L.). J Exp Mar Biol Ecol 453: 62–69. doi: 10.1016/j.jembe.2014.01.002

Clements JC, Hunt HL. 2017 Jan. Effects of CO2-driven sediment acidification on infaunal marine bivalves: A synthesis. Mar Pollut Bull, in press. doi: 10.1016/j.marpolbul.2017.01.053

Cline JD. 1969. Spectrophotometric determination of hydrogen sulfide in natural waters. Limnology and Oceanography 14(3): 454–458. doi: 10.4319/lo.1969.14.3.0454

Coen L, Brumbaugh R, Bushek D, Grizzle R, Luckenbach M, Posey M, Powers S, Tolley S. 2007. Ecosystem services related to oyster restoration. Mar Ecol Prog Ser 341: 303–307. doi: 10.3354/meps341303

Coen LD, Dumbauld BR, Judge ML. 2011. Expanding Shellfish Aquaculture: A Review of the Ecological Services Provided by and Impacts of Native and Cultured Bivalves in Shellfish-Dominated Ecosystems. In: Shellfish Aquaculture and the Environment. John Wiley & Sons, Ltd. p. 239–295. doi: 10.1002/9780470960967.ch9

Comeau, S., E. Tambutté, R. C. Carpenter, and others. 2017. Coral calcifying fluid pH is modulated by seawater carbonate chemistry not solely seawater pH. Proc. R. Soc. B Biol. Sci. 284: 20161669. doi:10.1098/rspb.2016.1669

Cornwall, C. E., C. D. Hepburn, C. M. McGraw, K. I. Currie, C. A. Pilditch, K. A. Hunter, P. W. Boyd, and C. L. Hurd. 2013. Diurnal fluctuations in seawater pH influence the response of a calcifying macroalga to ocean acidification. Proc. R. Soc. B Biol. Sci. 280: 20132201–20132201. doi:10.1098/rspb.2013.2201

Cornwall, C. E., and C. L. Hurd. 2015. Experimental design in ocean acidification research: problems and solutions. ICES J. Mar. Sci. J. Cons. fsv118. doi:10.1093/icesjms/fsv118

Cornwell JC, Morse JW. 1987. The characterization of iron sulfide minerals in anoxic marine sediments. Marine Chemistry 22(2–4): 193–206. doi: 10.1016/0304-4203(87)90008-9

Crame, J. A. 2000. Evolution of taxonomic diversity gradients in the marine realm: evidence from the composition of Recent bivalve faunas. Paleobiology 26: 188–214. doi:10.1666/0094-8373(2000)026<0188:EOTDGI>2.0.CO;2

Crompton TR. 2006. Analysis of Seawater: A Guide for the Analytical and Environmental Chemist. Berlin ; New York: Springer.

Cyronak T, Santos IR, McMahon A, Eyre BD. 2013. Carbon cycling hysteresis in permeable carbonate sands over a diel cycle: Implications for ocean acidification. Limnology and Oceanography 58(1): 131–143. doi: 10.4319/lo.2013.58.1.0131

Cyronak, T., K. G. Schulz, and P. L. Jokiel. 2016. The Omega myth: what really drives lower calcification rates in an acidifying ocean. ICES J. Mar. Sci. J. Cons. 73: 558–562. doi:10.1093/icesjms/fsv075

D'Andrea AF, Aller RC, Lopez GR. 2002. Organic matter flux and reactivity on a South Carolina sandflat: The impacts of porewater advection and macrobiological structures. Limnology and Oceanography 47(4): 1056–1070. doi: 10.4319/lo.2002.47.4.1056

Dame RF, Zingmark RG, Haskin E. 1984. Oyster reefs as processors of estuarine materials. J Exp Mar Biol Ecol 83(3): 239–247. doi: 10.1016/S0022-0981(84)80003-9

Dame RF, Spurrier JD, Wolaver TG. 1989. Carbon, nitrogen and phosphorus processing by an oyster reef. Mar Ecol Prog Ser 54: 249–256.

Dame RF. 2012. Ecology of Marine Bivalves: An Ecosystem Approach. 2nd ed. Boca Raton: Taylor & Francis. (CRC Series in marine science).

Davey E, Wigand C, Johnson R, Sundberg K, Morris J, Roman CT. 2011. Use of computed tomography imaging for quantifying coarse roots, rhizomes, peat, and particle densities in marsh soils. Ecological Applications 21(6): 2156–2171. doi: 10.1890/10-2037.1

de Melo CMR, Durland E, Langdon C. 2016. Improvements in desirable traits of the Pacific oyster, Crassostrea gigas, as a result of five generations of selection on the West Coast, USA. Aquaculture 460: 105–115. doi: 10.1016/j.aquaculture.2016.04.017

De Rijcke M, Vandegehuchte MB, Vanden Bussche J, Nevejan N, Vanhaecke L, De Schamphelaere KAC, Janssen CR. 2015. Common European harmful algal blooms affect the viability and innate immune responses of Mytilus edulis larvae. Fish Shellfish Immunol 47(1): 175–181. doi: 10.1016/j.fsi.2015.09.003

Deutsch C, Sarmiento JL, Sigman DM, Gruber N, Dunne JP. 2007. Spatial coupling of nitrogen inputs and losses in the ocean. Nature 445(7124): 163. doi: 10.1038/nature05392

Dickson AG. 1990. Thermodynamics of the dissociation of boric acid in synthetic seawater from 273.15 to 318.15 K. Deep Sea Res 37(5): 755–766.

Dillon ME, Woods HA, Wang G, Fey SB, Vasseur DA, Telemeco RS, Marshall K, Pincebourde S. 2016. Life in the Frequency Domain: the Biological Impacts of Changes in Climate Variability at Multiple Time Scales. Integrative and Comparative Biology 56(1): 14–30. doi: 10.1093/icb/icw024

Dillon ME, Woods HA. 2016. Introduction to the Symposium: Beyond the mean: Biological impacts of changing patterns of temperature variation. Integr Comp Biol 56(1): 11–13. doi: 10.1093/icb/icw020

Doney SC, Fabry VJ, Feely RA, Kleypas JA. 2009. Ocean Acidification: The Other CO2 Problem. Annual Review of Marine Science 1(1): 169–192. doi: 10.1146/annurev.marine.010908.163834

Dore JE, Lukas R, Sadler DW, Church MJ, Karl DM. 2009. Physical and biogeochemical modulation of ocean acidification in the central North Pacific. Proceedings of the National Academy of Sciences 106(30): 12235–12240. doi: 10.1073/pnas.0906044106

Du X, Peterson W, Fisher J, Hunter M, Peterson J. 2016. Initiation and development of a toxic and persistent Pseudo-nitzschia bloom off the Oregon coast in spring/summer 2015. PloS ONE 11(10): e0163977.

Duarte CM, Hendriks IE, Moore TS, Olsen YS, Steckbauer A, Ramajo L, Carstensen J, Trotter JA, McCulloch M. 2013. Is Ocean Acidification an Open-Ocean Syndrome? Understanding Anthropogenic Impacts on Seawater pH. Estuaries and Coasts 36(2): 221–236. doi: 10.1007/s12237-013-9594-3

Dufault, A. M., V. R. Cumbo, T.-Y. Fan, and P. J. Edmunds. 2012. Effects of diurnally oscillating pCO2 on the calcification and survival of coral recruits. Proc. R. Soc. B Biol. Sci. 279: 2951–2958. doi:10.1098/rspb.2011.2545

Dunn RP, Eggleston DB, Lindquist N. 2014 Dec 4. Oyster-Sponge Interactions and Bioerosion of Reef-Building Substrate Materials: Implications for Oyster Restoration. http://dx.doi.org/10.2983/035.033.0307. doi: 10.2983/035.033.0307

Eakin CM, Morgan JA, Heron SF, Smith TB, Liu G, Alvarez-Filip L, Bartels E, Bastidas C, Bouchon C, Brandt M, et al. 2010. Caribbean corals in crisis: Record thermal stress, bleaching, and mortality in 2005. PLoS ONE 5(11): e13969. doi: 10.1371/journal.pone.0013969

Eierman LE, Hare MP. 2013. Survival of oyster larvae in different salinities depends on source population within an estuary. J Exp Mar Biol Ecol 449: 61–68. doi: 10.1016/j.jembe.2013.08.015

Ekstrom JA, Suatoni L, Cooley SR, Pendleton LH, Waldbusser GG, Cinner JE, Ritter J, Langdon C, van Hooidonk R, Gledhill D, et al. 2015. Vulnerability and adaptation of US shellfisheries to ocean acidification. Nat Clim Change 5(3): 207–214. doi: 10.1038/nclimate2508

Emerson S, Jahnke R, Heggie D. 1984. Sediment-water exchange in shallow water estuarine sediments. Journal of Marine Research 42(3): 709–730. doi: 10.1357/002224084788505942

Engle VD, Kurtz JC, Smith LM, Chancy C, Bourgeois P. 2007. A classification of U.S. estuaries based on physical and hydrologic attributes. Environ Monit Assess 129(1–3): 397–412. doi: 10.1007/s10661-006-9372-9

Erftemeijer PLA, Middelburg JJ. 1993. Sediment-nutrient interactions in tropical seagrass beds: a comparision between a terrigenous and a carbonate sedimentary environment in South Sulawesi (Indonesia). Marine Ecology Progress Series 102: 187–198.

Eriander L, Wrange A-L, Havenhand JN. 2016. Simulated diurnal pH fluctuations radically increase variance in—but not the mean of—growth in the barnacle Balanus improvisus. ICES J Mar Sci J Cons 73(3): 596–603. doi: 10.1093/icesjms/fsv214

Evans W, Mathis JT, Ramsay J, Hetrick J. 2015. On the frontline: Tracking ocean acidification in an Alaskan shellfish hatchery. PLoS ONE 10(7): e0130384. doi: 10.1371/journal.pone.0130384

Fangue, N. A., M. J. O'Donnell, M. A. Sewell, P. G. Matson, A. C. MacPherson, and G. E. Hofmann. 2010. A laboratory-based, experimental system for the study of ocean acidification effects on marine invertebrate larvae. Limnol. Oceanogr. Methods 8: 441–452.

Fassbender, A. J., C. L. Sabine, and K. M. Feifel. 2016. Consideration of coastal carbonate chemistry in understanding biological calcification: Coastal zone calcification. Geophys. Res. Lett. doi:10.1002/2016GL068860

Feely RA. 2004. Impact of anthropogenic CO2 on the CaCO3 system in the oceans. Science 305(5682): 362–366. doi: 10.1126/science.1097329

Feely RA, Alin SR, Newton J, Sabine CL, Warner M, Devol A, Krembs C, Maloy C. 2010. The combined effects of ocean acidification, mixing, and respiration on pH and carbonate saturation in an urbanized estuary. Estuar Coast Shelf Sci 88(4): 442–449. doi: 10.1016/j.ecss.2010.05.004

Fodrie FJ, Rodriguez AB, Gittman RK, Grabowski JH, Lindquist NL, Peterson CH, Piehler MF, Ridge JT. 2017. Oyster reefs as carbon sources and sinks. Proceedings of the Royal Society B: Biological Sciences 284(1859): 20170891. doi: 10.1098/rspb.2017.0891

Frieder CA, Gonzalez JP, Bockmon EE, Navarro MO, Levin LA. 2014. Can variable pH and low oxygen moderate ocean acidification outcomes for mussel larvae? Global Change Biology 20(3): 754–764. doi: 10.1111/gcb.12485

Gallager SM, Mann R. 1986. Growth and survival of larvae of Mercenaria mercenaria (L.) and Crassostrea virginica (Gmelin) relative to broodstock conditioning and lipid content of eggs. Aquaculture 56(2): 105–121.

Gattuso, J.-P., K. Gao, K. Lee, B. Rost, and K. G. Schulz. 2010. Approaches and tools to manipulate the carbonate chemistry, p. 13. In U. Riebesell, V.J. Fabry, L. Hansson, and J.-P. Gattuso [eds.], Guide for Best Practices in Ocean Acidification Research and Data Reporting. Publications Office of the European Union.

Gazeau F, Quiblier C, Jansen JM, Gattuso J-P, Middelburg JJ, Heip CHR. 2007. Impact of elevated CO2 on shellfish calcification. Geophys Res Lett 34(7). doi: 10.1029/2006GL028554

Gazeau F, Gattuso J-P, Greaves M, Elderfield H, Peene J, Heip CHR, Middelburg JJ. 2011. Effect of carbonate chemistry alteration on the early embryonic development of the Pacific oyster (Crassostrea gigas). PLoS ONE 6(8): e23010. doi: 10.1371/journal.pone.0023010

Gazeau F, Parker LM, Comeau S, Gattuso J-P, O'Connor WA, Martin S, Pörtner H-O, Ross PM. 2013. Impacts of ocean acidification on marine shelled molluscs. Mar Biol 160(8): 2207–2245. doi: 10.1007/s00227-013-2219-3

Gazeau F, van Rijswijk P, Pozzato L, Middelburg JJ. 2014. Impacts of Ocean Acidification on Sediment Processes in Shallow Waters of the Arctic Ocean. Browman HI, editor. PLoS ONE 9(4): e94068. doi: 10.1371/journal.pone.0094068

Goñi MA, Monacci N, Gisewhite R, Ogston A, Crockett J, Nittrouer C. 2006. Distribution and sources of particulate organic matter in the water column and sediments of the Fly River Delta, Gulf of Papua (Papua New Guinea). Estuarine, Coastal and Shelf Science 69(1–2): 225–245. doi: 10.1016/j.ecss.2006.04.012

Grabowski JH, Brumbaugh RD, Conrad RF, Keeler AG, Opaluch JJ, Peterson CH, Piehler M, Powers SP, Smyth A. 2012. Economic Valuation of Ecosystem Services Provided by Oyster Reefs. BioScience 62(10): 900–909. doi: 10.1525/bio.2012.62.10.10

Gradoville, M. R., A. E. White, and R. M. Letelier. 2014. Physiological Response of Crocosphaera watsonii to Enhanced and Fluctuating Carbon Dioxide Conditions. PLOS ONE 9: e110660. doi:10.1371/journal.pone.0110660

Gray, M., C. Langdon, G. Waldbusser, B. Hales, and S. Kramer. 2017. Mechanistic understanding of ocean acidification impacts on larval feeding physiology and energy budgets of the mussel Mytilus californianus. Mar. Ecol. Prog. Ser. 563: 81–94. doi:10.3354/meps11977

Green MA, Aller RC, Aller JY. 1993. Carbonate dissolution and temporal abundances of Foraminifera in Long Island Sound sediments. Limnology and Oceanography 38(2): 331–345. doi: 10.4319/lo.1993.38.2.0331

Green MA, Aller RC. 1998. Seasonal patterns of carbonate diagenesis in nearshore terrigenous muds: Relation to spring phytoplankton bloom and temperature. Journal of Marine Research 56(5): 1097–1123. doi: 10.1357/002224098765173473

Green MA, Waldbusser GG, Reilly SL, Emerson K, O'Donnell S. 2009. Death by dissolution: Sediment saturation state as a mortality factor for juvenile bivalves. Limnology and Oceanography 54(4): 1037–1047. doi: 10.4319/lo.2009.54.4.1037

Green MA, Jones ME, Boudreau CL, Moore RL, Westman BA. 2004. Dissolution mortality of juvenile bivalves in coastal marine deposits. Limnology and Oceanography 49(3): 727–734. doi: 10.4319/lo.2004.49.3.0727

Green MA, Waldbusser GG, Hubazc L, Cathcart E, Hall J. 2013. Carbonate Mineral Saturation State as the Recruitment Cue for Settling Bivalves in Marine Muds. Estuaries Coasts 36(1): 18–27. doi: 10.1007/s12237-012-9549-0

Griffith AW, Gobler CJ. 2017. Transgenerational exposure of North Atlantic bivalves to ocean acidification renders offspring more vulnerable to low pH and additional stressors. Scientific Reports 7(1). doi: 10.1038/s41598-017-11442-3

Gruber N, Hauri C, Lachkar Z, Loher D, Frolicher TL, Plattner G-K. 2012. Rapid progression of ocean acidification in the California Current System. Science 337(6091): 220–223. doi: 10.1126/science.1216773

Gustafsson E, Wällstedt T, Humborg C, Mörth C-M, Gustafsson BG. 2014. External total alkalinity loads versus internal generation: The influence of nonriverine alkalinity sources in the Baltic Sea: Alkalinity in the Baltic Sea. Global Biogeochemical Cycles 28(11): 1358–1370. doi: 10.1002/2014GB004888

Gutiérrez JL, Jones CG, Strayer DL, Iribarne OO. 2003. Mollusks as ecosystem engineers: the role of shell production in aquatic habitats. Oikos 101(1): 79–90.

Gutiérrez JL, Jones CG, Byers JE, Arkema KK, Berkenbusch K, Commito JA, Duarte CM, Hacker SD, Lambrinos JG, Hendriks IE, et al. 2011. Physical ecosystem engineers and the

functioning of estuaries and coasts. Funct Estuaries Coast Ecosyst CHR Heip CJM Philippart JJ MiddelburgElsevier Amst.

Hadfield M, Paul V. 2001. Natural Chemical Cues for Settlement and Metamorphosis of Marine-Invertebrate Larvae. In: McClinTOCk J, Baker B, editors. Marine Chemical Ecology. CRC Press. p. 431–461. doi: 10.1201/9781420036602.ch13

Hagy JD, Boynton WR, Keefe CW, Wood KV. 2004. Hypoxia in Chesapeake Bay, 1950–2001: Long-term change in relation to nutrient loading and river flow. Estuaries 27(4): 634–658. doi: 10.1007/BF02907650

Hales B, Emerson S. 1997. Calcite dissolution in sediments of the Ceara Rise: In situ measurements of porewater O2, pH, and CO2(aq). Geochimica et Cosmochimica Acta 61(3): 501–514.

Hales B, Takahashi T, Bandstra L. 2005. Atmospheric CO2 uptake by a coastal upwelling system. Glob Biogeochem Cycles 19(1). doi: 10.1029/2004GB002295

Hales B, Suhrbier A, Waldbusser GG, Feely RA, Newton JA. 2017. The carbonate chemistry of the “fattening line,” Willapa Bay, 2011–2014. Estuaries Coasts 40(1): 173–186. doi: 10.1007/s12237-016-0136-7

Hargis Jr WJ, Haven DS. 1999. Chesapeake oyster reefs, their importance, destruction and guidelines for restoring them. Oyster Reef Habitat Restor Synop Synth Approaches Va Inst Mar Sci Press Glos Point VA: 329–358.

Harris KE, DeGrandpre MD, Hales B. 2013. Aragonite saturation state dynamics in a coastal upwelling zone. Geophys Res Lett 40(11): 2720–2725. doi: 10.1002/grl.50460

Hauri C, Gruber N, McDonnell AMP, Vogt M. 2013. The intensity, duration, and severity of low aragonite saturation state events on the California continental shelf. Geophysical Research Letters 40(13): 3424–3428. doi: 10.1002/grl.50618

Hauri C, Gruber N, Vogt M, Doney SC, Feely RA, Lachkar Z, Leinweber A, McDonnell AMP, Munnich M, Plattner G-K. 2013. Spatiotemporal variability and long-term trends of ocean acidification in the California Current System. Biogeosciences 10(1): 193–216. doi: 10.5194/bg-10-193-2013

Helmuth BST, Hofmann GE. 2001. Microhabitats, thermal heterogeneity, and patterns of physiological stress in the rocky intertidal zone. Biol Bull 201: 374–384.

Helmuth B. 2009. From cells to coastlines: how can we use physiology to forecast the impacts of climate change? J Exp Biol 212(6): 753–760. doi: 10.1242/jeb.023861

Helmuth B, Broitman BR, Yamane L, Gilman SE, Mach K, Mislan KAS, Denny MW. 2010. Organismal climatology: analyzing environmental variability at scales relevant to physiological stress. J Exp Biol 213(6): 995–1003. doi: 10.1242/jeb.038463

Helmuth B, Russell BD, Connell SD, Dong Y, Harley CD, Lima FP, Sará G, Williams GA, Mieszkowska N. 2014. Beyond long-term averages: making biological sense of a rapidly changing world. Clim Change Responses 1(1): 6. https://doi.org/10.1186/s40665-014-0006-0

Hernández AB, Brumbaugh RD, Frederick P, Grizzle R, Luckenbach MW, Peterson CH, Angelini C. 2018. Restoring the eastern oyster: how much progress has been made in 53 years? Front Ecol Environ 16(8): 463–471. doi: 10.1002/fee.1935

Hettinger A, Sanford E, Hill TM, Russell AD, Sato KN, Hoey J, Forsch M, Page HN, Gaylord B. 2012. Persistent carry-over effects of planktonic exposure to ocean acidification in the Olympia oyster. Ecology 93(12): 2758–2768.

Hettinger, A., E. Sanford, T. M. Hill, E. A. Lenz, A. D. Russell, and B. Gaylord. 2013. Larval carry-over effects from ocean acidification persist in the natural environment. Glob. Change Biol. doi:10.1111/gcb.12307

Higgins C, Tobias C, Piehler M, Smyth A, Dame R, Stephenson K, Brown B. 2013. Effect of aquacultured oyster biodeposition on sediment N2 production in Chesapeake Bay. Marine Ecology Progress Series 473: 7–27. doi: 10.3354/meps10062

Hijmans RJ, Graham CH. 2006. The ability of climate envelope models to predict the effect of climate change on species distributions. Glob Change Biol 12(12): 2272–2281. doi: 10.1111/j.1365-2486.2006.01256.x

His, E., M. N. L. Seaman, and R. Beiras. 1997. A simplification the bivalve embryogenesis and larval development bioassay method for water quality assessment. Water Res. 31: 351–355.

His E, Beiras R, Seaman MNL. 1999. The assessment of marine pollution - bioassays with bivalve embryos and larvae. Adv Mar Biol 37: 1–178. doi: 10.1016/S0065-2881(08)60428-9

Hofmann GE, Barry JP, Edmunds PJ, Gates RD, Hutchins DA, Klinger T, Sewell MA. 2010. The Effect of Ocean Acidification on Calcifying Organisms in Marine Ecosystems: An Organism-to-Ecosystem Perspective. Annual Review of Ecology, Evolution, and Systematics 41(1): 127–147. doi: 10.1146/annurev.ecolsys.110308.120227

Holyoke RR. 2008. Biodeposition and Biogeochemical Processes in Shallow, Mesohaline Sediments of Chesapeake Bay. Available at http://drum.lib.umd.edu/handle/1903/8025. Accessed 2018 Nov 4.

Hönisch B, Ridgwell A, Schmidt DN, Thomas E, Gibbs SJ, Sluijs A, Zeebe R, Kump L, Martindale RC, Greene SE, et al. 2012. The geological record of ocean acidification. Science 335(6072): 1058–1063. doi: 10.1126/science.1208277

Hovd, M., and R. R. Bitmead. 2009. Feedforward for stabilization. IFAC Proc. Vol. 42: 602–606. doi:10.3182/20090712-4-TR-2008.00097

Howes, E. L., N. Bednaršek, J. Büdenbender, and others. 2014. Sink and swim: a status review of thecosome pteropod culture techniques. J. Plankton Res. 36: 299–315. doi:10.1093/plankt/fbu002

Hu X, Burdige DJ. 2008. Shallow marine carbonate dissolution and early diagenesis—Implications from an incubation study. Journal of Marine Research 66(4): 489–527. doi: 10.1357/002224008787157449

Hu X, Cai W-J. 2011. An assessment of ocean margin anaerobic processes on oceanic alkalinity budget. Global Biogeochemical Cycles 25(3): GB3003. doi: 10.1029/2010GB003859

Hulth S, Aller RC, Canfield DE, Dalsgaard T, Engstrom P, Gilbert F, Sundback K, Thamdrup B. 2005. Nitrogen removal in marine environments: recent findings and future research challenges. Marine Chemistry 94(1–4): 125–145. doi: 10.1016/j.marchem.2004.07.013

Humphries AT, Ayvazian SG, Carey JC, Hancock BT, Grabbert S, Cobb D, Strobel CJ, Fulweiler RW. 2016. Directly Measured Denitrification Reveals Oyster Aquaculture and Restored Oyster Reefs Remove Nitrogen at Comparable High Rates. Front Mar Sci 3. doi: 10.3389/fmars.2016.00074

Hunt CW, Salisbury JE, Vandemark D. 2011. Contribution of non-carbonate anions to total alkalinity and overestimation of pCO2 in New England and New Brunswick rivers. Biogeosciences 8(10): 3069–3076. doi: 10.5194/bg-8-3069-2011

Jackson M, Owens MS, Cornwell JC, Kellogg ML. In prep. A confirmation that live oyster clusters perform the majority of denitrification and nutrient fluxes on restored oyster reefs. , in press.

Jahnke RA, Jahnke DB. 2004. Calcium carbonate dissolution in deep sea sediments: reconciling microelectrode, pore water and benthic flux chamber results. Geochimica et Cosmochimica Acta 68(1): 47–59. doi: 10.1016/S0016-7037(03)00260-6

Jajo NK. 2005. A Review of Robust Regression and Diagnostic Procedures in Linear Regression. Acta Mathematicae Applicatae Sinica, English Series 21(2): 209–224. doi: 10.1007/s10255-005-0230-2

Jarrold, M. 2017. Diel CO2 cycles reduce severity of behavioural abnormalities in coral reef fish under ocean acidification.doi:10.4225/28/5923bfed71f8d

Jokiel, P. L. 2013. Coral reef calcification: carbonate, bicarbonate and proton flux under conditions of increasing ocean acidification. Proc. R. Soc. B Biol. Sci. 280: 20130031–20130031. doi:10.1098/rspb.2013.0031

Jones CG, Lawton JH, Shachak M. 1997. Positive and negative effects of organisms as physical ecosystem engineers. Ecology 7: 1946–1957.

Jørgensen BB. 1982. Mineralization of organic matter in the sea bed - the role of sulphate reduction. Nature 296: 643–645.

Jury, C. P., R. F. Whitehead, and A. M. Szmant. 2010. Effects of variations in carbonate chemistry on the calcification rates of Madracis auretenra (= Madracis mirabilis sensu Wells, 1973): bicarbonate concentrations best predict calcification rates. Glob. Change Biol. 16: 1632–1644. doi:10.1111/j.1365-2486.2009.02057.x

Kamenos NA, Burdett HL, Aloisio E, Findlay HS, Martin S, Longbone C, Dunn J, Widdicombe S, Calosi P. 2013. Coralline algal structure is more sensitive to rate, rather than the magnitude, of ocean acidification. Glob Change Biol 19(12): 3621–3628. doi: 10.1111/gcb.12351

Kapsenberg L, Kelley AL, Shaw EC, Martz TR, Hofmann GE. 2015. Near-shore Antarctic pH variability has implications for the design of ocean acidification experiments. Sci Rep 5: 9638. doi: 10.1038/srep09638

Kayanne H. 2017. Validation of degree heating weeks as a coral bleaching index in the northwestern Pacific. Coral Reefs 36(1): 63–70. doi: 10.1007/s00338-016-1524-y

Kearney M, Porter WP. 2004. Mapping the fundamental niche: physiology, climate, and the distribution of a nocturnal lizard. Ecology 85(11): 3119–3131.

Kearney M, Porter W. 2009. Mechanistic niche modelling: combining physiological and spatial data to predict species' ranges. Ecol Lett 12(4): 334–350. doi: 10.1111/j.1461-0248.2008.01277.x

Kellogg M, Cornwell J, Owens M, Paynter K. 2013. Denitrification and nutrient assimilation on a restored oyster reef. Mar Ecol Prog Ser 480: 1–19. doi: 10.3354/meps10331

Kellogg ML, Smyth AR, Luckenbach MW, Carmichael RH, Brown BL, Cornwell JC, Piehler MF, Owens MS, Dalrymple DJ, Higgins CB. 2014. Use of oysters to mitigate eutrophication in coastal waters. Estuar Coast Shelf Sci 151: 156–168. doi: 10.1016/j.ecss.2014.09.025

Kemp W, Boynton W, Adolf J, Boesch D, Boicourt W, Brush G, Cornwell J, Fisher T, Glibert P, Hagy J, et al. 2005. Eutrophication of Chesapeake Bay: historical trends and ecological interactions. Marine Ecology Progress Series 303: 1–29. doi: 10.3354/meps303001

Keppel A, Breitburg D, Wikfors G, Burrell R, Clark V. 2015. Effects of co-varying diel-cycling hypoxia and pH on disease susceptibility in the eastern oyster Crassostrea virginica. Mar Ecol Prog Ser 538: 169–183. doi: 10.3354/meps11479

Keul, N., G. Langer, L. J. de Nooijer, and J. Bijma. 2013. Effect of ocean acidification on the benthic foraminifera Ammonia sp. is caused by a decrease in carbonate ion concentration. Biogeosciences 10: 6185–6198. doi:10.5194/bg-10-6185-2013

Kidwell SM, Jablonski D. 1983. Taphonomic Feedback- Ecological consequences of shell accumulation. In: Biotic Interactions in Recent and Fossil Benthic Communities.

Ko GWK, Vera CBS, R D, Dennis CKS, Adela LJ, Yu Z, Thiyagarajan V. 2013. Larval and post-larval stages of Pacific oyster (Crassostrea gigas) are resistant to elevated CO2. PLoS ONE 8(5): e64147. doi: 10.1371/journal.pone.0064147

Ko GWK, Dineshram R, Campanati C, Chan VBS, Havenhand J, Thiyagarajan V. 2014. Interactive effects of ocean acidification, elevated temperature, and reduced salinity on early-life stages of the Pacific oyster. Environ Sci Technol 48(17): 10079–10088. doi: 10.1021/es501611u

Koroleff F. 1976. Determination of nutrients. In: Grasshof E, Kremling E, editors. Methods of Seawater Analysis. New York: Verlag Chemi Weinhein.

Kroeker KJ, Kordas RL, Crim RN, Singh GG. 2010. Meta-analysis reveals negative yet variable effects of ocean acidification on marine organisms: Biological responses to ocean acidification. Ecol Lett 13(11): 1419–1434. doi: 10.1111/j.1461-0248.2010.01518.x

Kroeker, K. J., F. Micheli, M. C. Gambi, and T. R. Martz. 2011. Divergent ecosystem responses within a benthic marine community to ocean acidification. Proc. Natl. Acad. Sci. 108: 14515–14520. doi:10.1073/pnas.1107789108

Kroeker KJ, Kordas RL, Crim R, Hendriks IE, Ramajo L, Singh GS, Duarte CM, Gattuso J-P. 2013. Impacts of ocean acidification on marine organisms: quantifying sensitivities and interaction with warming. Global Change Biology 19(6): 1884–1896. doi: 10.1111/gcb.12179

Krumins V, Gehlen M, Arndt S, Van Cappellen P, Regnier P. 2013. Dissolved inorganic carbon and alkalinity fluxes from coastal marine sediments: model estimates for different shelf

environments and sensitivity to global change. Biogeosciences 10(1): 371–398. doi: 10.5194/bg-10-371-2013

Kump, L. R., T. J. Bralower, and A. Ridgwell. 2009. Ocean acidification in deep time. Oceanography 22: 94–107.

Kurihara H, Kato S, Ishimatsu A. 2007. Effects of increased seawater pCO2 on early development of the oyster Crassostrea gigas. Aquat Biol 1: 91–98. doi: 10.3354/ab00009

Kwiatkowski, L., and J. C. Orr. 2018. Diverging seasonal extremes for ocean acidification during the twenty-first century. Nat. Clim. Change 8: 141–145. doi:10.1038/s41558-017-0054-0

Landschützer, P., N. Gruber, D. C. E. Bakker, I. Stemmler, and K. D. Six. 2018. Strengthening seasonal marine CO2 variations due to increasing atmospheric CO2. Nat. Clim. Change 8: 146–150. doi:10.1038/s41558-017-0057-x

Langdon C, Evans F, Jacobson D, Blouin M. 2003. Yields of cultured Pacific oysters Crassostrea gigas Thunberg improved after one generation of selection. Aquaculture 220(1–4): 227–244. doi: 10.1016/S0044-8486(02)00621-X

Lelong A, Hégaret H, Soudant P, Bates SS. 2012. Pseudo-nitzschia (Bacillariophyceae) species, domoic acid and amnesic shellfish poisoning: revisiting previous paradigms. Phycologia 51(2): 168–216.

Lewitus AJ, Horner RA, Caron DA, Garcia-Mendoza E, Hickey BM, Hunter M, Huppert DD, Kudela RM, Langlois GW, Largier JL, et al. 2012. Harmful algal blooms along the North American west coast region: History, trends, causes, and impacts. Harmful Algae 19: 133–159. doi: 10.1016/j.hal.2012.06.009

Li Y-H, Gregory S. 1974. Difussion of ions in seawater and in deep-sea sediments. Geochimica et Cosmochimica Acta 88: 703–714.

Li, F., Y. Wu, D. A. Hutchins, F. Fu, and K. Gao. 2016. Physiological responses of coastal and oceanic diatoms to diurnal fluctuations in seawater carbonate chemistry under two CO2 concentrations. Biogeosciences 13: 6247–6259. doi:10.5194/bg-13-6247-2016

Lisle J, Reich C, Halley R. 2014. Aragonite saturation states and nutrient fluxes in coral reef sediments in Biscayne National Park, FL, USA. Mar Ecol Prog Ser 509: 71–85. doi: 10.3354/meps10844

Liu G, Strong AE, Skirving W. 2003. Remote sensing of sea surface temperatures during 2002 Barrier Reef coral bleaching. Eos Trans Am Geophys Union 84(15): 137–144.

Liu H, Kelly M, Campbell D, Dong S, Zhu J, Wang S. 2007. Exposure to domoic acid affects larval development of king scallop Pecten maximus (Linnaeus, 1758). Aquat Toxicol 81(2): 152–158. doi: 10.1016/j.aquatox.2006.11.012

Long JS, Ervin LH. 2000. Using heteroscedasticity consistent standard errors in the linear regression model. Am Stat 54(3): 217. doi: 10.2307/2685594

Lord CJI, Church TM. 1983. The geochemistry of salt marshes: Sedimentary ion diffusion, sulfate reduction, and pyritization. Geochimica et Cosmochimica Acta 47(8): 1381–1391. doi: 10.1016/0016-7037(83)90296-X

Luckenbach, M. W.; Mann, R.; And Wesson, J. A. 1999. Oyster reef habitat restoration : a synopsis and synthesis of approaches; proceedings from the symposium, Williamsburg, Virginia, April 1995. , in press. doi: 10.21220/v5nk51

Lundholm N, Hansen PJ, Kotaki Y. 2004. Effect of pH on growth and domoic acid production by potentially toxic diatoms of the genera Pseudo-nitzschia and Nitzschia. Mar Ecol Progr Ser 273(1): 1–15 .

Malkin SY, Seitaj D, Burdorf LDW, Nieuwhof S, Hidalgo-Martinez S, Tramper A, Geeraert N, De Stigter H, Meysman FJR. 2017. Electrogenic Sulfur Oxidation by Cable Bacteria in Bivalve Reef Sediments. Front Mar Sci 4. doi: 10.3389/fmars.2017.00028

Marinelli RL, Jahnke RA, Craven DB, Nelson JR, Eckman JE. 1998. Sediment nutrient dynamics on the South Atlantic Bight continental shelf. Limnology and Oceanography 43(6): 1305–1320. doi: 10.4319/lo.1998.43.6.1305

Marvin-DiPasquale M, Capone D. 1998. Benthic sulfate reduction along the Chesapeake Bay central channel. I. Spatial trends and controls. Marine Ecology Progress Series 168: 213–228. doi: 10.3354/meps168213

Marvin-DiPasquale M, Boynton W, Capone D. 2003. Benthic sulfate reduction along the Chesapeake Bay central channel. II. Temporal controls. Marine Ecology Progress Series 260: 55–70. doi: 10.3354/meps260055

Maryland Department of Natural Resources. 2018. Eyes on the Bay: Maryland Tidal Water Quality Data. Available at http://eyesonthebay.dnr.maryland.gov/. Accessed 2018 Nov 13.

McCabe RM, Hickey BM, Kudela RM, Lefebvre KA, Adams NG, Bill BD, Gulland FMD, Thomson RE, Cochlan WP, Trainer VL. 2016. An unprecedented coastwide toxic algal bloom linked to anomalous ocean conditions. Geophys Res Lett 43(19): 10,366–10,376. doi: 10.1002/2016GL070023

McElhany P, Busch SD. 2013. Appropriate pCO2 treatments in ocean acidification experiments. Mar Biol 160(8): 1807–1812. doi: 10.1007/s00227-012-2052-0

McGraw, C. M., C. E. Cornwall, M. R. Reid, K. I. Currie, C. D. Hepburn, P. Boyd, C. L. Hurd, and K. A. Hunter. 2010. An automated pH-controlled culture system for laboratory-based ocean acidification experiments: Automated pH-controlled culture system. Limnol. Oceanogr. Methods 8: 686–694. doi:10.4319/lom.2010.8.0686

McKibben SM, Peterson W, Wood AM, Trainer VL, Hunter M, White AE. 2017. Climatic regulation of the neurotoxin domoic acid. Proc Natl Acad Sci USA 114(2): 239–244.

Miller C, Waldbusser G. 2016. A post-larval stage-based model of hard clam Mercenaria mercenaria development in response to multiple stressors: temperature and acidification severity. Mar Ecol Prog Ser 558: 35–49. doi: 10.3354/meps11882

Millero FJ. 1995. Thermodynamics of the carbon dioxide system in the oceans. Geochim Cosmochim Acta 59(4): 661–677.

Millero F, Huang F, Zhu X, Liu X, Zhang J-Z. 2001. Adsorption and Desorption of Phosphate on Calcite and Aragonite in Seawater. Aquatic Geochemistry 7(1): 33–56.

Millero FJ. 2010. Carbonate constants for estuarine waters. Mar Freshw Res 61(2): 139. doi: 10.1071/MF09254

Montalto V, Helmuth B, Ruti PM, Dell'Aquila A, Rinaldi A, Sarà G. 2016. A mechanistic approach reveals non linear effects of climate warming on mussels throughout the Mediterranean sea. Clim Change 139(2): 293–306. doi: 10.1007/s10584-016-1780-4

Moore JL, Remais JV. 2014. Developmental models for estimating ecological responses to environmental variability: Structural, parametric, and experimental issues. Acta Biotheor 62(1): 69–90. doi: 10.1007/s10441-014-9209-9

Moran A, Manahan D. 2004. Physiological recovery from prolonged 'starvation' in larvae of the Pacific oyster Crassostrea gigas. J Exp Mar Biol Ecol 306(1): 17–36. doi: 10.1016/j.jembe.2003.12.021

Morse JW, Millero FJ, Cornwell JC, Rickard D. 1987. The Chemistry of the Hydrogen Sulfide and Iron Sulfide Systems in Natural Waters. Earth-Science Reviews 24: 1–42.

Morse JW, Arvidson RS, Lüttge A. 2007. Calcium Carbonate Formation and Dissolution. Chem Rev 107(2): 342–381. doi: 10.1021/cr050358j

Mucci A. 1983. The solubility of calcite and aragonite in seawater at various salinities, temperatures, and one atmosphere total pressure. Am J Sci 283: 780–799.

National Oceanic and Atmospheric Adminisitration (NOAA). 2016. Analysis of monitoring data from Harris Creek Sactuary oyster reefs. Data on the first 102 acres/12 reefs restored. NOAA. Available at https://chesapeakebay.noaa.gov/images/stories/habitats/hc3ydcheckinjuly2016.pdf.

Nestlerode JA, Luckenbach MW, O'Beirn FX. 2007. Settlement and Survival of the Oyster Crassostrea virginica on Created Oyster Reef Habitats in Chesapeake Bay. Restor Ecol 15(2): 273–283. doi: 10.1111/j.1526-100X.2007.00210.x

Neuheimer AB, Taggart CT. 2007. The growing degree-day and fish size-at-age: the overlooked metric. Can J Fish Aquat Sci 64: 375–385.

Newell RIE. 2004. Ecosystem influences of natural and cultivated populations of suspension-feeding bivalve molluscs: A review. J Shellfish Res 23(1): 51–61.

Newell RIE, Fisher TR, Holyoke RR, Cornwell JC. 2005. Influence of Eastern Oysters on Nitrogen and Phosphorus Regeneration in Chesapeake Bay, USA. In: Dame RF, Olenin S, editors. The Comparative Roles of Suspension-Feeders in Ecosystems. Berlin/Heidelberg: Springer-Verlag. p. 93–120. doi: 10.1007/1-4020-3030-4_6

Orr JC, Fabry VJ, Aumont O, Bopp L, Doney SC, Feely RA, Gnanadesikan A, Gruber N, Ishida A, Joos F, et al. 2005. Anthropogenic ocean acidification over the twenty-first century and its impact on calcifying organisms. Nature 437(7059): 681–686. doi: 10.1038/nature04095

Pacella SR, Brown CA, Waldbusser GG, Labiosa RG, Hales B. 2018 Apr 2. Seagrass habitat metabolism increases short-term extremes and long-term offset of CO 2 under future ocean acidification. Proceedings of the National Academy of Sciences: 201703445. doi: 10.1073/pnas.1703445115

Pachauri, R. K., L. Mayer, and Intergovernmental Panel on Climate Change, eds. 2015. Climate change 2014: synthesis report, Intergovernmental Panel on Climate Change.

Papke LE, Wooldridge JM. 1996. Econometric methods for fractional response variables with an application to 401 (K) Plan participation rates. J Appl Econom 11: 619–632.

Parker LM, Ross PM, O'Connor WA. 2009. The effect of ocean acidification and temperature on the fertilization and embryonic development of the Sydney rock oyster Saccostrea glomerata. Glob Change Biol 15(9): 2123–2136. doi: 10.1111/j.1365-2486.2009.01895.x

Parker, L. M., W. A. O'Connor, D. A. Raftos, H.-O. Pörtner, and P. M. Ross. 2015. Persistence of Positive Carryover Effects in the Oyster, Saccostrea glomerata, following Transgenerational Exposure to Ocean Acidification V. Thiyagarajan (Rajan) [ed.]. PLOS ONE 10: e0132276. doi:10.1371/journal.pone.0132276

Pawlik JR. 1992. Chemical ecology of the settlement of benthic marine invertebrates. Ocean Mar Biol Annu Rev 30: 273–335.

Pechenik JA. 1990. Delaed metamorphosis by larvae of benthic marine invertebrates: Does it occur? Is there a price to pay? Ophelia 32(1–2): 63–94.

Pechenik JA. 1999. On the advantages and disadvantages of larval stages in benthic marine invertebrate life cycles. Mar Ecol Prog Ser 177(1): 269–297.

Pechenik JA. 2006. Larval experience and latent effects—metamorphosis is not a new beginning. Integr Comp Biol 46(3): 323–333. doi: 10.1093/icb/icj028

Peng C, Zhao X, Liu S, Shi W, Han Y, Guo C, Peng X, Chai X, Liu G. 2017. Ocean acidification alters the burrowing behaviour, Ca2+/Mg2+-ATPase activity, metabolism, and gene expression of a bivalve species, Sinonovacula constricta. Mar Ecol Prog Ser 575: 107–117. doi: 10.3354/meps12224

Rao AMF, Malkin SY, Montserrat F, Meysman FJR. 2014. Alkalinity production in intertidal sands intensified by lugworm bioirrigation. Estuar Coast Shelf Sci 148: 36–47. doi: 10.1016/j.ecss.2014.06.006

Rassmann J, Lansard B, Pozzato L, Rabouille C. 2016. Carbonate chemistry in sediment porewaters of the Rhône River delta driven by early diagenesis (northwestern Mediterranean). Biogeosciences 13(18): 5379–5394. doi: https://doi.org/10.5194/bg-13-5379-2016

Rassmann J, Lansard B, Gazeau F, Guidi-Guilvard L, Pozzato L, Alliouane S, Grenz C, Rabouille C. 2018 May. Impact of ocean acidification on the biogeochemistry and meiofaunal assemblage of carbonate-rich sediments: Results from core incubations (Bay of Villefranche, NW Mediterranean Sea). Mar Chem, in press. doi: 10.1016/j.marchem.2018.05.006

Rebreanu L, Vanderborght J-P, Chou L. 2008. The diffusion coefficient of dissolved silica revisited. Marine Chemistry 112(3–4): 230–233. doi: 10.1016/j.marchem.2008.08.004

Reum JCP, Alin SR, Harvey CJ, Bednaršek N, Evans W, Feely RA, Hales B, Lucey N, Mathis JT, McElhany P, et al. 2016. Interpretation and design of ocean acidification experiments in upwelling systems in the context of carbonate chemistry co-variation with temperature and

oxygen. ICES Journal of Marine Science: Journal du Conseil 73(3): 582–595. doi: 10.1093/icesjms/fsu231

Rosenberg R, Davey E, Gunnarsson J, Norling K, Frank M. 2007. Application of computer-aided tomography to visualize and quantify biogenic structures in marine sediments. Marine Ecology Progress Series 331: 23–34. doi: 10.3354/meps331023

Rost, B., I. Zondervan, and D. Wolf-Gladrow. 2008. Sensitivity of phytoplankton to future changes in ocean carbonate chemistry: current knowledge, contradictions and research directions. Mar. Ecol. Prog. Ser. 373: 227–237. doi:10.3354/meps07776

Rusch A, Huettel M, Reimers CE, Taghon GL, Fuller CM. 2003. Activity and distribution of bacterial populations in Middle Atlantic Bight shelf sands. FEMS Microbiology Ecology 44: 89–100.

Sabine CL, Feely RA, Key RM, Bullister JL, Millero FJ, Lee K, Peng T-H, Tilbrook B, Ono T, Wong CS. 2002. Distribution of anthropogenic CO 2 in the Pacific Ocean. Global Biogeochemical Cycles 16(4): 30-1-30–17. doi: 10.1029/2001GB001639

Schneider, K., and J. Erez. 2006. The effect of carbonate chemistry on calcification and photosynthesis in the hermatypic coral Acropora eurystoma. Limnol. Oceanogr. 51: 1284–1293. doi:10.4319/lo.2006.51.3.1284

Seabra R, Wethey DS, Santos AM, Lima FP. 2015. Understanding complex biogeographic responses to climate change. Sci Rep 5(1). doi: 10.1038/srep12930

Siedlecki SA, Kaplan IC, Hermann AJ, Nguyen TT, Bond NA, Newton JA, Williams GD, Peterson WT, Alin SR, Feely RA. 2016. Experiments with Seasonal Forecasts of ocean conditions for the Northern region of the California Current upwelling system. Scientific Reports 6: 27203. doi: 10.1038/srep27203

Smyth A, Geraldi N, Piehler M. 2013. Oyster-mediated benthic-pelagic coupling modifies nitrogen pools and processes. Mar Ecol Prog Ser 493: 23–30. doi: 10.3354/meps10516

Soetaert K, Hofmann AF, Middelburg JJ, Meysman FJR, Greenwood J. 2007. The effect of biogeochemical processes on pH. Marine Chemistry 105(1–2): 30–51. doi: 10.1016/j.marchem.2006.12.012

Sordo, L., R. Santos, J. Reis, A. Shulika, and J. Silva. 2016. A direct CO2 control system for ocean acidification experiments: testing effects on the coralline red algae Phymatolithon lusitanicum. PeerJ 4: e2503. doi:10.7717/peerj.2503

Strathmann RR. 1985. Feeding and nonfeeding larval development and life-history evolution in marine invertebrates. Annu Rev Ecol Syst 16(1): 339–361.

Strickland JDH, Parsons TR. 1972. A Practical Handbook of Seawater Analysis. 2nd edition. (Vol. FIsheris Research Board of Canada Bulletin). Available at https://epic.awi.de/39262/1/Strickland-Parsons_1972.pdf. Accessed 2018 Nov 9.

Sun J, Hutchins DA, Feng Y, Seubert EL, Caron DA, Fu F-X. 2011. Effects of changing pCO2 and phosphate availability on domoic acid production and physiology of the marine harmful bloom diatom Pseudo-nitzschia multiseries. Limnol Oceanogr 56(3): 829–840. doi: 10.4319/lo.2011.56.3.0829

Takahashi, T., S. C. Sutherland, D. W. Chipman, J. G. Goddard, C. Ho, T. Newberger, C. Sweeney, and D. R. Munro. 2014. Climatological distributions of pH, pCO2, total CO2, alkalinity, and CaCO3 saturation in the global surface ocean, and temporal changes at selected locations. Mar. Chem. 164: 95–125. doi:10.1016/j.marchem.2014.06.004

Takeshita Y, Frieder CA, Martz TR, Ballard JR, Feely RA, Kram S, Nam S, Navarro MO, Price NN, Smith JE. 2015. Including high-frequency variability in coastal ocean acidification projections. Biogeosciences 12(19): 5853–5870. doi: 10.5194/bg-12-5853-2015

Talmage SC, Gobler CJ. 2010. Effects of past, present, and future ocean carbon dioxide concentrations on the growth and survival of larval shellfish. Proc Natl Acad Sci USA 107(40): 17246–17251. doi: 10.1073/pnas.0913804107

Talmage S, Gobler C. 2012. Effects of CO2 and the harmful alga Aureococcus anophagefferens on growth and survival of oyster and scallop larvae. Mar Ecol Prog Ser 464: 121–134. doi: 10.3354/meps09867

Tamburri MN, Zimmer RK, Zimmer CA. 2007. Mechanisms reconciling gregarious larval settlement with adult cannibalism. Ecological Monographs 77(2): 255–268.

Thomsen J, Haynert K, Wegner KM, Melzner F. 2015. Impact of seawater carbonate chemistry on the calcification of marine bivalves. Biogeosciences 12(14): 4209–4220. doi: 10.5194/bg-12-4209-2015

Timmins-Schiffman E, O'Donnell MJ, Friedman CS, Roberts SB. 2013. Elevated pCO2 causes developmental delay in early larval Pacific oysters, Crassostrea gigas. Mar Biol 160(8): 1973–1982. doi: 10.1007/s00227-012-2055-x

Trainer VL, Bates SS, Lundholm N, Thessen AE, Cochlan WP, Adams NG, Trick CG. 2012. Pseudo-nitzschia physiological ecology, phylogeny, toxicity, monitoring and impacts on ecosystem health. Harmful Algae 14: 271–300. doi: 10.1016/j.hal.2011.10.025

Trimborn S, Lundholm N, Thoms S, Richter K-U, Krock B, Hansen PJ, Rost B. 2008. Inorganic carbon acquisition in potentially toxic and non-toxic diatoms: the effect of pH-induced changes in seawater carbonate chemistry. Physiologia Plantarum 133(1): 92–105. doi: 10.1111/j.1399-3054.2007.01038.x

Underwood AJ, Fairweather PG. 1989. Supply-side ecology and benthic marine assemblages. Trends Ecol Evol 4(1): 16–20.

Utting SD, Millican PF. 1997. Techniques for the hatchery conditioning of bivalve broodstocks and the subsequent effect on egg quality and larval viability. Aquaculture 155: 45–54. doi: https://doi.org/10.1016/S0044-8486(97)00108-7

Van Cappellen P, Berner R. 1991. Fluorapatite Crystal-Growth from Modified Seawater Solutions. Geochim Cosmochim Acta 55(5): 1219–1234.

Vance JM. 2012. Proof-of-concept: Automated high-frequency measurements of PCO2 and TCO2 and real-time monitoring of the saturation state of calcium carbonate. Oregon State University. Available at http://ir.library.oregonstate.edu/concern/graduate_thesis_or_dissertations/br86b7957.

Wahl M, Saderne V, Sawall Y. 2016. How good are we at assessing the impact of ocean acidification in coastal systems? Limitations, omissions and strengths of commonly used experimental approaches with special emphasis on the neglected role of fluctuations. Mar Freshw Res 67(1): 25. doi: 10.1071/MF14154

Waldbusser GG, Steenson RA, Green MA. 2011. Oyster shell dissolution rates in estuarine waters: effects of pH and shell legacy. Journal of Shellfish Research 30(3): 659–669.

Waldbusser GG, Voigt EP, Bergschneider H, Green MA, Newell RIE. 2011. Biocalcification in the Eastern oyster (Crassostrea virginica) in relation to long-term trends in Chesapeake Bay pH. Estuaries Coasts 34(2): 221–231. doi: 10.1007/s12237-010-9307-0

Waldbusser GG, Brunner EL, Haley BA, Hales B, Langdon CJ, Prahl FG. 2013a. A developmental and energetic basis linking larval oyster shell formation to acidification sensitivity. Geophys Res Lett 40(10): 2171–2176. doi: 10.1002/grl.50449

Waldbusser GG, Powell EN, Mann R. 2013b. Ecosystem effects of shell aggregations and cycling in coastal waters: an example of Chesapeake Bay oyster reefs. Ecology 94(4): 895–903. doi: 10.1890/12-1179.1

Waldbusser GG, Salisbury JE. 2014. Ocean acidification in the coastal zone from an organism's perspective: Multiple system parameters, frequency domains, and habitats. Annu Rev Mar Sci 6(1): 221–247. doi: 10.1146/annurev-marine-121211-172238

Waldbusser GG, Hales B, Langdon CJ, Haley BA, Schrader P, Brunner EL, Gray MW, Miller CA, Gimenez I. 2015a. Saturation-state sensitivity of marine bivalve larvae to ocean acidification. Nat Clim Change 5(3): 273–280. doi: 10.1038/nclimate2479

Waldbusser GG, Gray MW, Hales B, Langdon CJ, Haley BA, Gimenez I, Smith SR, Brunner EL, Hutchinson G. 2016a. Slow shell building, a possible trait for resistance to the effects of acute ocean acidification. Limnol Oceanogr 61: 1969–1983. doi: 10.1002/lno.10348

Waldbusser GG, Hales B, Haley BA. 2016b. Calcium carbonate saturation state: on myths and this or that stories. ICES Journal of Marine Science: Journal du Conseil 73(3): 563–568. doi: 10.1093/icesjms/fsv174

Waldbusser GG, Hales B, Langdon CJ, Haley BA, Schrader P, Brunner EL, Gray MW, Miller CA, Gimenez I, Hutchinson G. 2015b. Ocean acidification has multiple modes of action on bivalve larvae. PLoS ONE 10(6): e0128376. doi: 10.1371/journal.pone.0128376

White MM, McCorkle DC, Mullineaux LS, Cohen AL. 2013. Early exposure of bay scallops (Argopecten irradians) to high CO2 causes a decrease in larval shell growth. PLoS ONE 8(4): e61065. doi: 10.1371/journal.pone.0061065

White M, Mullineaux L, McCorkle D, Cohen A. 2014. Elevated pCO2 exposure during fertilization of the bay scallop Argopecten irradians reduces larval survival but not subsequent shell size. Mar Ecol Prog Ser 498: 173–186. doi: 10.3354/meps10621

Whiting MC, McIntire CD. 1985. An investigation of distributional patterns in the diatom flora of Netarts Bay, Oregon, by correspondence analysis. J Phycol 21: 655–661.

Whitman E, Reidenbach M. 2012. Benthic flow environments affect recruitment of Crassostrea virginica larvae to an intertidal oyster reef. Marine Ecology Progress Series 463: 177–191. doi: 10.3354/meps09882

Wittmann, A. C., and H.-O. Pörtner. 2013. Sensitivities of extant animal taxa to ocean acidification. Nat. Clim. Change 3: 995–1001. doi:10.1038/nclimate1982

Wolf-Gladrow DA, Zeebe RE, Klaas C, Körtzinger A, Dickson AG. 2007. Total alkalinity: The explicit conservative expression and its application to biogeochemical processes. Mar Chem 106(1–2): 287–300. doi: 10.1016/j.marchem.2007.01.006

Xu Y-Y, Pierrot D, Cai W-J. 2017. Ocean carbonate system computation for anoxic waters using an updated CO2SYS program. Marine Chemistry 195: 90–93. doi: 10.1016/j.marchem.2017.07.002

Zeebe RE, Wolf-Gladrow DA. 2001. CO2 in Seawater: Equilibrium, Kinetics, Isotopes. 1st ed. Elsevier Science. (Elsevier Oceanography Series; Vol. 65).

Zeebe RE, Ridgwell A, Zachos JC. 2016. Anthropogenic carbon release rate unprecedented during the past 66 million years. Nat Geosci 9(4): 325–329. doi: 10.1038/ngeo2681

Zeebe RE. 2012. History of seawater carbonate chemistry, atmospheric CO2, and ocean acidification. Annu Rev Earth Planet Sci 40(1): 141–165. doi: 10.1146/annurev-earth-042711-105521

Zu Ermgassen PSE, Spalding MD, Blake B, Coen LD, Dumbauld B, Geiger S, Grabowski JH, Grizzle R, Luckenbach M, McGraw K, et al. 2012. Historical ecology with real numbers: past and present extent and biomass of an imperilled estuarine habitat. Proceedings of the Royal Society B: Biological Sciences 279(1742): 3393–3400. doi: 10.1098/rspb.2012.0313